SCUOLA DI DOTTORATO

UNIVERSITÀ DEGLI STUDI DI MILANO-BICOCCA

Department of Biotechnology and Biosciences

PhD program in Biology e Biotechnology Cycle XXXI

Molecular Curriculum

# New insights into the regulation of DNA end processing and DNA damage checkpoint

Surname: Colombo Name: Chiara Vittoria

Registration number: 727667

Tutor: Prof. Maria Pia Longhese

Coordinator: Prof. Paola Branduardi

**ACADEMIC YEAR 2017/2018**

**University of Milano-Bicocca**

**Department of Biotechnology and Biosciences**

**PhD program in Biology e Biotechnology – Cycle XXXI – Molecular curriculum**


# New insights into the regulation of DNA end processing and DNA damage checkpoint

Colombo Chiara Vittoria

Registration number: 727667

Tutor: Prof. Maria Pia Longhese

Coordinator: Prof. Paola Branduardi

**Academic year 2017/2018**

# *INDEX*

# *ABSTRACT*

The maintenance of genome integrity is essential for every living organism in order to transmit a full and faithful genetic inheritance to its progeny. However, genomic stability is continuously threatened by DNA damage that, if not rapidly and properly repaired, can be converted into mutations. Accumulation of mutations leads to genomic instability, which is one of the ten hallmarks of cancer in human cells.

Eukaryotic cells deal with DNA damage by activating DNA damage response (DDR), which includes pathways devoted to repair DNA lesions. One of the most dangerous DNA lesions is DNA double strand break (DSB), since it can cause both chromosomal rearrangements and loss of genetic material. In *Saccharomyces cerevisiae*, DSBs are mainly repaired by Homologous Recombination (HR), which exploits the sister chromatid or the homologous chromosome as a template to repair the damage. HR-mediated repair requires the DSB ends to be nucleolytically degraded in order to generate long 3'-ended single-stranded DNA (ssDNA) tails, in a process known as DSB end resection. Resection initiates with an endonucleolytic cleavage by the MRX (Mre11-Rad50-Xrs2) complex, together with Sae2 protein, while resection extension is carried out by the nucleases Exo1 and Dna2, the latter in association with the helicase Sgs1.

DSB repair is coordinated with the cell cycle progression through the DNA damage checkpoint, a signal transduction cascade that halts the cell cycle, in order to give cells sufficient time to repair the damage. In *Saccharomyces cerevisiae*, DNA damage checkpoint is activated by the two highly conserved kinases Tel1 and Mec1, orthologues of human ATM and ATR, respectively. Tel1 recognizes unprocessed DSBs, while Mec1 is activated by the RPA-coated ssDNA, produced by DNA end resection. Once activated, Mec1 and Tel1 phosphorylate different substrates including the adaptor Rad9 and the effector kinases Rad53 and Chk1, which allow signal amplification and subsequent cell cycle arrest.

Both DNA end resection and DNA damage checkpoint have to be finely regulated in order to ensure efficient DSB repair, albeit avoiding excessive ssDNA generation, and to properly coordinate repair with cell cycle progression. In this PhD thesis, we provide evidence of a new level of regulation of DSB resection, based on the modulation of the

amount of Exo1 exonuclease by the RNA-binding protein Npl3. Furthermore, we have studied the role of Sae2 protein in DNA damage repair and checkpoint activation.

Npl3 is a *S. cerevisiae* RNA-binding protein, which shares structural homologies with both the heterogeneous nuclear ribonucleoprotein (hNRP) and the mammalian serine-arginine-rich (SR) protein families. It plays a central role in the RNA metabolism, from transcription to translation, and counteracts the accumulation of harmful DNA-RNA hybrids during replication-coupled-transcription. Since emerging evidence supports strong connections between RNA metabolism and genome integrity, we investigated whether Npl3 was involved in DSB response. We demonstrated that the absence of Npl3 impairs both the Mec1-dependent checkpoint activation and the generation of long ssDNA tails at DSB ends. In particular, Npl3 promotes resection extension by acting in the same pathway of Exo1 nuclease. Moreover, both the lack of Npl3 protein and the inactivation of its RNA-binding domains cause the reduction of Exo1 protein level, thus indicating that Npl3 promotes resection extension and the subsequent Mec1-dependent checkpoint activation by regulating *EXO1* at the RNA level. Indeed, we proved that the decrease of Exo1 protein level is due to the presence of unusual and not properly terminated *EXO1* RNA species. These findings, together with the observation that *EXO1* overexpression partially suppresses the resection defect of *npl3Δ* cells, suggest that Npl3 participates in DSB end resection regulation by promoting the proper biogenesis of *EXO1* mRNA.

Concerning the second PhD project, it is already known that Sae2 protein participates in both DSB repair and DNA damage checkpoint. In particular, it promotes the endonucleolytic activity of MRX complex during DSB end resection and negatively regulates Tel1-dependent checkpoint response. Indeed, Sae2 limits MRX accumulation at the damage site, thus reducing Tel1 recruitment at the lesion and its signalling activity. How Sae2 functions in supporting DNA damage resistance and in inhibiting the DNA damage checkpoint are connected to each other is still unclear. Similarly, the mechanism by which Sae2 modulates MRX, Tel1 and Rad53 signalling activities has still to be elucidated. By performing a genetic screen, we identified the *sae2-ms* mutant

that, similarly to Sae2 absence, upregulates Tel1 signalling activity, thus suppressing the sensitivity of *mec1Δ* cells to hydroxyurea (HU) and methyl methanesulphonate (MMS). Indeed, Sae2-ms is able to increase both MRX and Tel1 recruitment to the DSBs, like the absence of Sae2. However, unlike *SAE2* deletion, Sae2-ms does not cause any resection or tethering defect, nor any sensitivity to genotoxic agents. Moreover, Sae2-ms induces Tel1 hyperactivation, but not Rad53 hyperactivation, suggesting that Sae2 plays distinct functions in controlling Tel1 and Rad53 activation. In accordance with these findings, we demonstrated that Sae2 absence, but not Sae2-ms presence, increases Rad53-Rad9 interaction even in the absence of DNA damage, thus indicating that Sae2 directly inhibits Rad53 activation by counteracting Rad53-Rad9 interaction. In conclusion, these data indicate that Sae2 regulates checkpoint activation both by controlling MRX removal from the damage site and by limiting Rad53-Rad9 interaction and that Rad53 activity downregulation is the main responsible for the DNA damage resistance promoted by Sae2.

Taken together, the results shown in this PhD thesis allow to better understand the molecular mechanisms involved in the control of the DNA damage response processes and so in the maintenance of genomic integrity.

# *PUBLICATIONS*

- Manfrini, N., Clerici, M., Wery, M., **Colombo, C.V.**, Descrimes, M., Morillon, A., d'Adda di Fagagna, F. & Longhese, M.P. Resection is responsible for loss of transcription around a double-strand break in Saccharomyces cerevisiae. *eLife* **4**, e08942 (2015)

- **Colombo, C.V.***, Trovesi, C.*, Menin, L., Longhese, M.P. & Clerici, M. The RNA binding protein Npl3 promotes resection of DNA double-strand breaks by regulating the levels of Exo1. *Nucleic Acids Res.* **45**, 6530-6545 (2017)

- **Colombo, C.V.**, Menin, L. & Clerici, M. Alkaline Denaturing Southern Blot Analysis to Monitor Double-Strand Break Processing. *Methods Mol Biol.* **1672**, 131-145 (2018)

- Bonetti, D., **Colombo, C.V.**, Clerici, M. & Longhese, M.P. Processing of DNA Ends in the Maintenance of Genome Stability. *Front. Genet* **9**, 390 (2018)

**Accepted for publication**

- **Colombo, C.V.**, Menin, L., Ranieri, R., Bonetti, D., Clerici, M. & Longhese, M.P. - Uncoupling Sae2 functions in downregulation of Tel1 and Rad53 signalling activities. *Genetics (early online December 2018)*

# *INTRODUCTION*

## DNA damage response and maintenance of genomic stability

Maintaining genomic integrity is essential for all of the organisms. In fact, preservation of genomic integrity guarantees life propagation and the transmission of a full and faithful genetic heritage to progeny. During evolution, cells have developed a series of mechanisms allowing them to protect their genetic heritage and to safeguard genomic stability.

In fact, our DNA is continuously affected by lesions that, if not properly and rapidly repaired, become mutations, which are transmitted to the progeny. It is estimated that every single cell has to deal with about $10^4$-$10^5$ lesions per day [1]. DNA damage can arise spontaneously from bases deamination, DNA depurination or depyrimidination, replication errors, uncontrolled recombination, collisions of replication and transcription machineries or from side-products of normal cellular metabolism like Reactive Oxygen Species (ROS). Otherwise DNA lesions can be caused by exogenous agents like ionizing radiations (IR), UltraViolet light (UV) and genotoxic chemicals, which include base analogues, alkylating agents, hydroxylating agents, intercalating agents, cross-linking agents and agents that cause Double Strand Breaks (DSBs) [2].

Cells face DNA damage by activating a sophisticated set of mechanisms that constitute a very complex cellular response, named DNA Damage Response (DDR), which is extremely conserved from the simplest prokaryotes to the most complex eukaryotes. DDR is a network of cellular pathways that sense, signal and repair the lesions. Since there are different types of DNA lesions, cells have developed a great number of different repair mechanisms to protect their genetic heritage. Repair mechanisms include Base Excision Repair (BER), Nucleotide Excision Repair (NER), MisMatch Repair (MMR), Non Homologous End Joining (NHEJ) and Homologous Recombination (HR). Apart from repair mechanisms, DDR comprises damage tolerance mechanisms, which allow cells to bypass a replicative fork stall and to proceed with normal DNA replication downstream of the unrepaired damage, and DNA damage checkpoint mechanisms that allow cells to arrest cell cycle progression until the lesion has been repaired [3] *( Figure* **1***)*.

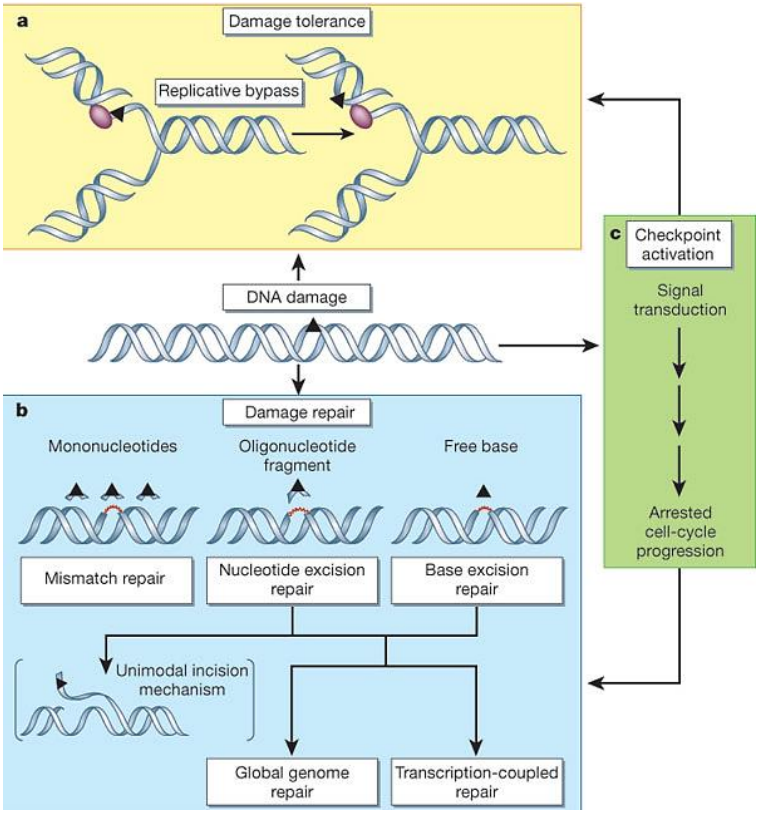


***Figure 1 – DNA Damage Response***

In the presence of DNA lesions, cells activate DDR, which includes repair mechanisms, damage tolerance mechanisms and checkpoint mechanisms. Damage tolerance mechanisms **(a)** are activated by a replication fork stall and they allow cells to bypass the damage without repairing it. DNA damage repair **(b)** comprises different mechanisms for different kinds of lesions, such as MMR, NER and BER. DNA damage checkpoint **(c)** is a network of complex signalling pathways that allow cells to arrest the cell cycle till the damage has been repaired.

*Adapted from [3]*

Therefore, DDR functionality is essential to maintain genomic integrity, avoiding the conversion of the lesions into mutations. In fact, unrepaired or wrongly repaired DNA lesions result in single base-pair mutations, like point mutations, deletions, insertions and microsatellite contractions or expansions, in chromosomal rearrangements like duplications, deletions, inversions or translocations, or in genome alterations like gross chromosomal rearrangements (GCRs), copy number variants (CNVs), hyper-recombination events and loss of heterozygosity (LOH). Even if mutations are important to guarantee genetic variability, which is a pre-requisite for cells evolution, accumulation of mutations causes genomic instability. Genomic instability has been defined as an "enabling" characteristic of cancer, allowing cells to acquire the capability to survive, proliferate and disseminate [4,5] *(Figure 2)*. Cancer cells genome is, indeed,

characterized by a great number of genetic, chromosomic or genomic mutations. In particular, 90% of somatic cancer mutations are dominant and usually affect oncogenes which, once mutated, promote tumour transformation. The remaining 10% mutations are recessive and usually affect tumour suppressors, which normally counteract neoplastic transformation [6]. In precancerous lesions, that originate when the first mutations arise, there is an evident activation of the DDR that delays or prevents cancer. Additional mutational events, which compromise this response, might allow cell proliferation, survival, genomic instability and promote tumour progression [7]. In accordance with this hypothesis, loss-of-function mutations in genes encoding for proteins involved in the DDR, known as care-takers genes, are thought to be responsible for hereditary cancers. Furthermore, diseases caused by mutations in DDR genes, like Ataxia Telangectasia, Bloom syndrome or Werner syndrome are characterized by an increased tumour incidence. This evidence strongly supports the "mutator hypothesis" which states that genomic instability, due to mutations in DDR genes, drives tumour development by increasing the spontaneous mutation rate [5]. Unlike hereditary cancers, genomic instability in sporadic cancers does not seem to be caused by mutations in care-takers genes. For this kind of tumours it is, instead, supported the "oncogene-induced DNA replication stress model" that attributes genomic instability to the replicative forks collapse caused by oncogenes activation [5]. In conclusion, the tight correlation between genome instability and tumour incidence is definitely clear by now, as well as the dependence of genome stability from the proper efficiency and reliability of the DDR. For this reason, increasing our knowledge about the molecular basis of the DDR is fundamental to develop new therapies against cancer and genetic diseases and to try to prevent them.

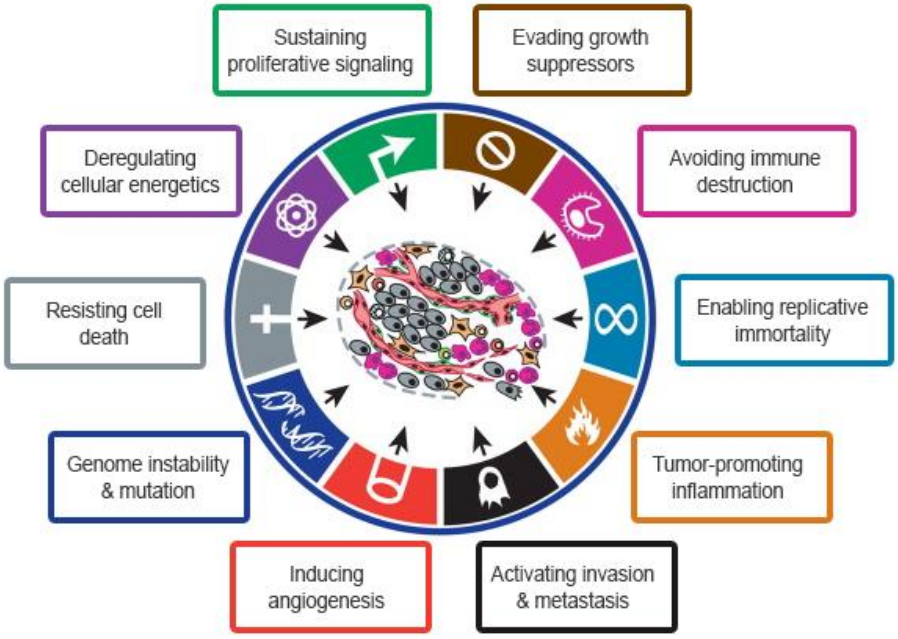


***Figure 2 – Hallmarks of cancer***

Schematic representation of the 10 hallmarks of cancer. The first 6 acquired cancer capabilities, proposed in 2000, were proliferative signalling sustainment, growth suppressors evasion, invasion and metastasis activation, replicative immortality, angiogenesis induction and cell death resistance. In 2011 cellular energetics deregulation and immune destruction avoidance have been added as emerging hallmarks. In the same year, genome instability & mutation and tumor-promoting inflammation have been recognized as tumour enabling characteristics.

*Adapted from [4]*

## DNA Double Strand Breaks repair mechanisms

DNA double strand breaks are breakages at the double helix of DNA, generated when the phospho-sugar backbone of two complementary DNA strands is broken in the same position or in very close proximity, causing the dissociation of the double helix into two molecules separated by the lesion. DSBs are one of the most dangerous lesions for cells, indeed if they are not rapidly and properly repaired they can lead to loss of genetic material next to the lesion or to chromosomic rearrangements like deletions, inversions or translocations [8]. DSBs can either arise spontaneously or they can be caused by physical agents (like ionizing radiations) or by chemicals. Spontaneous DSBs can be due to ROS or other by-products of normal cellular metabolism that can interact with DNA, oxidise the bases of opposite DNA strands and trigger Single Strand Breaks (SSBs) or DSBs. However the mayor source of spontaneous DSBs in proliferating cells is the replication process, especially in the presence of replication stress. In fact, DNA replication intermediates are fragile and susceptible to breakage, so every situation in which replication forks stall and replisome collapses can give rise to DSBs. Transcription has also been implicated as one of the leading causes of DSBs. Indeed, collision between replication and transcription machineries, as well as the presence of hybrids between DNA and RNA, cause replication stress and the arrest of replication forks progression [9]. Chemical agents that cause DSBs are widely used as chemotherapeutic drugs, since cancer cells are usually more sensitive to DSBs than healthy cells. Among the chemicals that cause DSBs there are radiomimetic agents, like Phleomycin (Phleo) or bleomycin, which mimic the action of IR, alkylating agents, like Methyl Methane Sulphonate (MMS) or temozolomide, which stall replication forks and inhibit transcription, cross-linking agents, like mitomycin C, cisplatin and psoralens, which covalently link bases of the same strand (intrastrand) or of complementary strands (interstrand). Drugs like HydroxyUrea (HU) and aphidicoline impair replication fork progression by depleting deoxyribonucleotides pool and inhibiting DNA polymerase, respectively. Moreover, topoisomerase inhibitors, like camptothecin (CPT) and

etoposide, trap covalently linked topoisomerase-DNA cleavable complexes, causing SSBs and the arrest of the replication fork, which generates replication intermediates that are resolved producing DSBs [8,9].

Defects in the response to DSBs are linked to a series of genetic hereditary human diseases like LIG4-syndrome, Severe Combined Immunodeficiency with Sensitivity to Ionizing Radiation, Ataxia Telangiectasia, Ataxia Telangiectasia-Like Disorder, Nijmegen Breakage Syndrome, ATR-Seckel syndrome and Fanconi Anaemia [10]. Furthermore, DSB repair defects can cause increased cancer susceptibility, immunodeficiencies and neurological defects [8].

Although DSBs are so toxic and dangerous for genomic stability, during specific physiological processes programmed DSBs are induced. In particular, T- and B-lymphocytes inflict themselves DSBs through the RAG complex, to initiate V(D)J recombination that allows them to produce T-cell receptors and immunoglobulin antigen receptors, able to recognize every different type of antigen. DSBs are also induced by lymphocytes during immunoglobulin class switching [11]. Another example of self-inflicted DSBs are the meiotic ones. Indeed, during early meiotic prophase, after DNA replication has ended, the highly conserved topoisomerase-like protein Spo11 creates a single DSB on every chromosome. These programmed DSBs are not randomly located, but they are only generated in chromosome regions with specific features. Repair of these auto-inducted DSBs by homologous recombination leads to an exchange of genetic material between homologous chromosomes, which guarantees genetic variability. Repair by homologous recombination also keeps the homologous chromosomes linked through X-structures named chiasma during metaphase I, which allows them to segregate correctly during the first meiotic division [12].

Cells have developed two main mechanisms to repair DSBs: Non Homologous End Joining (NHEJ), which simply re-ligates broken ends kept close to each other, and Homologous Recombination (HR), which uses the homologous chromosome or the sister chromatid as a template for the repair.

## Non Homologous End Joining (NHEJ)

NHEJ is a repair mechanism in which two broken ends are joined together, without any particular attention to their sequence. Indeed, Lig4 enzyme re-constitutes the phosphodiester bond between two broken ends even if they are not perfectly compatible, following a small processing by nucleases and polymerases. For this reason NHEJ is considered an error prone mechanism that could lead to genic mutations like deletions, insertions or base substitutions, but also to chromosomal rearrangements like inversions or translocations. Thus, a lack of regulation and efficiency of NHEJ repair could cause genomic instability and subsequent tumoral transformation [13,14].

NHEJ is highly conserved from prokaryotes to complex eukaryotes and it is the main DSB repair pathway in mammals. The first step of NHEJ is the recognition of the lesion and its binding by the highly conserved heterodimeric complex KU, composed by Ku70 and Ku80 subunits both in yeast and in mammals. KU complex has the shape of an asymmetrical ring, with positively charged amino acids inside the hole, which allow for sequence-independent interaction with DNA that perfectly accommodates into the hole [13]. After binding to the lesion, KU recruits the other factors involved in NHEJ and protects the DSB ends from nucleolytic degradation. Indeed, NHEJ can occur only on blunt or minimally processed DNA ends. If DSBs are nucleolytically processed they have to be repaired by HR [15]. In order to re-ligate the correct broken ends it is essential they are kept close to each other in a process named bridging or tethering. In mammals this role is performed by the DNA-PKcs protein, which is recruited to the lesion by Ku. DNA-PKcs is a member of the phosphoinositide 3-kinase related protein kinase (PI3KK) family, and it forms an active complex with Ku and the DNA, named DNA-PK. This active complex tethers the broken ends together and phosphorylates downstream targets involved in NHEJ processing or repair, in order to recruit them to the lesion [13,14]. In yeast, the broken ends bridging is carried out by the MRX complex, composed by Mre11, Rad50 and Xrs2 subunits. MRX is orthologue of the human MRN (MRE11-RAD50-NBS1) complex that, however, does not seem to perform the same role in

mammalian cells. Rad50 subunit of the MRX complex is responsible for tethering of DNA ends in yeast thanks to its particular structure. In fact, Rad50 has two central coiled-coil domains separated by a Cys-X-X-Cys (CXXC) motif that corresponds to a zinc hook. CXXC motifs of two different Rad50 molecules coordinate a single zinc ion, allowing the interaction between two Rad50 proteins linked to different DNA ends [13,16–18] *(Figure 3)*. Sae2 protein also contributes to intrachromosomal bridging of DSB ends in yeast, by acting in the same pathway of the MRX complex [19].

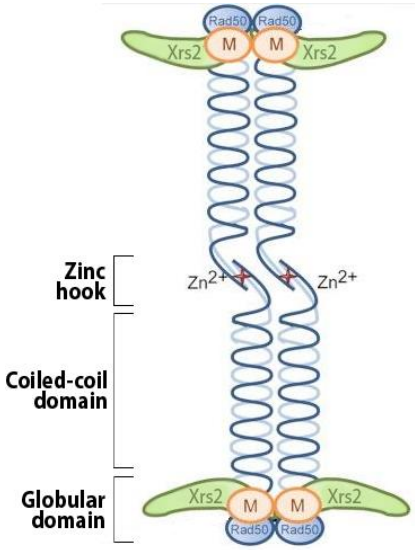


***Figure 3 – Rad50 zinc hook role in DNA ends tethering***

Schematic representation of the MRX complex structure. Rad50 interacts with Mre11 and Xrs2 through its globular domain, thus forming a DNA-binding motif. Between the coiled-coil domains of Rad50 there is a zinc hook domain, characterized by a conserved CXXC motif. The zinc hook domains of 2 different Rad50 molecules coordinate the same zinc ion, resulting in the tethering of DNA ends.

*Adapted from [18]*

After DSB recognition and tethering of the broken ends, the other factors involved in NHEJ repair are recruited to the damage. Most of the DSB ends are not perfectly compatible, due to DNA-protein adducts or mismatching overhangs, thus some processing is needed before the ligation reaction can occur. In mammals, blocking end groups are removed by factors like polynucleotide kinase (PNKP) or aprataxin. Mismatching nucleotides at the DSB ends are eliminated through nucleolytical processing by ARTEMIS nuclease, APLF nuclease, MRN complex, CtIP protein, FEN1 endonuclease, EXO1 exonuclease and WRN helicase. Gap-filling of protruding ends is

performed by the family of X polymerases, which includes μ and γ polymerases [13,20]. In yeast, the main endonuclease involved in the removal of mismatching overhangs is Rad27, even though we cannot exclude a contribution of the Mre11 subunit of the MRX complex. Gap-filling is accomplished by the Pol4 polymerase, which belongs to the same family of human μ and γ polymerases [13,21]. Once the DSB ends are made compatible, they can be ligated by a DNA ligase through an ATP-dependent reaction. In mammals, DNA ligase IV (DNL4) enzyme, in association with its cofactors XRCC4 and XLF is recruited to the lesion by the DNA-PK complex. XRCC4 stimulates DNA ligase IV activity, while XLF allows it to re-join mismatched DNA ends [13,20]. In yeast, DNA Ligase 4 (Dnl4/Lig4) enzyme, in association with its cofactor Lif1, is recruited to the DSB by a direct interaction between Lif1 and the Xrs2 subunit of the MRX complex. The recruitment of Lig4-Lif1 also requires Ku70 presence at the lesion, while nuclear localization of Lif1 seems to require Nej1 factor [13,16].

NHEJ mechanism in mammals and yeast is shown in *Figure 4*.

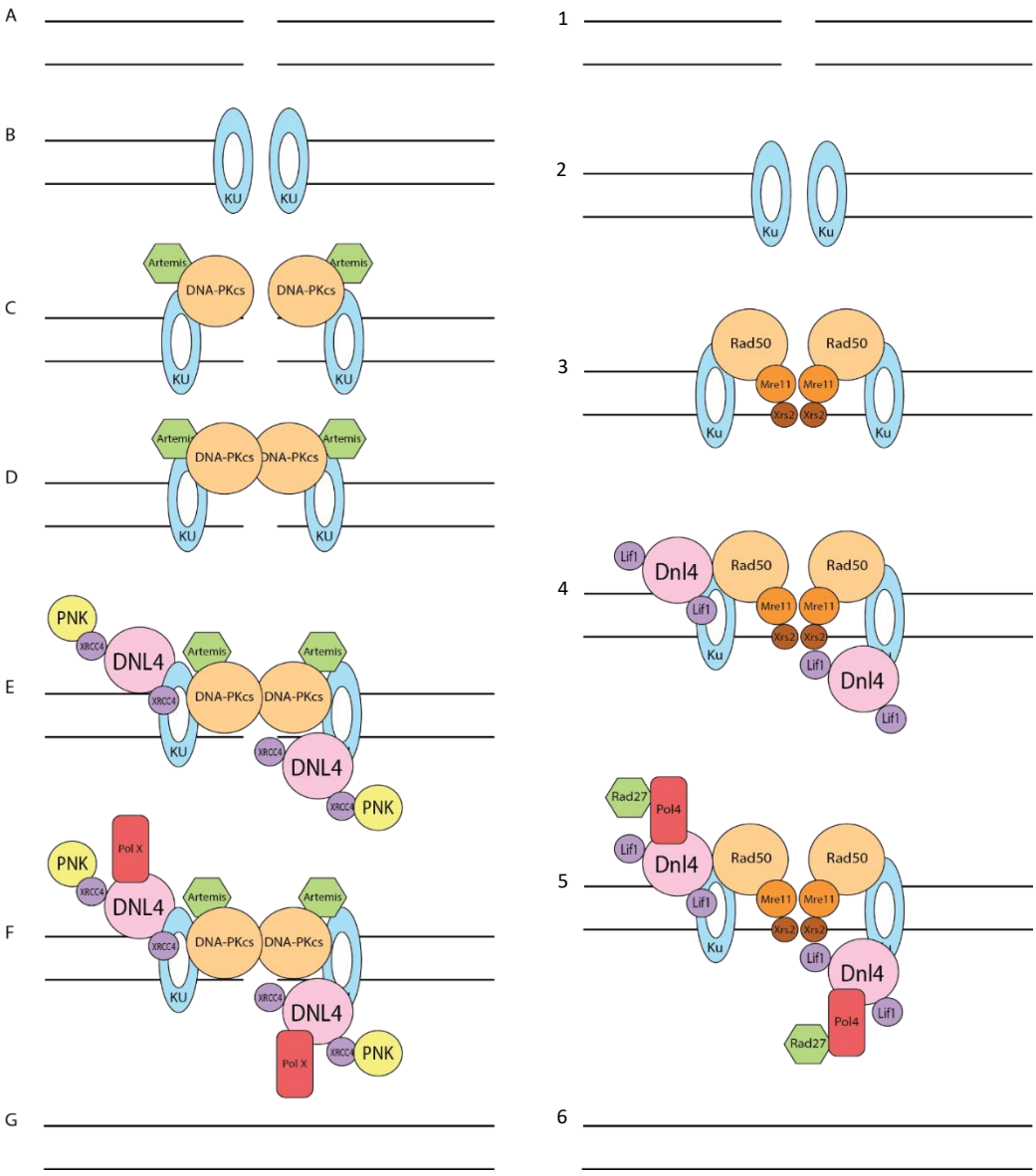


***Figure 4 – NHEJ mechanism in human and yeast cells***

When a DSB occurs **(A-1)** Ku complex recognises the lesion and binds to DSB ends **(B-2)**. DNA-PKcs in mammals **(C)** and the MRX complex in yeast **(3)** are recruited to the lesion and tether DNA broken ends **(D-3)**. In human cells ARTEMIS nuclease is recruited to the break together with DNA-PKcs **(C-D)**.DNA ligase IV (DNL4/Dnl4) enzyme, in association with its cofactor XRCC4/Lif1 is recruited to the DSB **(E-4)**. End processing enzymes, like polynucleotide kinase (PNK), ARTEMIS nuclease and Pol X family polymerases (μ and γ) localise to the lesion to make the broken ends compatible in human cells **(F)**. In yeast cells the same role is accomplished by Rad27 nuclease and Pol4 polymerase **(5)**. Once the ends are made compatible DNA ligase re-joins the broken ends **(G-6)**.

*Adapted from [13]*

## Homologous Recombination (HR)

Homologous recombination is a highly conserved repair mechanism that exploits a homologous DNA sequence, like the sister chromatid or the homologous chromosome, as a template to repair the lesion. For this reason, unlike NHEJ, it is considered an error-free mechanism. Thus, HR consists in the exchange of genetic material from an intact DNA molecule, defined as donor, to a damaged recipient DNA molecule, with identical or very similar sequence. Since availability of a homologous DNA template is essential for HR repair, this mechanism is highly dependent on the ploidy and on the cell cycle phase [22]. Indeed, HR is performed only in S/G2 phase, after DNA has been completely replicated, while NHEJ is the predominant mechanism in G1 phase. Cell cycle regulation of HR is mainly obtained by the restriction to S/G2 phase of its first step, which consists in the nucleolytic degradation of DSB ends. This cell cycle-related restriction is carried out by cyclin-CDK (Cyclin-Dependent Kinase) complexes, which alter their kinase activity relying on cell cycle phases [9,15,23]. Apart from homologous DNA sequence presence, other factors influence substrate availability for HR, such as donor and recipient proximity, chromatin structure and nuclear compartmentalisation. In fact, HR preferentially involves sister chromatids, which are linked by cohesin, rather than homologous chromosomes, which are distant inside the nucleus. Furthermore, HR cannot occur if chromatin structure is too condensed, so several chromatin-remodelling factors are recruited to the DSB during this repair mechanism. Finally, HR can occur only in nucleoplasm, while it is inhibited both in the nucleolus and in the nuclear periphery [22].

HR mechanism can be divided into three main phases:

1) Nucleolytical degradation of DSB ends *(Figure 5)*
2) Strand invasion and DNA synthesis
3) Repair process completion and Holliday junctions resolution

Nucleolytical processing of 5'-ends of the DSB allows for the generation of long 3'-protruding single strand DNA (ssDNA) tracts. ssDNA tails are then covered by a series

of proteins, generating a nucleofilament that can invade the homologous DNA helix. After strand invasion, homologous recombination occurs through DNA synthesis, employing the homologous DNA as a template, with different mechanisms during mitosis or meiosis. Homologous recombination generates X-structures on DNA, named Holliday junctions, which have to be resolved by nucleases or helicases-topoisomerases complexes to complete repair [22,24–26].

### 1) Nucleolytic degradation of DSB ends (DNA end resection)

DSB end resection consists in the nucleolytic degradation of the 5' DSB ends, in order to produce long 3'-protruding ssDNA stretches. Resection can be divided into two steps: resection initiation, which removes about 50-200 nucleotides from DSB ends, and resection extension that elongates ssDNA tails [22]. These long ssDNA tracts are very important both to induce checkpoint activation, allowing cell cycle arrest until the lesion has been repaired [27], and to invade the homologous strand, thus guaranteeing template-directed repair [22].

The main factors involved in DSB end resection are extremely conserved from yeast to humans, and analogous proteins are found in prokaryotes, as well [15,28,29]. In particular, the MRX complex, which consists of Mre11, Rad50 and Xrs2 subunits, is responsible for resection initiation in yeast, in association with the protein Sae2. Similarly, the MRN complex, composed by MRE11, RAD50 and NBS1, is involved in short-range resection in mammals, together with Sae2 orthologue CtIP [30–33]. Thus, MRX/MRN catalyses the endonucleolytic cleavage of 5' ends, producing a short 3' overhang, but it has also a role in the recruitment of other factors involved in resection. Resection extension is performed by Exo1 and Dna2 nucleases in yeast, and by their orthologues EXO1 and DNA2 in human cells. In yeast, Dna2 acts in association with the helicase Sgs1, while both EXO1 and DNA2 act together with the helicase BLM in humans [25,30,32–34]. Short-range resection is essential on "dirty" DNA ends, like in the presence of DNA-protein

adducts. Conversely on “clean” DSB ends, such as the enzyme-induced ones, the nucleases involved in long-range resection can directly process DNA ends, even in the absence of MRX/MRN and Sae2/CtIP [32].

Resection initiation is a key step for the choice of the proper DSB repair mechanism, both in yeast and in mammals. Indeed, once DNA ends processing has begun, the long ssDNA tails do not allow Ku to bind to the DSB ends anymore. Thus, after resection initiation, NHEJ repair is prevented and cells are committed to HR repair [15,25]. For this reason, resection has to be strictly controlled during cell cycle progression, so that HR only occurs in S/G2 phase, when the sister chromatid is available as a template for the repair. Moreover, a tight regulation of the nucleolytic degradation of DSB ends is essential to avoid excessive processing, which would be detrimental for genomic stability [25,31].

The mechanism of DSB end resection in yeast, showing the main factors and regulators involved in the process, is shown in *Figure 5*.

**Nucleases and helicases involved in DSB end resection**

One of the first protein complexes recruited to a DSB is the MRX (Mre11-Rad50-Xrs2) complex in yeast and its orthologue MRN (MRE11-RAD50-NBS1) complex in mammals [35]. MRX/MRN is a heterohexameric complex composed by dimers of the three different subunits and it has both a catalytic and a structural role in DSB end resection. Mre11/MRE11 and Rad50/RAD50 subunits are highly conserved also in prokaryotic cells, while Xrs2/NBS1 is the less conserved subunit of the complex, with no orthologue in prokaryotes [25].

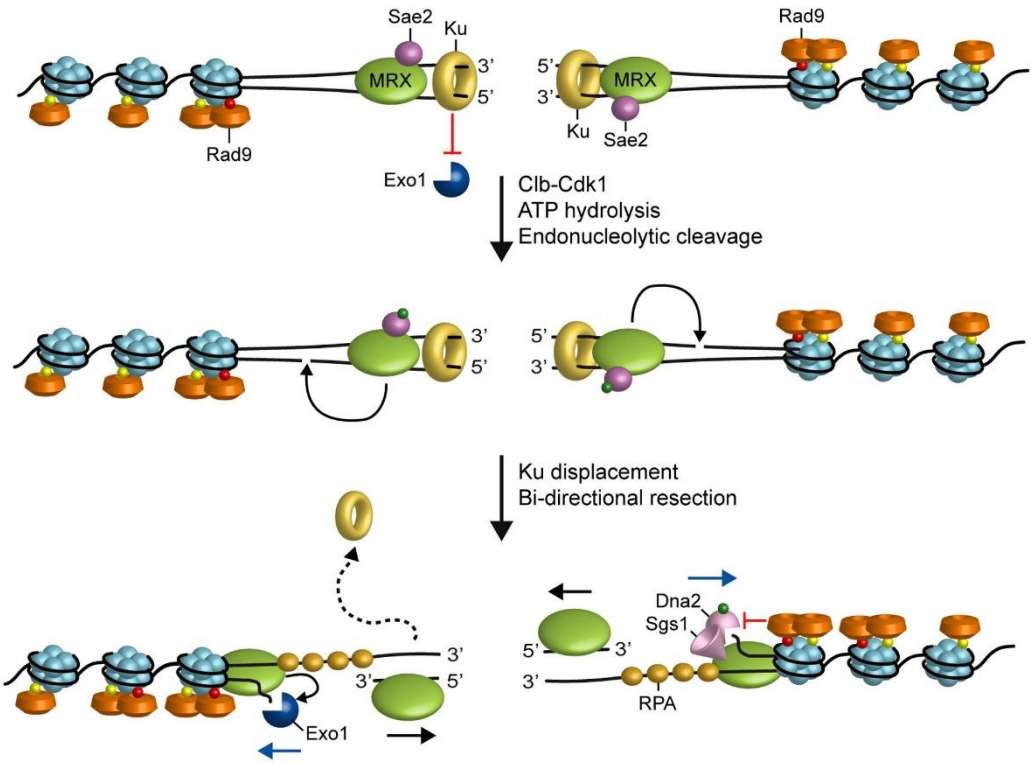


***Figure 5 - Model for DSB end resection in yeast***

The first factors recruited to the DSB are MRX, Sae2 and Ku. Ku inhibits Exo1 access to DNA ends, while Rad50, in its ATP-bound state, blocks the Mre11 nuclease activity. After ATP hydrolysis by Rad50, Mre11 catalyses the endonucleolytic cleavage of the 5' strands of the DSB. Mre11-dependent processing is promoted by Sae2, once it has been phosphorylated by Cdk1. The initial incision by MRX-Sae2 creates an entry site for Exo1 and Sgs1-Dna2, that process DNA in the 5'–>3' direction from the nick (blue arrows), while MRX degrades in the 3'–>5' direction toward the DSB ends (black arrows). The MRX complex also promotes Exo1 and Sgs1-Dna2 association at the DSB ends, whereas Rad9 inhibits the resection activity of Sgs1-Dna2. Phosphorylation events by Mec1 and Tel1 are indicated by red dots, green dots indicate phosphorylation events by Cdk1, while methylation of histone H3 is indicated by yellow dots.

*Adapted from [33]*

Mre11/MRE11 has an N-terminal region containing the Xrs2/NBS1 binding site and five phosphodiesterase domains, which are fundamental for its nuclease activity. In the C-terminal domain, it has two DNA binding sites and the Rad50/RAD50 interaction region [25,33,36,37]. Mre11/MRE11 acts as a homodimer and preferentially binds to DNA ends, mainly to double-stranded DNA and branched substrates. It seems to be supported by Rad50/RAD50 and Xrs2/NBS1 for the binding [37,38]. Once bound to DNA ends, Mre11/MRE11 catalyses the degradation of 5'-terminated ends through its nuclease activity. *In vitro*, Mre11/MRE11 exhibits manganese-dependent endonuclease and 3' to 5' exonuclease activities [32,33,39]. Mre11/MRE11 nuclease activities are enhanced by Xrs2/NBS1 and Rad50/RAD50, *in vivo* [32]. The endonucleolytic activity of Mre11 in yeast, which is strongly promoted by Sae2 [40], is dispensable on "clean DNA ends", like the ones generated by endonucleases, while it is essential on DNA ends with altered secondary structures or blocked by proteins, defined as "dirty DNA ends". Examples of dirty DNA ends are the ones that form hairpin structures or are bound by Ku complex, by Spo11 protein or by topoisomerases. The DSB ends generated after exposure to IR, CPT, bleomycin or alkylating agents are also dirty ones [25,35,41]. In human cells, the MRE11 endonucleolytic activity, supported by CtIP, is, instead, fundamental also on clean DNA ends, suggesting they are less accessible than the yeast ones [25]. Thus, Mre11/MRE11, in association with Sae2/CtIP, performs an endonucleolytic cleavage about 50-200 nucleotides apart from the 5' DNA ends, allowing the removal of ssDNA oligonucleotides that leave 3'-protruding overhangs [25,41].

Rad50/RAD50 is a member of the ABC ATPase superfamily and its domains organization is characteristic of the SMC proteins family, which is implicated in the maintenance of chromosomes stability through the control of chromatin structure [36,42]. Rad50/RAD50 has an N-terminal domain, containing a Walker A motif, and a C-terminal domain, containing a Walker B motif. These two motifs associate together, making a bipartite ATPase domain, typical of ATP-binding cassettes [33,36,37]. As previously described, the central portion of Rad50/RAD50 is constituted by two coiled-coil domains, separated by a Cys-X-X-Cys motif that coordinates a zinc atom, allowing DSB ends tethering

[17,18,33,36]. The zinc hook motif is important both for Rad50/RAD50 dimerization and for its interaction with Mre11/MRE11 C-terminal portion. Another interaction site is between the capping domain of Mre11/MRE11 and the ATPase domain of Rad50/RAD50 [17,43]. In particular, it has recently been demonstrated that when Rad50/RAD50 binds ATP, MRX/MRN complex adopts a closed conformational state, in which Rad50/RAD50 head domains dimerize and cover the nuclease domain of Mre11/MRE11. This closed state allows DNA binding, but not resection. After ATP hydrolysis, a conformational change happens and MRX/MRN complex is shifted to an open conformation, in which the active site of Mre11/MRE11 is exposed and resection can start. Thus, the closed conformation promotes MRX/MRN roles in NHEJ and checkpoint activation, while the open MRX/MRN conformation favours resection and HR [25,33,39,44,45].

Xrs2/NBS1 is the less conserved subunit of the MRX/MRN complex and it mainly exerts regulatory functions or recruits other factors to the damage site [25,37]. The N-terminal portion Xrs2/NBS1 contains a ForkHead-Associated (FHA) domain, which allows the interaction with Sae2/CtIP and Lif1/XRCC4 [46–49]. It also contains two tandem BRCA1 C-Terminal (BRCT) domains that are important for the interaction with other proteins involved in the DDR, such as the phosphorylated checkpoint adaptor MDC1 that binds the phosphorylated H2AX histone, allowing checkpoint signalling amplification and maintenance [25,36,37,50]. In the C-terminal portion, Xrs2/NBS1 contains the interaction sites for Mre11/MRE11 and for the checkpoint kinase Tel1/ATM. In the same region there is also a Nuclear Localization Sequence (NLS) which allows the translocation of the MRX/MRN complex from the cytoplasm to the nucleus, once its subunits are synthesised and assembled [25,36,51,52]. Xrs2/NBS1 also promotes the binding of the MRX/MRN complex to the DNA and the nuclease activity of Mre11/MRE11 subunit [53,54]. A recent study demonstrated that Xrs2 is not essential for resection, but it is fundamental for the nuclear localization of the MRX complex, for canonical NHEJ and for Tel1 recruitment to the lesion [46].

Together with the MRX/MRN complex, Sae2 protein in *S. cerevisiae* and its orthologue CtIP in humans, is involved in resection initiation. Both Sae2 and CtIP are, for most of their sequences, intrinsically disordered proteins, but they both contain a structurally conserved N-terminal portion, which is essential for their oligomerization. They also have a conserved C-terminal region, involved in resection stimulation and regulation [55]. Moreover, they both can interact with DNA and with the MRX/MRN complex, thus promoting its endonuclease activity [19,33,40,56,57]. Sae2/CtIP activity (and oligomerization state in the case of Sae2) is strongly dependent on its phosphorylation state. In particular, Sae2/CtIP is phosphorylated by CDK and by the checkpoint kinases Mec1/ATR and Tel1/ATM and these phosphorylation events are fundamental to stimulate HR repair and to restrict DSB end resection to S/G2 phases [31,47,48,58–60]. Concerning cell cycle-dependent Sae2 regulation, the most important residue for Cdk1 phosphorylation is Serine 267, while Serine 134 has only a secondary role [61]. How Sae2 participates in resection is still not completely clear. It has been demonstrated that it activates the dsDNA-specific endonuclease activity of Mre11 within the MRX complex, generating an entry site for Mre11 itself and for Exo1 and Dna2 nucleases [33,40]. The efficiency of this endonucleolytic cleavage by MRX-Sae2 is strongly enhanced by the presence of physiological protein blocks, *in vitro* [33,40,62,63]. On the contrary, Paull's laboratory has biochemically proved an endonuclease activity of Sae2 itself [64,65]. Furthermore, it is quite evident that Sae2 has not only the role of promoting Mre11 endonucleolytic activity, since *sae2Δ* cells are more sensitive to genotoxic agents than *mre11* nuclease defective (*mre11-nd*) cells. Indeed, it has been proved that Sae2 also participates in DSB ends tethering, in MRX removal from DSB ends and in the negative regulation of checkpoint signalling [19,66–68]. Like Sae2, CtIP also stimulates resection initiation with a not completely known mechanism. It physically interacts with NBS1 and localizes to the lesion together with the MRN complex [31,69]. Phosphorylation by CDKs enhances CtIP activity as a co-factor, thus allowing it to promote the nuclease activity of the MRN complex [69]. *In vitro*, CtIP also shows an endonuclease activity on branched DNA structures, independent from the MRN complex [70]. Furthermore, CtIP

interacts with the tumour suppressor BRCA1, which seems to increase DSB end resection speed [71]. Recent studies also demonstrated that CtIP positively influences the activity of the nucleases involved in the resection extension [72].

After 50-200 nucleotides are removed from the 5' ends of the DSB by MRX/MRN-Sae2/CtIP, the nucleases Exo1/EXO1 and Dna2/DNA catalyse resection extension by two parallel and partially redundant pathways [56,73–75]. In fact, inactivation of a single pathway results in only a small resection defect, since the other pathway compensates for it, while inactivation of both pathways results in a very strong resection defect [33,74]. Exo1/EXO1 is part of the Rad2/XPG nucleases family and it shows exonuclease activity in the 5'->3' direction, which leads to the release of mononucleotide products from dsDNA ends [30,33,76]. Yeast Exo1 does not need any helicase activity for DNA unwinding, while human EXO1 requires BLM helicase, which increases its DNA affinity [73,76]. The MRX complex enhances both the affinity to DNA ends and the processivity of Exo1 nuclease [33,57,73,77,78]. This promoting activity by MRX does not require the Mre11 nuclease activity and it is further enhanced by Sae2 [78]. Recent findings support a model in which MRX promotes a local unwinding of the DSB DNA ends, which facilitates Exo1 persistence on DNA [79]. This enhanced processivity seems to be particularly critical in the presence of RPA, since Exo1 is rapidly stripped from DNA by RPA, thus multiple cycles of Exo1 rebinding at the same DNA end would be required for extensive resection [80]. Anyway, Exo1-dependent resection also occurs in the absence of MRX-Sae2, suggesting that other factors may promote the nuclease activity of Exo1 [25,30,74]. Human EXO1 protein also shows an enhanced enzymatic activity in the presence of the MRN complex *in vitro*, even if it does not physically interact with any subunit of the complex [73,81]. Furthermore, CtIP allows the recruitment of EXO1 to the lesion, by a physical interaction between the two proteins [81]. Thus, in human cells, resection initiation by MRN-CtIP is essential to recruit EXO1 and promote its activity [73,81]. CtIP also negatively regulates EXO1 nucleolytic activity, by avoiding unscheduled and excessive strands degradation [81]. Both in yeast and in mammals, Exo1/EXO1 activity is inhibited by cyclin-dependent and checkpoint kinases. Indeed, Rad53 limits ssDNA accumulation in

yeast, while ATR induces EXO1 degradation in human cells, while CDK restricts EXO1 action to S/G2 phase of the cell cycle [30,82,83].

Dna2/DNA2 is a bifunctional helicase-nuclease, which possesses both 5'->3' and 3'->5' nuclease activities, as well as a helicase activity with 5'->3' polarity [84,85]. Dna2 participates to both the elimination of DNA flaps arising during lagging strand synthesis and to the endonucleolytic cleavage of 5' or 3' ssDNA ends [74,84–87]. The resection activity of Dna2/DNA2 relies on the RecQ helicase Sgs1/BLM, which provides the proper substrates for the nuclease by unwinding the dsDNA [33,73,74,86,87]. In human cells, DNA2 also physically interacts with the RecQ helicase WRN [88,89]. However, recent studies have demonstrated that also the helicase activity of Dna2/DNA2 itself supports its role in resection by acting as a ssDNA translocase [90,91]. In particular, its ATP-dependent helicase activity promotes Dna2 translocation in the 5'->3' direction, thus resulting in the formation of degradation products of 12-100 nucleotides in length. By contrast, in the absence of Dna2 helicase activity, the cleavage products are only 5-12 nucleotides long [91]. The correct polarity of Dna2 translocation and degradation during the resection process is maintained by the RPA complex. In fact, RPA binds and protects the 3' strands from Dna2 access, allowing the resection activity of the nuclease only on the 5' strands [86,87]. Moreover, in mammals, RPA and CtIP enhance the activity of DNA2-BLM complex [72,73].

Sgs1/BLM is a member of the RecQ helicases family and it is able to unwind dsDNA ends with an ATP dependent 3'->5' translocation on the 3' terminated strands [87,92]. The unwound ssDNA is then covered by RPA on the 3' strand, while the 5' strand can be nucleolitically degraded by Dna2/DNA2 [73,74]. In yeast, the MRX complex physically interacts with Sgs1 and it is involved in its recruitment to the DSBs, as well as in the stimulation of its helicase activity [78,86]. In the same way, the MRN complex recruits BLM and promotes its helicase activity in human cells [73]. Sgs1 physically interacts with Top3 topoisomerase and with Rmi1 protein, thus forming the STR complex [86,87]. Both Top3 and Rmi1 are required for DSB end resection *in vivo*, independently from Top3 topoisomerase function. Indeed, the heterodimer formed by Rmi1 and Top3 strongly

stimulates the helicase activity of Sgs1, thus suggesting a structural function of the complex rather than a catalytic function [28,74,93]. Similarly, BLM interacts with TOP3α and RMI1/RMI2 in mammals and the resulting complex promotes the helicase activity of BLM [73,94].

**Regulators of DSB end resection**

The first level of resection regulation, which restricts the resection process to only S and G2 phases of the cell cycle, avoiding it to occur during G1 phase, relies on the activity of cyclin-CDK (cyclin-dependent kinase) complexes [25]. Indeed, CDKs are proteins whose catalytic activity and substrate specificity depends on their binding to cyclins, which are differently expressed during the different phases of the cell cycle [23]. In yeast, a single cyclin-dependent kinase, Cdk1, is responsible for both G1/S and G2/M transitions through the association to different cyclins [23,95]. Conversely, in human cells four different CDKs are present [23]. In yeast, Cdk1-dependent phosphorylation of Sae2 and Dna2 regulates short and long range resection processes, respectively [33,61,75,96–98]. In particular, the main Cdk1-dependent phosphorylation site of Sae2 is serine 267, which is located in the C-terminal portion of the protein. Similarly, in mammals, CDK phosphorylates CtIP protein in its C-terminal domain, on threonine 847. These phosphorylation events promote resection initiation during S/G2 phases of the cell cycle [23,56,61,99]. During the same cell cycle phases, resection extension is stimulated by the phosphorylation of threonine 4, serine 17 and serine 237 of Dna2 by Cdk1, in yeast. This phosphorylation events enhance Dna2 recruitment to the DSBs and its nuclease activity [23,97]. Conversely, human DNA2 does not have any consensus site for CDK-dependent phosphorylation, while the phosphorylation of mammalian EXO1 seems to have a regulatory role on resection extension [23]. However consensus sites for cyclin-CDK complexes are also present on Mre11/MRE11, Xrs2/NBS1, Exo1, RPA and Ku [23,81].

Another level of resection regulation, both in yeast and in mammals, relies on the heterodimeric complex Ku/KU [33,41]. Ku is rapidly recruited to the DSBs during G1 phase and it avoids the generation of ssDNA, favouring NHEJ rather than HR during this phase, by inhibiting the recruitment and the activity of factors involved in resection [41,100]. In particular, it hides the DSB ends from the degradation by Exo1 [101]. Conversely, during S/G2 phase, Cdk1-dependent phosphorylation of Sae2 promotes MRX function in the displacement of Ku from the DSB ends. In fact, Ku and MRX complexes bind simultaneously and independently to the site of damage and seem to compete for the binding to the DSB ends [33,41,78,100,102,103]. Moreover, MRX-Sae2 endonucleolytic cleavage limits Ku association to the DSBs by generating ssDNA tracts that are less suitable for Ku engagement, since it prefers dsDNA ends as binding substrates [101,104]. Furthermore, MRX could also indirectly limit Ku association to DSB ends by promoting Exo1 resection activity [79]. The negative regulation of DSB end resection by the Ku complex is conserved in human cells, where KU inhibits the EXO1-mediated processing of DNA ends [105].

Another negative regulator of DSB end resection is the checkpoint adaptor protein Rad9 in yeast, and its orthologue 53BP1 in mammals [33,41,106–109]. Rad9 is recruited to the DSB ends through different pathways, involving both chromatin modifications and protein-protein interactions. In particular, the Tudor domain of Rad9 interacts with the methylated lysine 79 (H3-K79me) of histone H3, as well as 53BP1 interacts with methylated lysine 79 of histone H3 and methylated lysine 20 of histone H4 [106,110–113]. Furthermore, Rad9 tandem-BRCT domain interacts with the histone H2A after it has been phosphorylated on serine 129 (γH2A) by Mec1 and Tel1 checkpoint kinases [114–118]. In the same way, 53BP1 is recruited to the lesion after the phosphorylation, and the subsequent ubiquitination by RNF8 and RNF168 U3-ubiquitin ligases, of the H2A and H2AX histones [113]. Moreover, Cdk1-dependent phosphorylation of Rad9 allows its interaction with Dpb11 protein, which mediates a chromatin-independent binding of Rad9 to the damage site [119,120]. Conversely, the chromatin remodeler Fun30, as well as its human orthologue SMARCAD1, counteracts Rad9 association to the DSB ends, by

promoting resection extension by Exo1 and Dna2-Sgs1 [121–123]. Another protein complex able to promote resection by limiting Rad9 binding to the DSBs is the Slx4-Rtt107 complex, which competes with Rad9 for the interaction with Dpb11 and γH2A [124,125]. Once recruited to the DSBs, Rad9 acts as a barrier towards the nucleases involved in resection. In particular, Rad9 mainly inhibits the processing activity of Sgs1-Dna2, by limiting Sgs1 association to the DSB ends [106–108,113]. In human cells, during G1 phase, 53BP1 inhibits BRCA1-CtIP mediated resection by recruiting RIF1 at the DSB sites, thus favouring NHEJ repair [109,126,127]. However, during S/G2 phase, Cdk1-dependent phosphorylation events lead to the activation of BRCA1-CtIP that displace 53BP1-RIF1 from DSB ends, thus allowing resection and subsequent repair by HR [109].

The resection process is also both positively and negatively controlled by DNA damage checkpoint [33] *(Figure 6)*. Indeed, the checkpoint kinase Tel1, which is recruited and loaded at the DSBs by the MRX complex, supports MRX persistence at the damage site in a positive feedback loop, thus promoting DSB end resection. The promoting activity of Tel1 does not depend on its kinase activity, but Tel1 rather seems to exert a structural role in stabilizing MRX retention at the DSBs [106,128]. Conversely, the checkpoint kinase Mec1 negatively regulates DSB end resection in, at least, two different ways. On one hand, Mec1 induces the phosphorylation of Exo1 by the effector checkpoint kinase Rad53, which inhibits Exo1 processing activity [129,130]. On the other hand, Mec1 phosphorylates the serine 129 of H2A histone, thus promoting the binding of the resection inhibitor Rad9 to the DSB ends [123,131,132]. Interestingly, Mec1 also exerts a positive control on DSB end resection. In fact, it phosphorylates Sae2 protein and activates its functions in the processing of DSBs [59,133]. Moreover, Mec1 phosphorylates Slx4 leading to the formation of the Dpb11-Slx4-Rtt107 complex, which limits Rad9 accumulation at the DSB ends, thus favouring resection [124,125,134]. The same mechanism was also observed in mammalian cells [135]. Furthermore, ATM and ATR, the human orthologues of Tel1 and Mec1 kinases, regulate resection by phosphorylating CtIP, EXO1 and DNA2 [136]. Moreover, in both yeast and mammals, the 9-1-1 complex

exerts both a negative regulation of resection by promoting Rad9/53BP1 association at the DSBs, and a positive regulation by stimulating the nuclease activity of Dna2/DNA2 and Exo1/EXO1 [137,138].

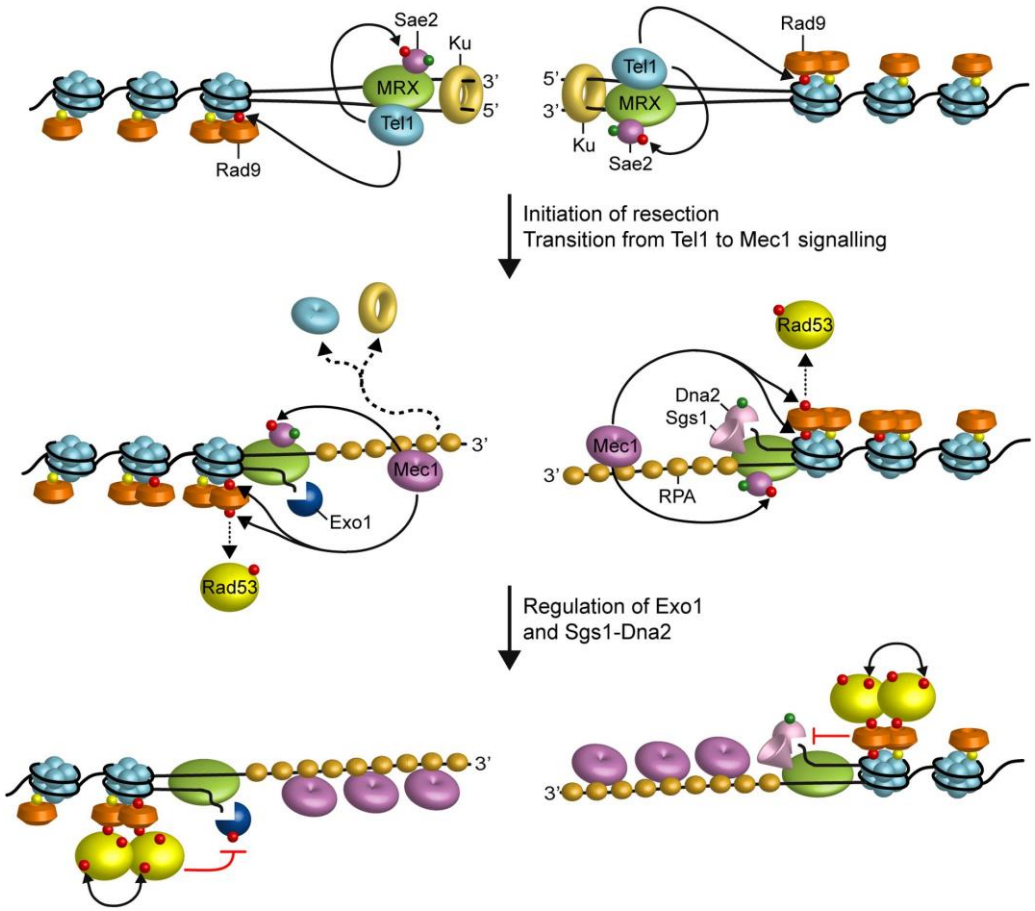


***Figure 6 – Interplay between DSB end resection and DNA damage checkpoint in yeast***

MRX, Sae2, and Ku rapidly localize to the DSB ends when the damage occurs. MRX recruits, loads and activates Tel1, which promotes resection by stabilizing MRX association to the DNA ends. Tel1 also phosphorylates H2A histone, thus contributing to the recruitment of Rad9 to the DSB. MRX-Sae2 then initiate resection, followed by Exo1 and Dna2-Sgs1. This generates ssDNA tracts that promote a switch from Tel1 to Mec1 signalling. Mec1 phosphorylates H2A histone, increasing Rad9 accumulation at the DSB ends, which inhibits the processing activity of Dna2-Sgs1. Furthermore, Mec1 phosphorylates Rad9, allowing Rad53 in-trans autophosphorylation that leads to the full activation of the effector kinase. Activated Rad53 phosphorylates Exo1, thus inhibiting DSB end resection. Red dots indicate phosphorylation events by Mec1 and Tel1, green dots indicate phosphorylation events by Cdk1, while yellow dots indicate methylation of histone H3.

*Adapted from [33]*

### 2) Strand invasion and DNA synthesis

The ssDNA generated during resection has to be covered by proteins in order to stabilise it and to allow the subsequent strand invasion of the intact donor DNA *(Figure 7)*. The heterotrimeric complex RPA (Replication Protein A), which is constituted by Rfa1, Rfa2 and Rfa3 proteins in yeast and by RPA70, RPA32 and RPA14 proteins in mammals, coats the ssDNA protecting it from the nucleolytic degradation [24,25].

However, RPA-ssDNA is not able to invade the homologous strand. Thus, RPA is replaced by the Rad51/RAD51 recombinase, whose structure is highly conserved among the eukaryotes and resembles the one of the RecA bacterial recombinase [24]. Rad51 assembles onto ssDNA forming a right-handed nucleofilament which comprises about 18 nucleotides and 6 Rad51 monomers per helical turn. The Rad51-ssDNA nucleofilament, also referred as pre-synaptic filament, can span thousands of bases and it is essential for strand invasion [24].

Since Rad51 itself is not able to displace RPA from ssDNA, a series of proteins, known as recombination mediators, support the replacement of RPA with Rad51 in both yeast and mammals [24,139]. The main recombination mediator in yeast is Rad52, a multimeric ring-shaped protein, whose C-terminal domain can interact with ssDNA and Rad51, while its central portion can bind RPA [24,139]. Thus, Rad52 brings Rad51 close to RPA-ssDNA and, working in multimers, it delivers a high number of molecules of Rad51 near the ssDNA, statistically favouring the exchange between RPA and Rad51 [24,139]. Rad55 and Rad57 proteins, paralogues of Rad51, are other recombination mediators in yeast. They form a highly stable heterodimer, which binds ssDNA and exchanges RPA with Rad51 by a mechanism analogous to that of Rad52 protein [139]. Rad55-Rad57 heterodimer can also form co-filaments with Rad51 and this makes the nucleofilament more resistant to the action of negative regulators, like the Srs2 helicase [139]. In addition, the Shu complex, which is constituted by Shu1, Psy3, Shu2 and Csm2 subunits, has been recognized as a recombination mediator, even if the mechanism by which it promotes Rad51 filament formation is still unknown [139]. In human cells, RAD52

protein, the structural orthologue of yeast Rad52, does not seem to exert a particularly important role as a recombination mediator [24]. In fact, the most important mediator in mammals is the tumour suppressor BRCA2, which shows functional homology with the yeast protein Rad52 [24,140]. BRCA2 binds the DNA through 3 OB fold domains, while it associates with RPA through its N-terminal portion. Both the BRC domain and the C-terminal CTRB domain of BRCA2 mediate its interaction with RAD51 [24]. In particular, the BRC domain recruits the first RAD51 molecules on ssDNA, while the CTRB domain allows the nucleofilament extension [24]. Furthermore, DSS1 and PALB2 proteins regulate BRCA2 function as a recombination mediator. In particular, DSS1 binds BRCA2 on its DNA-binding domain, probably favouring its interaction with ssDNA. Instead, PALB2 maintains BRCA2 stability in chromatin and nuclear matrix by binding its N-terminal portion [24,139]. Apart from BRCA2, other recombination mediators in mammals are the RAD51 paralogues RAD51B, RAD51C, RAD51D, XRCC2 and XRCC3, which allow the stabilization of the nucleofilament [24,139].

Once the pre-synaptic Rad51 nucleofilament has been assembled, it is able to invade an intact dsDNA molecule, in order to find homology regions with the strand that has to be repaired. From studies conducted in *E. coli*, it is probable that the homology search process occurs by random collisions between the pre-synaptic nucleofilament and the intact duplex DNA molecule [24]. Thus, the intact donor regions are tested, in a reiterative way, until homology is found and a stable connection between the nucleofilament and the donor is established [24,141]. The generated three-stranded intermediate is referred as synaptic complex and it assumes a peculiar secondary structure, known as D-loop [24,141]. In yeast, the homology search process, as well as the stabilization of the D-loop, are positively regulated by the Rad54 protein [24,75,141]. Rad54 is a member of the Swi2/Snf2 protein family and it has both ATPase, translocase and chromatin remodelling activities. In particular, Rad54 physically interacts with Rad51 and it promotes the strand separation within the intact donor DNA, by generating supercoilings through ATP hydrolysis. Thus, it facilitates the pairing between the nucleofilament and the donor DNA [24,141]. Moreover, it stabilizes the D-loop structure

through chromatin remodelling [24]. Finally, after strand invasion, Rad54 removes some Rad51 molecules from the 3'-OH end of the nucleofilament, in order to guarantee the access of the DNA polymerases responsible for the reparative synthesis [24,75,141]. Like in yeast, the human orthologues of Rad54 protein, RAD54 and RAD54B, interact with RAD51 and promote the homology search process, D-loop formation and its stabilization [24,141].

After strand invasion, the invading strand primes DNA synthesis, by using the intact DNA molecule as a template. In both yeast and mammals, the reparative synthesis is carried out by the proteins involved in DNA replication such as PCNA and RFC complexes, Dpb11/TOPBP1 protein and δ, η and ζ polymerases [22,75,142].

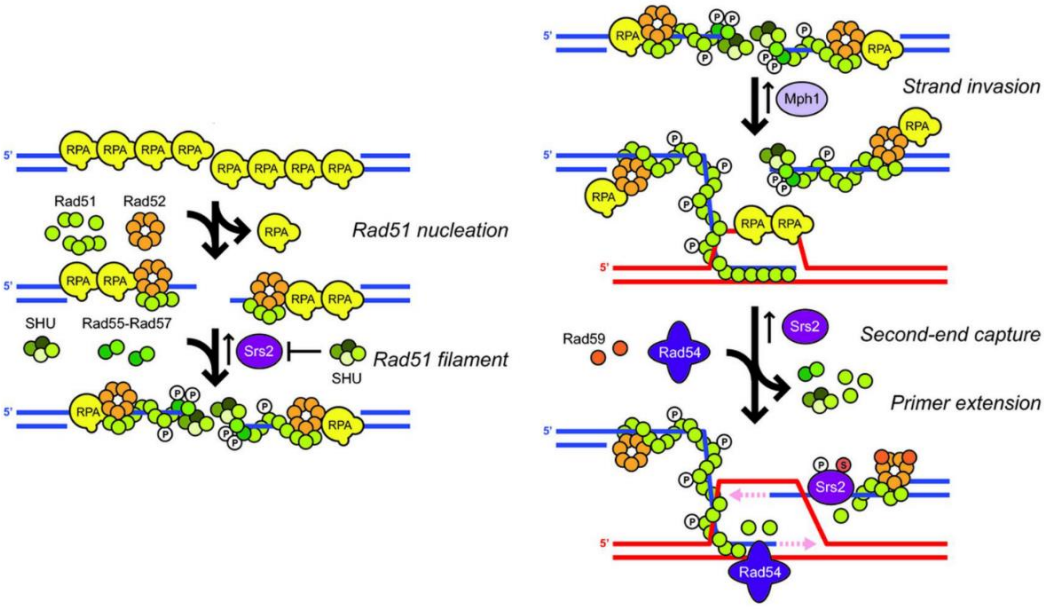


***Figure 7 – Nucleofilament formation, strand invasion and reparative DNA synthesis in yeast***

RPA complex rapidly coats the ssDNA generated by the resection process. RPA is then substituted by Rad51 recombinase, with the help of the recombination mediators Rad52, Rad55, Rad57 and Shu. The mediators load Rad51 onto ssDNA and stabilize the generated nucleofilament. After assembly, the nucleofilament invades a homologous intact DNA molecule and it is assisted by Rad54 protein in the homology search process. Strand invasion causes the formation of a D-loop structure. Then replicative enzymes, including δ polymerase, PCNA and RFC, perform reparative DNA synthesis. Both Srs2, whose action is inhibited by the Shu complex, and Mph1 negatively regulate HR repair by destabilizing the D-loop structure.

*Adapted from [22]*

### 3) Repair process completion and Holliday junctions resolution

Homologous recombination repair can be concluded at least in 3 different ways *(Figure 8)* [22,139,143].

The first model proposed is the Double Strand Break Repair (DSBR) model *(Figure 8B)*, in which the second 3'-OH strand of the damaged molecule anneals with the D-loop, in a step called "second end capture". This primes a new round of DNA synthesis that results in the formation of 2 four-way intermediates, known as Holliday junctions (HJs) [22,24,139]. HJs are then resolved by specialized nucleases, called resolvases, which perform an endonucleolytic cleavage to produce both Cross-Over (CO) and Non-Cross-Over (NCO) products [22,26,139]. Yeast resolvases include the Mus81-Mms4 complex and the Yen1 protein, while in mammals the same function is carried out by their orthologues MUS81-EME1 complex and GEN1 protein [26,144,145]. Otherwise HJs are dissolved by helicase-topoisomerase complexes, which exclusively generate NCO products [93,139,146]. In particular, the STR complex, which is constituted by Sgs1 Top3 and Rmi1 in yeast and their orthologues BLM, TOP3α and RMI1/2 in human cells, is able to dissolve HJs without causing any rearrangement [93,146].

The Synthesis Dependent Strand Annealing (SDSA) model *(Figure 8C)*, is the second possible mechanism of HR repair. In this model, the invading strand is displaced from the D-loop after limited DNA synthesis and before the second end capture. If sufficient DNA synthesis has occurred, in order to overcome the lesion, the displaced strand can re-anneal to the other strand of the damaged molecule and the repair can be concluded by fill-in synthesis and ligation [22,143,147]. Therefore, only NCO products are generated, thus SDSA is the preferred HR repair mechanism during mitosis. Conversely, DSBR is essential during meiosis, since it guarantees genetic variability and keeps the homologous chromosomes linked through the Holliday junctions [22,139,147]. The propensity for SDSA repair during mitosis is achieved through the destabilization of the D-loop structure by the Srs2 helicase in yeast and by the helicases RECQ5, FANCJ and BLM in mammals [139,148].


***Figure 8 – Models of homologous recombination repair***

**(A)** DSB end resection generates 3'-protruding ssDNA ends, which are coated by Rad51 to form a nucleofilament that can invade a homologous intact DNA molecule, thus forming a D-loop structure. After DNA synthesis, starting from the 3'-OH end of the invading strand, HR repair can be concluded in 3 different ways. **(B)** DSBR mechanism is characterized by second end capture followed by the generation of double Holliday junctions. HJs can be resolved by nucleases, leading to the formation of both CO and NCO products, or dissolved by the Sgs1-Top3-Rmi1 complex, producing only NCO products. **(C)** In SDSA mechanism the invading strand is displaced from the D-loop and re-anneals with the other strand of the damaged DNA molecule. DNA synthesis and ligation complete the process, leading to the generation of only NCO products. **(D)** In BIR mechanism the D-loop is converted into a replication fork and synthetises DNA until the end of the template chromosome.

*Adapted from [139]*

The last model of homologous recombination is the Break Induced Replication (BIR) *(Figure 8D)*, which occurs when there is only one end of the damaged DNA, due to the loss of the second end. During this repair mechanism the D-loop assembles into a replicative fork and copies the entire intact chromosome arm in a single-ended invasion process [22,24,139].

## The DNA Damage Checkpoint

The DNA damage checkpoint is a signal transduction cascade that allows cells to arrest the cell cycle during G1/S transition, S phase or G2/M transition, until the lesion has been completely repaired. This surveillance mechanism, which involves a lot of factors and has to be tightly regulated, guarantees sufficient time to properly repair the damage and to activate specific transcriptional programs. Moreover, if the lesions are too severe to be properly repaired, DNA damage checkpoint can induce senescence or apoptosis [144,149]. The DNA damage checkpoint is highly conserved from yeast to humans and alterations in checkpoint factors and mechanisms can lead to genomic instability. Indeed, checkpoint factors encoding genes are often mutated in cancer cells. Moreover, tumoral transformation is more rapid if DNA damage checkpoint does not act correctly [150]. Physical and genetic interactions between the factors involved in repair and checkpoint allow a fine coordination between these two mechanisms, in order to arrest the cell cycle in the presence of any DNA lesion and to keep the checkpoint active until the damage has been completely repaired [151]. The DNA damage checkpoint response involves four major groups of proteins that allow to transduce the signal and to arrest the cell cycle. In particular, sensor proteins recognize the damage and activate the transduction cascade, adaptor/mediator proteins allow sensors to activate the effectors, effector proteins amplify the signal by activating a series of molecular targets, target proteins induce the arrest of the cell cycle [27,149].

## DNA damage checkpoint activation

The DNA damage checkpoint sensors, which recognize the damage and activate the signalling cascade, are the highly conserved kinases Tel1 and Mec1 in *S. cerevisiae* and their orthologues ATM (Ataxia-Telangectasia Mutated) and ATR (Ataxia-Telangectasia mutated and Rad53-related) in human cells [150] (Figure 9). Tel1/ATM and Mec1/ATR are members of the phosphatidylinositol 3-kinase-related kinase (PIKK) family, which phosphorylates serine and threonine residues within Ser/Thr-Gln consensus sequences. PIKK family includes proteins that share common structural features and domain organization. In particular, PIKK kinases are characterized by the presence of repeated HEAT domains in the N-terminal region, which allow protein-protein and protein-DNA interactions. In the C-terminal portion is located a relatively small kinase domain, flanked by FAT (FRAP-ATM-TRRAP) and FATC (FAT-C-terminal) domains, which regulate its enzymatic activity [41,152–154]. Tel1/ATM and Mec1/ATR are activated by different kinds of DNA damage, indeed Tel1/ATM recognizes unprocessed DSBs, while Mec1/ATR is activated by ssDNA intermediates, which can be generated from a broad spectrum of DNA lesions [144,155].

Tel1/ATM is recruited to the lesion through a physical interaction with the C-terminal domain of the Xrs2/NBS1 subunit of the MRX/MRN complex [150,155–157]. Moreover, MRX/MRN is required for complete Tel1/ATM activation, even if the molecular mechanism of this activation is still not completely clear. In particular, the DNA ends tethering activity of the MRN complex seems to be important for the transition from ATM inactive dimers to active monomers [157,158]. Furthermore, Xrs2/NBS1 could act as a cofactor for Tel1/ATM activation [158], while the ATPase activity of Rad50/RAD50 may induce a conformational change of MRX/MRN complex, thus promoting Tel1/ATM activation [150,159]. Conversely, in both yeast and mammals, evidence demonstrates that Tel1/ATM activation is independent from MRX/MRN nuclease activity [156,159,160]. Full activation of human ATM kinase depends on phosphorylation events [41,155]. Indeed, upon DNA damage, ATM autophosphorylation on serine 1981 determines ATM

transition from inactive homodimers to active monomers [155,159]. An analogous mechanism could also account for Tel1 activation in yeast. ATM autophosphorylation requires a previous acetylation of the FATC domain of ATM by TIP60 [161]. Moreover, serine 367, serine 1893 and serine 2996 are other ATM autophosphorylation sites, which play a role in the ATM activation process. In summary, upon DSB occurrence, the MRX/MRN complex binds to the damaged DNA ends. Here, it is able to recruit and activate Tel1/ATM both directly, by Xrs2/NBS1 interaction with Tel1/ATM, and indirectly, by tethering together the DSB ends. Once activated, Tel1/ATM phosphorylates different substrates in order to propagate the checkpoint signal and to arrest the cell cycle *(*Figure 9*)*.

ATM-dependent checkpoint has a preponderant role in humans, while the checkpoint activated by Tel1 has only a minor role respect to the Mec1-dependent one, in yeast [149]. This is probably due to the yeast high resection efficiency, which allows a rapid conversion of the DSB ends into ssDNA intermediates that are the preferred substrates for Mec1 kinase [41]. Moreover, differences in the kinase activity and in the interaction capability of Tel1 and ATM could also explain the different importance of the checkpoint activated by these kinases in yeast and humans [41].

Mec1/ATR kinase recognizes ssDNA intermediates, thus it preferentially acts during S/G2 phase of the cell cycle in response to replicative stress, but also to nucleolytically processed DSBs [41]. Both in yeast and in mammals, Mec1/ATR recruitment to the damage site requires the presence of ssDNA coated by RPA. ssDNA-RPA intermediates are usually generated by the resection process or by helicase-polymerase uncoupling during replicative fork arrest [155,162]. Recognition of RPA-coated ssDNA by Mec1/ATR requires the Ddc2/ATRIP protein. Indeed, a highly conserved N-terminal domain of Ddc2/ATRIP can directly interact with RPA and recruit Mec1/ATR to the lesion [162–165]. Although the interaction among Mec1, Ddc2 and RPA, as well as the interaction among ATR, ATRIP and RPA, is required for Mec1/ATR localization to the lesion, it is not sufficient for full Mec1/ATR activation [149,166]. Indeed, Mec1/ATR activation, in both yeast and mammals, requires the presence of the 9-1-1 complex, constituted by Ddc1,

Rad17 and Mec3 in *S. cerevisiae* and by RAD9, RAD1 and HUS1 in human cells [149,167]. 9-1-1 is a ring-shaped heterotrimeric complex, which is loaded onto the DNA, at the junctions between ssDNA and dsDNA, by the clamp-loader RFC-like complex, which is composed by Rad24, Rfc2 and Rfc5 in yeast and by RAD17, RFC2 and RFC5 in mammals [149]. In *S. cerevisiae*, the Ddc1 subunit of the 9-1-1 complex physically interacts with Mec1, thus promoting its kinase activity [149,167,168]. Conversely, there is no evidence of interactions between the 9-1-1 complex and ATR kinase in humans. However, it has been demonstrated an interaction between the phosphorylated RAD9 subunit of the human 9-1-1 complex and the TOPBP1 protein, which is recruited to the lesion by the MRN complex [155,169]. Thus, once recruited to the ssDNA by MRN, the interaction with 9-1-1 leads to a conformational change of TOPBP1 that exposes its ATR activating domain, which can directly activate ATR kinase activity [155,169,170]. The yeast orthologue of TOPBP1, Dpb11 protein, is also involved in the full activation of Mec1 checkpoint kinase [41,149]. Indeed, the Ddc1 subunit of the 9-1-1 complex recruits Dpb11 to the lesion site and the interaction between Dpb11 and Mec1 stimulates Mec1 enzymatic activity [120,149,171]. Phosphorylation of Ddc1 by Mec1 is essential to recruit Dpb11, indicating that a partial Mec1 activation occurs even in the absence of Dpb11 [172]. In summary, in yeast, RPA-coated ssDNA recruits Mec1-Ddc2 by a physical interaction between Ddc2 and RPA. 9-1-1 is recruited at the interface between ssDNA and dsDNA, and partially activates Mec1, which phosphorylates its Ddc1 subunit. Phosphorylated Ddc1 recruits Dpb11 protein, which, in turn, allows full Mec1 activation [41,120,149]. On the contrary, in mammals, after ATR recruitment to RPA-coated ssDNA by ATR-ATRIP-RPA interaction, the RAD9 subunit of the 9-1-1 complex recruits TOPBP1, which directly activates ATR kinase activity [41,155,169] *(*Figure 9*)*.

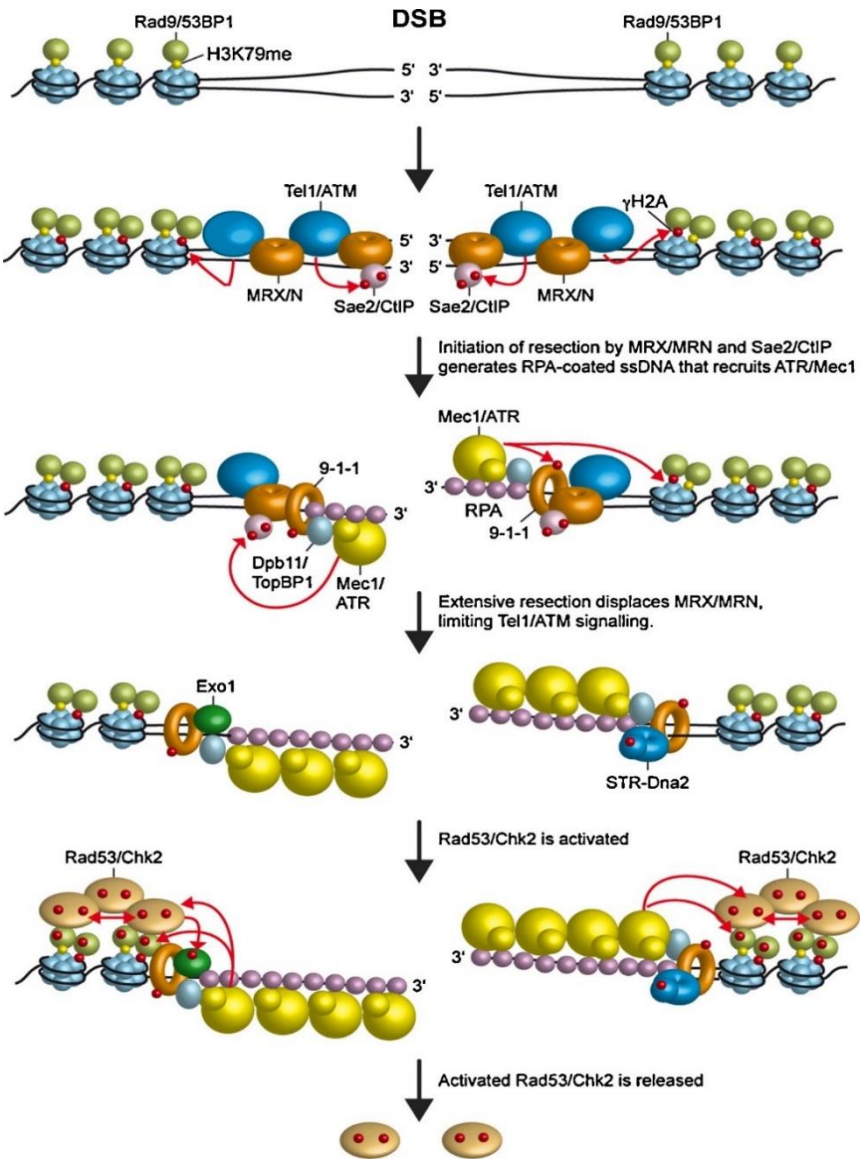


***Figure 9 – Tel1/ATM and Mec1/ATR checkpoint kinases activation after DSB occurrence***

MRX/MRN recognizes the DSBs and recruits Tel1/ATM, which phosphorylates Sae2/CtIP and H2A histone (γH2A). MRX/MRN, Sae2/CtIP and the other nucleases involved in resection nucleolytically process the DSB ends, thus generating 3'-protruding ssDNA tails that are rapidly coated by RPA. RPA-coated ssDNA recruits Ddc2-Mec1 and ATRIP-ATR complexes. Full Mec1/ATR activation requires the presence of Dpb11/TOPBP1 and of 9-1-1 complex. Activated Mec1/ATR phosphorylates Rad9/53BP1 adaptor and Rad53/CHK2 effector kinase, thus activating the checkpoint transduction cascade. Mec1/ATR also regulates ssDNA generation by phosphorylating Sae2/CtIP and H2A histone and promoting Rad53-dependent inhibition of Exo1 nuclease activity.

*Adapted from [41]*

How Tel1/ATM and Mec1/ATR checkpoint activities are coordinated is a challenging question. However, it is evident that the activation of either Tel1/ATM or Mec1/ATR depends on the different length of ssDNA, with Tel1/ATM acting on blunt or minimally processed ends, and Mec1/ATR acting in the presence of long ssDNA tracts [41,173,174]. In this context, DSB end resection has two different consequences: it generates ssDNA that activates Mec1/ATR and it displaces MRX/MRN from the DSB ends, thus attenuating Tel1/ATM signalling. In both yeast and mammals, Tel1/ATM stimulates ssDNA accumulation at the damage site, thus promoting the transition from Tel1/ATM-dependent checkpoint to Mec1/ATR-dependent one [173,174]. Therefore, the actual working model assesses that, upon DSB generation, the MRX/MRN complex binds to the damaged DNA ends and recruits Tel1/ATM kinase, thus activating Tel1/ATM-dependent checkpoint. MRX/MRN initiates resection, which is also promoted by Tel1/ATM. The resection process causes ssDNA accumulation, which displaces MRX/MRN, thus attenuating Tel1/ATM-dependent checkpoint signalling, and which recruits Mec1/ATR, thus promoting Mec1/ATR-dependent checkpoint activation [41,174] *(*Figure 9*)*.

## DNA damage checkpoint signal transduction: the mediators

The DNA damage checkpoint mediators are a class of proteins that have the role to propagate the checkpoint signal from Tel1/ATM and Mec1/ATR upstream kinases to the downstream effector kinases [150].

In yeast, the activation of Rad53 and Chk1 effector kinases requires the checkpoint adaptor Rad9. As previously reported (section *"Regulators of DSB end resection"*), Rad9 can be recruited to the DSB ends through multiple pathways, involving both chromatin modifications and protein-protein interactions. In particular, upon DNA damage, Mec1- and Tel1-dependent H2A histone phosphorylation on serine 129 is recognized by the two tandem BRCT domains of Rad9. Moreover, lysine 79 of H3 histone, which is

constitutively methylated by Dot1 methyl transferase, is bound by Rad9 Tudor domain [114–118,149]. However, Rad9 can also be recruited to the DSBs through a histone-independent pathway, relying on Rad9-Dpb11 interaction. Indeed, Dpb11 physically interacts with Rad9 BRCT domain, after Rad9 has been phosphorylated by either Cdk1 kinase or other kinases different from Mec1, Tel1 and Cdk1 [119,120,175]. Once recruited to the damage site, Rad9 S/T-Q cluster domain is phosphorylated by Mec1 and Tel1 and these phosphorylation events cause the association between the BRCT domains of two Rad9 molecules, thus generating active Rad9 dimers [119,176]. Phosphorylated Rad9 physically interacts with the ForkHead-Associated (FHA) domains of Rad53 effector kinase, thus allowing the recruitment of lots of Rad53 molecules to the lesion. The proximity among Rad53, Mec1 and Tel1 molecules, favours Mec1- and Tel1-dependent Rad53 phosphorylation, which partially activates the effector kinase. Moreover, it allows the subsequent *in-trans* autophosphorylation of Rad53, which fully activates its kinase activity [177,178]. Rad9 also contributes to Chk1 effector kinase activation, with a mechanism involving Rad9 N-terminal portion, which could interact with Chk1, thus promoting a conformational change that may allow Chk1 activation by Mec1 [149,150].

As described before (section *"Regulators of DSB end resection"*), Rad9 human orthologue, 53BP1, is recruited to the lesion by a physical interaction between its Tudor domain and methylated lysine 79 of H3 histone and lysine 20 of H4 histone [106,110–113]. The association between 53BP1 and the methylated residues requires a previous ubiquitination of the H2A and H2AX histones by RNF8 and RNF168 ubiquitin ligases [113,149]. Furthermore, 53BP1 localization to the damage site is promoted by its physical interaction with phosphorylated H2AX histone [179]. Moreover, 53BP1 recruitment could also be promoted by its interaction with TOPBP1, in a Cdk1-dependent way [149]. Although 53BP1 is more implicated in DNA repair than in checkpoint signalling, it seems to interact with CHK1 effector kinase and to promote its activation by ATM and ATR [179]. However, the most important checkpoint mediator in human cells is MDC1, which shares some structural homologies with 53BP1, such as the presence of FHA domains, involved in protein-protein interactions, and of tandem BRCT domains, involved in the

recognition of phosphorylated residues [180,181]. MDC1 is recruited to the lesion by phosphorylated H2A histone, in particular its BRCT domains are able to associate with the γH2AX phosphorylated histone variant [180]. Once recruited to the damage site, ATM-dependent phosphorylation of MDC1 allows its oligomerization and accumulation, thus favouring its mediator role [182,183]. Indeed, MDC1 role as a checkpoint adaptor seems to be mainly dependent on its ability to keep different checkpoint proteins in close proximity. In particular, MDC1 physically interacts with NBS1 subunit of the MRN complex, and this may promote ATM recruitment to the damage site [182,184,185]. Moreover, the N-terminal FHA domain of MDC1 is able to directly associate with ATM kinase [180,182]. Furthermore, MDC1 indirectly supports the recruitment of 53BP1 and BRCA1 mediator proteins, by interacting with RNF8, which in turn promotes H2A-H2AX ubiquitination, thus altering chromatin structure around the lesion [180,183,185,186]. Therefore, MDC1 seems to mainly support checkpoint activation by bringing the ATM apical kinase and the CHK1 effector kinase close to each other.

The last checkpoint adaptor is Mrc1 protein in yeast and its orthologue Claspin in humans [149,155,187]. Mrc1/Claspin participates only to S-phase checkpoint and allows full Rad53/CHK1 activation in response to replication stress [155,187]. The S-phase checkpoint, which is mainly activated in the presence of UV-induced damage or stalled replication forks, induces cell cycle arrest, increases dNTPs synthesis, inhibits the firing of late replication origins and supports replisome stabilization. Mrc1 is a replicative protein, which is associated with the replisome even in the absence of DNA damage. After Mec1-dependent phosphorylation, Mrc1 interacts with Rad53 [188]. This association allows Mec1 and Rad53 molecules to be in close proximity, thus promoting Mec1-dependent full activation of Rad53 effector kinase [187,189]. In mammals, Claspin protein is recruited to stalled replication forks by Timeless and Tipin proteins. ATR-dependent phosphorylation allows the interaction between Claspin and the CHK1 effector kinase, thus increasing the local concentration of CHK1 and facilitating its phosphorylation by ATR [149,155].

## DNA damage checkpoint signal transduction: the effectors

The DNA damage checkpoint effector kinases, once phosphorylated and activated by the upstream checkpoint kinases, allow checkpoint signal amplification by phosphorylating a series of different targets, thus inducing different cellular responses. Both in yeast and in human cells two effector kinases are present: Rad53 and Chk1 in *S. cerevisiae* and their orthologues CHK1 and CHK2 in mammals [149]. Rad53 and Chk1 are activated by both Mec1 and Tel1 protein kinases. Conversely, in mammals, ATR and ATM activate CHK1 and CHK2, respectively [149]. Moreover, Rad53 acts in all the phases of the cell cycle, while Chk1 is only required for the G2/M checkpoint signalling. On the contrary, both CHK1 and CHK2 can activate the checkpoint in all cell cycle phases, even if CHK2 has only a subsidiary role respect to CHK1 [149].

Rad53 is the main effector kinase in yeast. It is a member of the serine/threonine kinases family, which is characterized by the presence of an N-terminal SQ/TQ cluster domain that creates a consensus sequence for Tel1/ATM and Mec1/ATR, and of a central ForkHead-Associated (FHA) domain that is responsible for protein-protein interactions [190]. Interestingly, Rad53 is the only kinase of this family to possess a second FHA domain at the C-terminus [190]. As described in the previous section, Rad53 is recruited to the lesion by a physical interaction between its FHA domain and the phosphorylated Rad9 adaptor. This allows the partial activation of Rad53 kinase, by Mec1- and Tel1- dependent phosphorylation. Moreover, it increases the local concentration of Rad53 molecules, thus promoting the subsequent Rad53 *in-trans* autophosphorylation, which fully activates the kinase [149,177,178]. Indeed, Rad53 is phosphorylated on more than twenty residues, most of them being autophosphorylation sites [177]. Once hyperphosphorylated, Rad53 is fully active and it is released from Rad9 and from the DNA, through an ATP-dependent reaction [178].

Like Rad53, Chk1 recruitment to the damage site requires Rad9 adaptor, and its activation is dependent on phosphorylation events by Mec1 and Tel1. However, Chk1

participates only in G2/M checkpoint arrest, while it is not activated during the other phases of the cell cycle [149,150].

In mammals, CHK1 has a preponderant role as an effector kinase and it is specifically activated by the ATR kinase. CHK1 structure is characterized by an N-terminal kinase domain, a regulatory SQ/TQ domain and a C-terminal domain with a putative regulatory function [191]. CHK1 is activated by ATR-dependent phosphorylation of its serine 317 and serine 345 residues. This phosphorylation events promote a conformational change that allows the exposition of CHK1 kinase domain, which was previously masked by its C-terminal regulatory domain [149,191,192]. This activates CHK1 kinase activity and allows the release of the protein from the chromatin, so that it can reach and phosphorylate its targets [149]. As described in the previous section, CHK1 activation is promoted by 53BP1, MDC1 and Claspin mediators.

CHK2 kinase has only a secondary and auxiliary role in checkpoint activation in mammals and it is specifically activated in the presence of DSBs [155,193,194]. In particular, ATM phosphorylates CHK2 on its threonine 68 residue. This induces CHK2 homodimerization, which promotes *in trans* autophosphorylation among CHK2 molecules, thus determining the full activation of CHK2 [155,194].

## DNA damage checkpoint molecular targets

Once activated, the checkpoint effector kinases phosphorylate several downstream targets in order to induce different cellular responses. The most important cellular response is the cell cycle arrest, which is obtained through the phosphorylation of different substrates, depending on the cell cycle phase in which the damage has been detected [149].

The G1-phase checkpoint allows cell cycle arrest during G1/S transition. In budding yeast, the main molecular targets of the G1-phase checkpoint are Swi6 and Gcn4 proteins. In particular, Rad53 directly phosphorylates Swi6, an inhibitory subunit of the

SBF transcriptional factor, thus reducing the transcription of S-phase cyclins Cln1 and Cln2. Conversely, the transcriptional factor Gcn4 is activated by Rad53 in an indirect manner and, once activated, it delays Cln2 cyclin accumulation. Thus, the reduced levels of Cln1 and Cln2 avoid the degradation of the B-type cyclin inhibitor Sic1, which leads to cell cycle arrest during the G1/S transition [149].

In human cells, the main targets of the G1-phase checkpoint are CDC25A, p53 and MDM2 proteins. In particular, ATM-activated CHK2 phosphorylates CDC25A phosphatase, targeting it for proteasomal degradation. Therefore, the inhibitory phosphorylation present on CDK2 kinase cannot be removed by the CDC25A phosphatase. The persistence of this inhibitory phosphorylation prevents CDK2 from interacting with cyclin E and avoids cells to enter S phase[195]. Moreover, activated CHK2 phosphorylates both p53 and its negative regulator MDM2. MDM2 phosphorylation targets the protein to proteasomal degradation, while p53 phosphorylation stabilizes it and avoids its interaction with MDM2. p53 stabilization allows the transcription and therefore the up-regulation of the cell cycle inhibitor p21, which inhibits CDK2-cyclin E activity [149,194,195].

The S-phase checkpoint promotes replication forks stabilization, inhibits late replication origins firing and avoids mitosis occurrence before the DNA has been completely replicated [149]. In yeast, the main S-phase checkpoint targets are the RPA complex and the DNA polymerase α-primase. In particular, Rad53-dependent phosphorylation inhibits pol α-primase, thus arresting DNA synthesis downstream from the lesion and slowing down S phase progression [149]. Moreover, Rad53 phosphorylates the Dbf4 regulatory subunit of Cdc7 kinase, thus delaying the firing of late replication origins. Furthermore, Rad53-dependent phosphorylation of Sld3 protein avoids its interaction with the replication factors Dpb11 and Cdc45, which are both required for replication initiation, thus preventing late replication origins firing [149]. Another target of S-phase checkpoint is Exo1 nuclease, which is inhibited by Rad53 phosphorylation. This prevents resection progression and the subsequent collapse of stalled replication forks [149]. During S phase, Rad53 also phosphorylates Dun1 kinase, which inhibits the

repressor of the ribonucleotide reductase (RNR) genes transcription, Crt1. Moreover, Dun1 phosphorylates the RNR inhibitor Sml1, targeting it for degradation. Therefore, Dun1 allows an increment of dNTPs pool in the presence of DNA damage arising during S phase [149].

In mammals, the S-phase checkpoint mainly involves the ATR apical kinase, which phosphorylates CHK1 effector kinase, with the help of Claspin, Tipin and Timeless mediators [155]. The main targets of this checkpoint are CDC25A and CDC25C phosphatases and WEE1 kinase. CHK1-dependent phosphorylation of CDC25A targets it for proteasomal degradation, while CDC25C phosphorylation inactivates the phosphatase through an interaction with the 14-3-3 complex [195]. On the other hand, phosphorylation-mediated WEE1 activation allows the kinase to inhibit CDK1 [155]. Furthermore, CHK1 inhibits the interaction between CDC45 and MCM7 helicase, thus preventing new replication origins firing in the presence of DNA damage [149].

The G2-phase checkpoint, which arrests the cell cycle during G2/M transition, by inhibiting metaphase to anaphase mitosis progression, is the most important checkpoint in most eukaryotic organisms [149]. In yeast, the G2-phase checkpoint involves both Rad53 and Chk1 effector kinases and their main target is the Pds1 securin, which needs to be degraded by APC-Cdc20 complex to allow mitosis initiation. In particular, Chk1 phosphorylates Pds1, thus preventing its ubiquitination by APC-Cdc20, while Rad53 modulates Cdc20 activity. All this events inhibit Pds1 degradation, thus preventing mitosis entrance [150].

In mammals, the G2-phase checkpoint also involves both CHK1 and CHK2 effector kinases [196]. In particular, ATM-CHK2 promote immediate G2 arrest, while ATR-CHK1 support G2 accumulation [155]. The main G2-phase target of CHK2 kinase is CDC25C phosphatase. In particular, CHK2-dependent phosphorylation inhibits the positive action of CDC25C on CDK1. Targets of CHK1-dependent phosphorylation are the CDK kinases, which are inhibited by the phosphorylation events [155].

## DNA damage checkpoint recovery and adaptation

Once DNA damage repair is completed, the DNA damage checkpoint can be terminated and cell cycle progression can restart. This process is known as recovery [150].

The main factor involved in recovery in budding yeast is the Srs2 helicase, which probably removes Rad51 recombinase from ssDNA ends [150]. Moreover, Ptc2 and Ptc3 phosphatases are required for Rad53 dephosphorylation and its subsequent inactivation [150].

In human cells, the checkpoint recovery process involves the WIP1 phosphatase, PLK1 polokinase, the Claspin mediator, the WEE1 kinase and the SCF ubiquitin ligase complex [27,150]. WIP1, the human orthologue of yeast Ptc2 and Ptc3 phosphatases, dephosphorylates both CHK1 and p53, thus inactivating them [150]. PLK1 promotes WEE1 kinase degradation, thus allowing CDC2 activation and mitosis initiation [150]. SCF ubiquitin ligase targets both the WEE1 kinase and the Claspin mediator for proteasomal degradation [27]. Claspin degradation removes the main CHK1 co-activator, thus allowing CDC25A re-accumulation and CDC25B and CDC25C activation, which in turn activates mitosis-promoting cyclin-CDK complexes [27].

If the lesion is irreparable, after a specific period of time cells downregulate the checkpoint and re-enter the cell cycle, even in the presence of the DNA damage. This process is known as adaptation [149]. However, after some cellular divisions from adaptation occurrence, accumulation of mutations induces programmed cell death through apoptosis. Both yeast and human cells have developed adaptation mechanisms [27,150]. In particular, PLK1 has a primary role in the adaptation process in human cells. In fact, after about 72 hours from checkpoint activation, it inhibits both CHK1 and CHK2 checkpoint effector kinases [197]. In *S. cerevisiae*, adaptation activation occurs about 12-14 hours after DNA damage induction [198]. Adaptation process involves different repair factors, including Ku70, Ku80, Rad51, Sae2 and Srs2, as well as chromatin remodelers, like INO80, and some phosphatases that remove the phosphorylation from checkpoint factors [198]. In particular, PPH3 phosphatase complex

dephosphorylates both H2A histone and Rad53 kinase, while Ptc2 and Ptc3 phosphatases only dephosphorylate Rad53 [198]. In the same way, human CHK1 and CHK2 dephosphorylation during adaptation is promoted by the Ptc2-Ptc3 orthologues WIP1 and PPM1D and by the PPH3 orthologue PP2A [198].

## RNA binding proteins and genome integrity maintenance

In the last few years, emerging evidence supports the presence of a strong connection between RNA metabolism and genome integrity. Indeed, defects in transcription elongation, splicing, RNA export or RNA degradation could be linked to genomic instability [199]. For this reason, several RNA-binding proteins (RPBs) have been found to participate in genomic stability preservation [199,200].

In particular, some RBPs are able to prevent the accumulation of R-loops, which arise during collisions between the transcription and the replication machineries and that impair replication fork progression as well as genome stability [199–201]. R-loops are particular nucleic acid structures, which consist of an RNA-DNA hybrid and of a displaced ssDNA strand, identical to the RNA molecule [201]. Co-transcriptional R-loops are source of genomic instability, thus inducing hyper-mutation, hyper-recombination and chromosomal rearrangements. Moreover, R-loops can affect the expression of key factors involved in genome maintenance, by influencing transcription termination, DNA methylation and chromatin modifications [199,201]. RBPs could prevent R-loop formation by packaging the nascent mRNA into a ribonucleoprotein particle, thus reducing its ability to anneal with the opened DNA strands [202].

Other RBPs are able to modulate the expression of DDR genes at either transcriptional or post-transcriptional level [199,200]. In fact, in the presence of DNA damage, there is a global repression of gene expression, but the mRNAs encoding for DDR proteins have to escape this repression. Thus, RPBs are important to guarantee the expression of DDR genes, by acting on both pre-mRNAs and mRNAs [200]. In particular, RBPs can regulate

the splicing of pre-mRNAs, the co-transcriptional processing of pre-mRNAs 3' end (endonuclelytic cleavage and polyadenylation), the export of the mature transcripts from the nucleus to the cytoplasm, the stability of the mRNAs and their translation [199,200]. Furthermore, some RPBs directly participate to the repair processes, by localizing to the lesion and interacting with DNA or with repair proteins [200]. For example, in mammals, YB-1 interacts with mismatched DNA and regulates mismatch repair. DSB repair pathways are, instead, influenced by PSF, NonO/p54$^{nrb}$, RBMX, hnRNP C and hnRNP U-like. In particular, PSF interacts with both DNA, RAD51D and TOPBP1 and affects both HR and NHEJ. NonO/p54$^{nrb}$ stimulates NHEJ, but it represses HR. RBMX interacts with the DNA and protects the DSB ends from degradation, thus favouring NHEJ fidelity. hnRNP C and hnRNP U-like are components of BRCA1/BRCA2/PALB2 and MRN complexes, respectively, and they promote HR repair [200].

## The RNA binding protein Npl3

One of the most abundant RBPs in *Saccharomyces cerevisiae* is Npl3. It shares structural and functional homologies with two highly conserved RBP families: the heterogeneous Nuclear RibonucleoProteins (hNRP) and the Serine-Arginine-rich (SR) proteins [203]. In particular, Npl3 seems to be a putative orthologue of the human SR protein SRSF1, which is involved in genomic stability maintenance thanks to its capability to prevent R-loop accumulation. Moreover, Npl3 is the putative orthologue of the hnRNP proteins TET (TLS-EWS-TAF15), which are also involved in DDR, since EWS participates to the alternative splicing of *MDM2* and *CHK2* genes, while TLS1 is involved in the transcriptional repression of D1 cyclin, thus controlling the coordination between repair and cell cycle progression [200,204,205].

Npl3 structure is characterized by the presence of two central RRM (RNA Recognition Motif) domains, which allow the protein to recognize and to bind the RNA, and of a C-terminal SR/RGG domain, which supports Npl3 dimerization and protein-protein

interactions [206–210]. The RRM domains are specific for G/U-rich sequences, thus ensuring an enhanced binding of Npl3 to weak or cryptic sites of transcription termination [206].The SR/RGG domain is required for the interaction of Npl3 with more than 70 proteins involved in different steps of RNA metabolism. Post-translational modifications on this domain control Npl3 localization between the nucleus and the cytoplasm, as well as its association to the interactor proteins [207,210,211].

Npl3 takes part to all the steps of RNA metabolism, ranging from transcription to pre-mRNA splicing, mRNA export from the nucleus and translation into proteins [212]. Moreover, it is probably involved in chromatin remodelling, telomere ends preservation and in the maintenance of genomic stability [213–215]. In particular, Npl3 physically interacts with the RNA polymerase II and promotes transcription elongation, as well as proper transcription termination [207]. Indeed, Npl3 preferentially binds to the 3'-terminus of highly transcribed genes and competes with polyadenylation factors in order to prevent premature transcription termination on cryptic or weak termination sites [216,217]. While methylation on its C-terminal domain is essential for transcription promotion, once phosphorylated Npl3 no longer interacts with either RNA polymerase or RNA [207,218]. Npl3 also supports splicing by interacting with U1 and BBP splicing factors and recruiting them to the nascent transcripts that need to be processed [209]. Transcription-coupled splicing promoted by Npl3 is particularly critical for proper pre-rRNA processing [219]. Furthermore, Npl3 regulation of chromatin structure, through both genetic and physical interactions with factors that ubiquitinate or de-ubiquitinate H2B histone, seems to be responsible for the coordination between chromatin remodelling and splicing [213]. Moreover, chromatin remodelling is strictly related to the export of mature mRNAs from the nucleus to the cytoplasm, thus Npl3 could also coordinate these two processes [220]. Indeed, Npl3 is a fundamental carrier for the export of polyadenylated mRNAs from the nucleus to the cytoplasm [221]. In particular, in the nucleus Npl3 associates with the RNA and with the heterodimeric receptor Mex67-Mtr2, which is part of the nuclear pore complex, thus allowing mRNA export from the nucleus to the cytoplasm [210,221]. Once in the cytoplasm, Npl3 releases the

mRNA, dissociates from Mex67-Mtr2 and associates with Mtr10, which allows the re-import of Npl3 into the nucleus [210,221]. Export-import cycles are linked to post-translational modifications on the RGG domain of Npl3. In particular, dephosphorylated Npl3 interacts with the mature mRNA and with Mex67 receptor, while the cytoplasmic phosphorylation of Npl3 promotes its dissociation from the above factors and its association with Mtr10 [210]. After exporting mRNAs into the cytoplasm, Npl3 is also able to affect translation initiation. Two opposite roles of Npl3 have been reported by different groups for what concerns the regulation of translation initiation. In particular, Parker's group demonstrated that Npl3 interaction with the eIF4G subunit of eIF4F complex prevents the recruitment of the 43S multifactorial complex of translation pre-initiation, thus inhibiting translation initiation and protecting the mRNAs from decapping [208]. Conversely, Krebber's group proved that Npl3 promotes translation initiation by ensuring proper monosome formation [222].

Interestingly, a role for Npl3 protein in the maintenance of genomic integrity was recently reported by Aguilera's group. In fact, they demonstrated that Npl3 absence causes hypersensitivity to genotoxic agents, as well as a marked replication stress [203,215]. This is due to the capability of Npl3 to prevent the accumulation of R-loops arising during replication-coupled-transcription [203,215].

This evidence, as well as the roles of the human orthologues of Npl3 in the maintenance of genomic integrity, let us think that Npl3 could also have other functions in DNA damage response, as we will demonstrate in the first part of the results.

# *RESULTS*

**Nucleic Acids Research**

June 2017

Volume 45, Issue 11, Pages 6530–6545

doi: 10.1093/nar/gkx347

# The RNA binding protein Npl3 promotes resection of DNA double-strand breaks by regulating the levels of Exo1

Chiara Vittoria Colombo*, Camilla Trovesi*, Luca Menin, Maria Pia Longhese, and Michela Clerici

Dipartimento di Biotecnologie e Bioscienze, Università di Milano-Bicocca, 20126 Milano, Italy

* These authors contributed equally to this work as first authors

Eukaryotic cells deal with DNA damage through a multifaceted cellular response, known as DNA damage response (DDR), which promotes DNA repair and couples it with cell cycle progression [144]. DNA double-strand breaks (DSBs) are among the most severe lesions. DSBs can be repaired by either non-homologous end-joining (NHEJ), which directly rejoins together the two broken ends, or homologous recombination (HR) that uses intact homologous duplex DNA sequences as a template for accurate repair [223].

HR is promoted by the nucleolytic degradation of the 5′ DSB ends (a process referred to as resection) to yield 3′ single-stranded DNA (ssDNA) tails that invade the homologous duplex and prime reparative DNA synthesis [223]. DSB resection is a two-step process that involves multiple nucleases and helicases. A protein complex, which is called MRX (Mre11–Rad50–Xrs2) in the budding yeast *Saccharomyces cerevisiae* and MRN (Mre11–Rad50–Nbs1) in mammals, initiates resection together with the Sae2/CtIP protein by catalyzing an endonucleolytic cleavage of the 5′-terminated DNA strands. This cleavage creates a substrate for two partially overlapping pathways, which depend on the nucleases Exo1 and Dna2, respectively, and promote the generation of long ssDNA tails (reviewed in [32,224]). While Exo1 is a 5′-3′ exonuclease capable of efficiently degrading the 5′ end on duplex DNA, the endonuclease Dna2 requires the helicase activity of Sgs1 (orthologue of mammalian BLM) to efficiently remove small fragments from DNA ends [32,224].

DSB end degradation is tightly controlled by both positive and negative regulators, which tune the action of specific resection factors. While the cyclin-dependent kinase (Cdk1 in yeast)-Clb complexes stimulate the activities of both Sae2 and Dna2, the Ku complex and Rad9 inhibit the action of Exo1 and Sgs1-Dna2, respectively [32,108,224]. Exo1 action is also inhibited through phosphorylation by the checkpoint kinase Rad53 [129] and regulated by the ssDNA-binding complex Replication Protein A (RPA), which promotes Exo1 action *in vivo*, and limits Exo1-dependent degradation by increasing Exo1 turnover at DNA ends *in vitro* [77,80]. Given the efficiency of Exo1 exonuclease [80], these multiple controls on its action can be important to prevent excessive DNA degradation that could lead to genome instability.

DSB repair is coupled with cell cycle progression by a checkpoint pathway, whose key players are the protein kinases Mec1 and Tel1, orthologs of mammalian ATR and ATM, respectively [144]. While Tel1 is recruited to blunt or minimally processed DNA ends through interaction with MRX [156], Mec1 and its interactor Ddc2 (ATRIP in mammals) are activated by extended RPA-coated ssDNA that is produced by resection [162]. Once activated, Mec1 and Tel1 propagate the checkpoint signal to the effector kinases Rad53 and Chk1 (Chk2 and Chk1 in mammals, respectively), whose activation requires the adaptor Rad9 (53BP1 in mammals) and leads to temporarily arrest cell cycle progression [144].

Increasing evidence suggests the existence of intimate connections between RNA metabolism, DDR and genome integrity [225]. Pre-mRNA molecules are co-transcriptionally processed by the addition of both a 5′-methylguanosine cap and a 3′ poly(A) tail, and eventually spliced before they are exported to the cytoplasm and translated. These events are mediated by RNA-binding proteins (RBPs), most of which belong to the conserved protein families of heterogeneous nuclear ribonucleo-proteins (hnRNPs) and mammalian serine-arginine-rich (SR) proteins [225]. RBPs also protect mRNAs from degradation and contribute to quality control systems that recognize and target to degradation improperly processed mRNAs [212,226]. In eukaryotes, mRNAs are mainly degraded either by the exosome multi-subunit complex, which includes both endo- and 3′-5′ exoribonuclease activities, or by the Xrn family of 5′-3′ exoribonucleases [226,227].

In both yeast and mammals, several RBPs participate to the DDR and the stress response. Many of these RBPs bind to nascent transcripts and prevent transcription-associated genome instability by packaging pre-mRNAs into ribonucleoprotein particles. This packaging limits the generation of DNA:RNA hybrids, which could induce replication stress and DNA damage by interfering with the progression of DNA replication forks (reviewed in [225,228]). Factors involved in RNA metabolism play also more direct roles in the DDR by either recruiting DDR proteins to the site of damage or regulating the expression of repair and checkpoint genes at different levels [225]. Finally,

the conserved nonsense-mediated decay (NMD) pathway was recently found to limit HR in *S. cerevisiae* undamaged cells by controlling the transcript and protein levels of HR factors [229].

One of the most abundant *S. cerevisiae* RBPs is Npl3, which shares structural homologies with both SR and hnRNPs protein families, as it possesses two conserved RNA-recognition motifs (RRMs) and a serine- and arginine-rich C-terminal domain [206]. Npl3 is recruited to transcribed regions through the interaction with RNA polymerase II [207,230], and participates in pre-mRNA processing and packaging as well as in mRNA export and translation [212]. Npl3 accumulates at the 3′ end of transcribed genes [215] and seems to play a role in transcription termination, although this role is somehow controversial. In fact, studies with reporter constructs indicated that Npl3 prevents both early transcription termination and recognition of polyadenylation cryptic sites by competing with polyadenylation/termination factors [207,217,218]. However, recent genome-wide analyses showed significant termination defects in the absence of Npl3, suggesting that Npl3 promotes transcription termination [231].

Similar to other RBPs, Npl3 prevents transcription-associated genome instability by limiting the accumulation of DNA:RNA hybrids [215]. Interestingly, several findings suggest additional Npl3 functions in the DDR. In particular, cells lacking Npl3 are highly sensitive to DSB-inducing agents [215] and to the expression of the EcoRI endonuclease [232]. Furthermore, Npl3 shows negative genetic interactions with the MRX complex [233], and Npl3 inactivation increases the sensitivity of *rad52* or *ku* mutants to genotoxic agents [215]. Finally, checkpoint-dependent Npl3 phosphorylation after methyl methanesulfonate (MMS) treatment suggests that Npl3 activity may be regulated in response to DNA damage [134].

Here, we show that Npl3 promotes both checkpoint activation and the generation of long ssDNA tails at the DSB ends. These functions are at least partially linked to the regulation of Exo1 abundance through the control of *EXO1* mRNA biogenesis. Altogether, our results identify a new function of Npl3 in the response to DSBs and contribute to define the role of this multifunctional RBP in preserving genome stability.

## Npl3 promotes the activation of a Mec1-dependent checkpoint

The hypersensitivity of *npl3* mutant cells to DSB-inducing agents [215,232] suggests that Npl3 is involved in the response to DSBs. To explore further this hypothesis, we asked whether the lack of Npl3 affects the checkpoint response to a single DSB that is generated by the HO endonuclease, whose gene is expressed from a galactose-inducible promoter in JKM139 haploid cells [234]. Galactose addition to these cells induces the generation at the *MAT* locus of a single DSB that cannot be repaired by HR because the homologous donor loci *HML* and *HMR* are deleted [234]. This HO-induced DSB triggers a Mec1-dependent checkpoint that causes a G2/M cell cycle arrest, as well as the phosphorylation of both the checkpoint effector kinase Rad53 and the Mec1 interactor Ddc2 [163,173,235]. We analyzed cell cycle progression and phosphorylation of Rad53 and Ddc2 after the induction of a single irreparable DSB in wild type and *npl3Δ* cells carrying a fully functional Ddc2-HA tagged variant. The cleavage efficiency was evaluated by quantitative PCR (qPCR) at the HO cut site 2 h after galactose addition. Cells carrying the deletion of *MEC1* and kept viable by the lack of the ribonucleotide reductase inhibitor Sml1 were used as a control [236].

When G1-arrested cell cultures were spotted on galactose-containing plates, wild type cells arrested as large-budded cells for at least 8 hours after HO induction, while *mec1Δ sml1Δ* cells, which are unable to activate the checkpoint, formed microcolonies with more than two cells within 4–6 hours *(Figure 10A)*. Although the cleavage efficiency was reduced to 82% in *npl3Δ* cells compared to wild type (95%), 60% of *npl3Δ* cells formed microcolonies 8 hours after HO induction, when >80% wild type cells were still arrested *(Figure 10A)*, indicating that Npl3 contributes to arrest the cell cycle in response to an irreparable DSB.

Rad53 and Ddc2 phosphorylation, which causes decreased electrophoretic mobility of the proteins, was analyzed by western blot of comparable amounts of protein extracts *(Loading control is shown in Figure 11)* after galactose addition to cell cultures exponentially growing in raffinose. As the HO cleavage efficiency was reduced in *npl3Δ*

cells compared to wild type (85% versus 97%), we also performed quantitative analyses of Rad53 and Ddc2 phosphorylation by calculating the ratio of slowly-migrating phosphorylated forms to total protein amount, and normalizing this value with respect to the efficiency of DSB formation evaluated by qPCR. Slowly-migrating Rad53 bands appeared 2–3 hours after HO induction and then became prevalent in wild type extracts *(Figure 10B)*. Conversely, the unphosphorylated Rad53 species remained abundant until the end of the experiment in *npl3Δ* extracts although some slowly-migrating bands appeared 3–4 hours after HO induction *(Figure 10B)*, indicating that Npl3 promotes the HO-induced Rad53 phosphorylation. Npl3 enhances also the phosphorylation of the Mec1-specific target Ddc2, as the amount of phosphorylated Ddc2 was lower in *npl3Δ* extracts than in wild type after HO induction *(Figure 10C)*. Altogether, these results indicate that Npl3 promotes the activation of the Mec1-dependent checkpoint in response to a single irreparable DSB.

As cells lacking Npl3 showed growth defects [215], we asked whether their checkpoint defect could be ascribed to alterations in cell cycle progression. This was not the case, because Rad53 phosphorylation was defective in *npl3Δ* cells even when the HO cut was induced in cells arrested in G2 with nocodazole and kept in G2 throughout the experiment *(Figure 10D)*.

To test whether Npl3 participates to checkpoint activation specifically after a single HO-induced DSB, we analyzed Rad53 phosphorylation in wild type and *npl3Δ* cells treated with different genotoxic agents. Cell cultures were arrested in G1 with α-factor and released in the presence of the topoisomerase poison camptothecin (CPT) or the alkylating agent MMS. As expected [237], Rad53 phosphorylation was slightly induced by CPT in wild type cells *(Figure 10E)*. However, this phosphorylation was further reduced in *npl3Δ* cells *(Figure 10E)*. Similarly, Rad53 was less phosphorylated in MMS-treated *npl3Δ* cells than in wild type *(Figure 10F)*. Conversely, Rad53 was efficiently phosphorylated in both wild type and *npl3Δ* cells arrested in G2 and treated with the DSB-inducing drug phleomycin *(Figure 10G)*. As checkpoint activation in all these conditions depends specifically on Mec1 [237,238], these results suggest that Npl3 is not

directly required to activate Mec1 but rather to generate specific signals that activate Mec1.

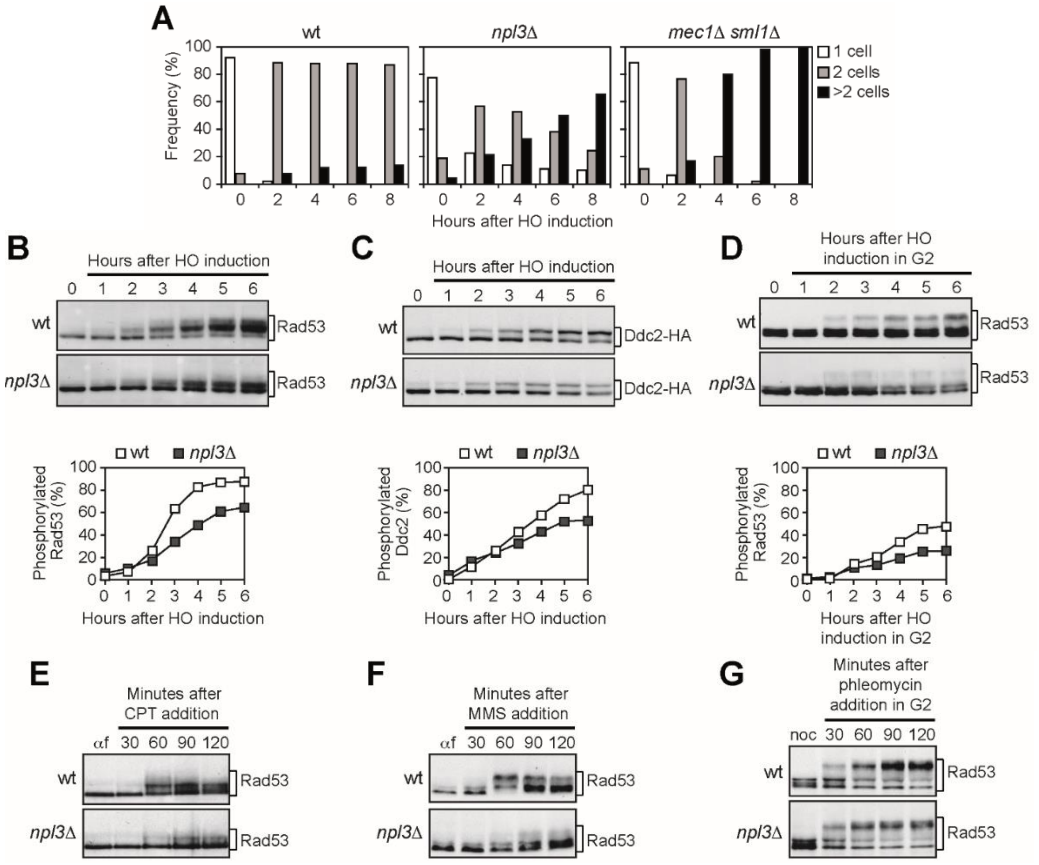


***Figure 10 - The lack of NPL3 impairs Mec1 signaling activity.***

**(A)** YEPR G1-arrested cell cultures of JKM139 derivative strains were plated on galactose-containing plates to induce HO expression (time zero). At the indicated time points, 200 cells for each strain were analyzed to determine the frequency of unbudded cells, large budded cells and microcolonies with more than two cells. **(B and C)** Exponentially growing YEPR cell cultures expressing a fully functional Ddc2-HA protein were transferred to YEPRG (time zero). Protein extracts prepared at the indicated time points were subjected to western blot with anti-Rad53 **(B)** or anti-HA **(C)** antibodies. Quantitative analysis of Rad53 and Ddc2 phosphorylation was performed by calculating the ratio of band intensities for slowly-migrating bands to total amount of protein, and dividing the obtained values by the HO cleavage efficiency. Cut efficiency was evaluated as the difference in the normalized amount of qPCR products obtained with a primer pair that amplifies only the uncut *MAT* locus before and 2h after galactose addition. **(D)** YEPR G2-arrested cell cultures were transferred in YEPRG (time zero) in the presence of nocodazole. Protein extracts were analyzed by western blot with anti-Rad53 antibodies. Quantitative analysis of Rad53 phosphorylation was performed as in **(B)**. **(E and F)** YEPD G1-arrested cell cultures were released in fresh medium containing camptothecin (CPT) (50 μM) **(E)** or methyl methanesulfonate (MMS) (0,02%) **(F)**. Rad53 phosphorylation was monitored by western blot with anti-Rad53 antibodies. **(G)** Phleomycin (15 μg/ml) was added to YEPD G2-arrested cell cultures kept arrested in G2. Protein extracts were subjected to western blot with anti-Rad53 antibodies.

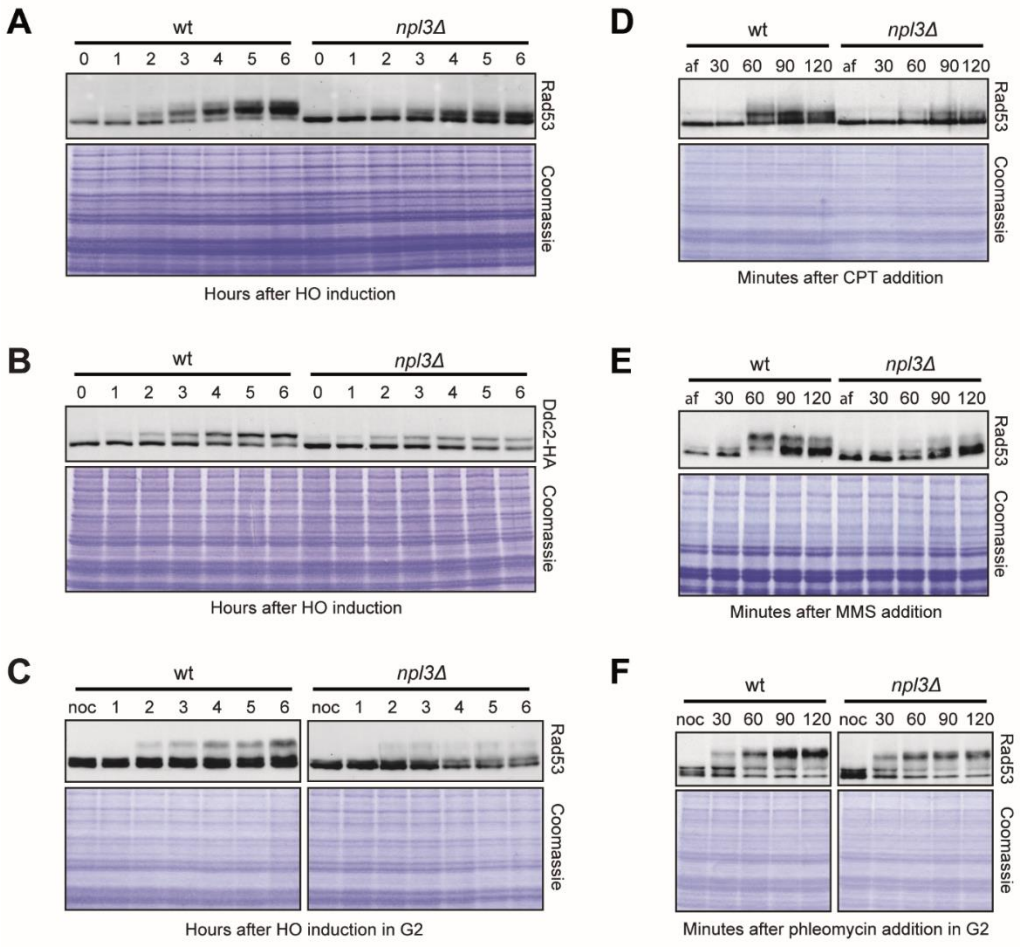


***Figure 11 - Loading control of western blot in Figure 10.***

**(A-C)** Galactose was added to exponentially growing **(A,B)** or G2-arrested **(C)** YEPR cell cultures to induce HO. Protein extracts were subjected to western blot with anti-Rad53 **(A,C)** or anti-HA **(B)** antibodies or stained with Coomassie as a loading control. **(D-E)** YEPD G1-arrested cell cultures (αf) were released in fresh medium containing CPT (50 µM) **(D)** or MMS (0,02%) **(E)**. Protein extracts were subjected to western blot with anti-Rad53 antibodies or stained with Coomassie. **(F)** Phleomycin (15 µg/ml) was added to YEPD G2-arrested cell cultures in the presence of nocodazole to maintain the G2 arrest. Protein extracts were analysed by western blot with anti-Rad53 antibodies or stained with Coomassie.

## Npl3 promotes the generation of ssDNA at DSBs

Mec1 activation requires the formation of RPA-coated ssDNA, which is generated by the 5′-3′ nucleolytic degradation of the DSB ends [162]. In both *Schizosaccharomyces pombe* and human cells, RPA loading at DSB ends was found to be inhibited by the presence of DNA:RNA hybrids [239,240]. As Npl3 counteracts the accumulation of DNA:RNA hybrids during transcription [215], the reduced Mec1 activation in *npl3Δ* cells could be due to the inability of these cells to remove DNA:RNA hybrids from the DSB ends. If this were the case, the checkpoint defect of *npl3Δ* cells should be alleviated by high levels of ribonuclease H1 (RNase H1), which is known to remove DNA:RNA hybrids in vivo [241]. We therefore transformed wild type and *npl3Δ* cells carrying the HO system with a centromeric plasmid carrying the RNase H1-encoding gene (*RNH1*) under the control of *tetO* promoter, which acts as a strong promoter in the absence of tetracyclin [241]. As expected [215], the *tetO-RNH1* plasmid suppressed the hypersensitivity of *npl3Δ* cells spotted on plates with MMS *(Figure 12A)*. However, the hypersensitivity to CPT of the same cells was only very slightly suppressed by RNase H1 overproduction *(Figure 12A)*, which was also unable to restore the HO-induced checkpoint in cells lacking Npl3. In fact, *npl3Δ* cells carrying either the *tetO-RNH1* plasmid or the empty vector showed similar defects in both Rad53 phosphorylation *(Figure 12B)* and cell cycle arrest after HO induction compared to wild type cells *(Figure 13)*. This finding indicates that the checkpoint defect of *npl3Δ* cells is not likely due to DNA:RNA hybrid accumulation.

We then asked whether Npl3 promotes DSB processing by directly monitoring ssDNA generation at the DSB ends. Galactose was added to cell cultures arrested in G2 with nocodazole to produce the HO-induced DSB in cells that were then maintained in G2. Because ssDNA is resistant to cleavage by restriction enzymes, we measured the 5′ strand degradation of one DSB end by following the loss of SspI restriction fragments at different time points after galactose addition by Southern blot of genomic DNA under alkaline conditions, using a single-stranded RNA probe that anneals to the unresected 3′ strand on one side of the break *(Figure 12C and D)*. We then evaluated

the resection efficiency by calculating the ratio of band intensities for ssDNA to total amount of DNA, normalized with respect to the efficiency of DSB formation for each time point *(Figure 12E)*. The 1.7 and 3.5 kb resection fragments (r1-r2 in *Figure 12C–E*) appeared with similar kinetics in both wild type and *npl3Δ* cells, suggesting that the lack of Npl3 does not affect initiation of DSB resection. However, the generation of resection fragments longer than 3.5 kb (r3–r7 in *Figure 12C–E*) was severely affected by the absence of Npl3 *(Figure 12D and E)*, indicating that *npl3Δ* cells are specifically impaired in extensive resection. Thus, Npl3 is dispensable to initiate DSB resection, whereas it is required to produce long ssDNA tails.

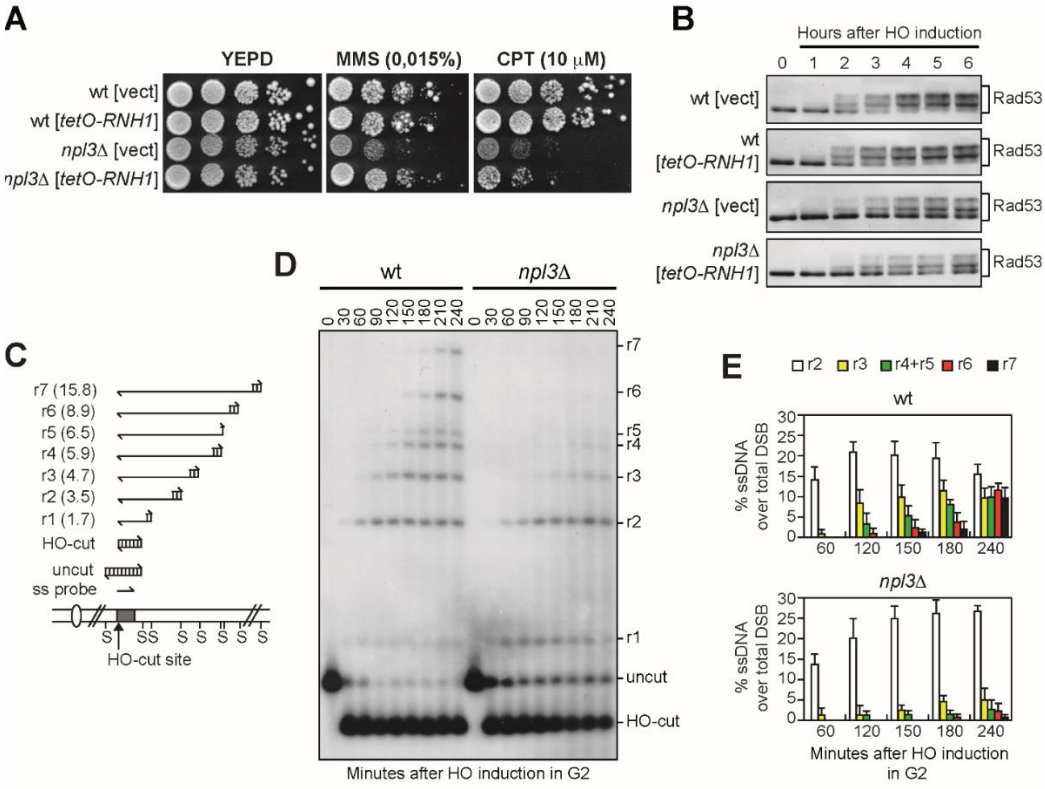


***Figure 12 - The lack of NPL3 impairs extensive resection of DSB ends.***

**(A and B)** Exponentially growing cell cultures of wild type and *npl3Δ* strains, both carrying a centromeric plasmid either expressing the *RNH1* gene from the *tetO* promoter or empty (vect), were either serially diluted (1:10) before being spotted out onto YEPD plates with or without MMS or CPT **(A)**, or transferred to YEPRG to monitor Rad53 phosphorylation by western blot **(B)**. **(C)** System to detect DSB resection. Gel

blots of SspI-digested genomic DNA separated on alkaline agarose gel were hybridized with a single-stranded RNA *MAT* probe (ss probe) that anneals to the unresected strand. 5′-3′ resection progressively eliminates SspI sites (S), producing larger SspI fragments (r1 through r7) detected by the probe. **(D and E)** Exponentially growing YEPR cell cultures were arrested in G2 with nocodazole and transferred to YEPRG (time zero) in the presence of nocodazole. **(D)** DSB resection as described in **(C)**. **(E)** Resection products in **(D)** were analyzed by densitometry. The mean values are represented with error bars denoting SD (n = 5).

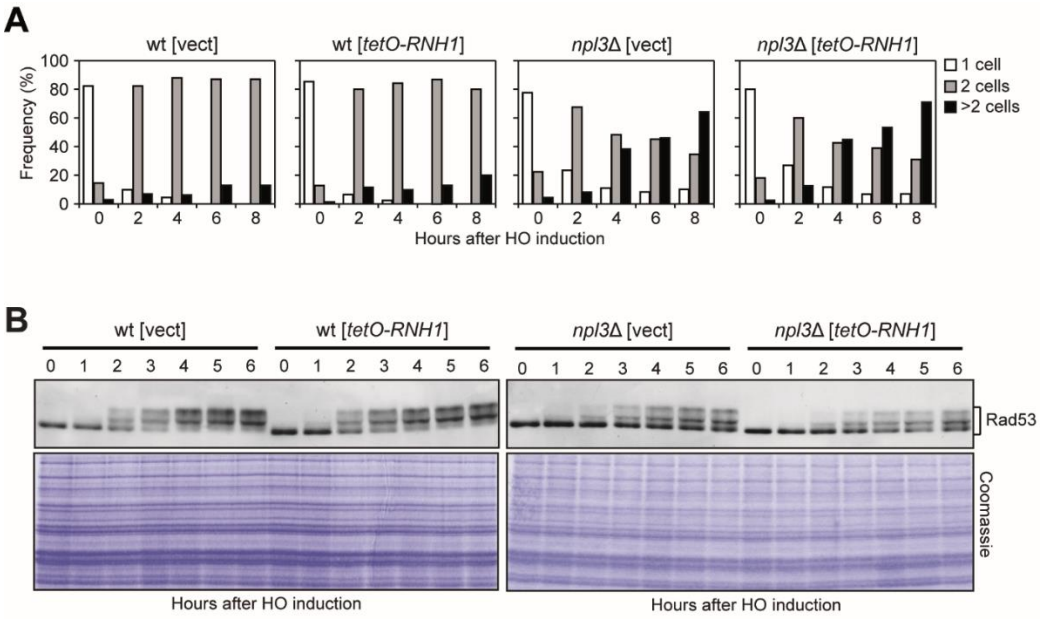


***Figure 13 - High levels of RNase H1 do not suppress the checkpoint defect of cells lacking Npl3.***

**(A)** Exponentially growing cell cultures of wild type JKM139 and an otherwise isogenic *npl3Δ* strain, both carrying a centromeric plasmid either expressing the *RNH1* gene from the *tetO* promoter or empty (vect), were arrested in G1 with α-factor and plated on galactose-containing plates (time zero) to follow microcolonies formation. **(B)** YEPR exponentially growing cell cultures were transferred in YEPRG to monitor Rad53 phosphorylation by western blot. The same amounts of protein extracts were separated on SDS-PAGE and stained with Coomassie as a loading control.

### The Npl3 RNA-binding domains are required for Npl3 functions in the DDR

Npl3 binds RNA through the RNA recognition motifs RRM1 and RRM2 [206]. We therefore investigated whether the integrity of Npl3 RRMs is required for cell survival in the presence of DNA damage and/or HO-induced checkpoint activation. We transformed *npl3Δ* cells with either an empty centromeric plasmid or with similar plasmids carrying wild type *NPL3*, the *npl3-F160L* allele, which inactivates RRM1, the *npl3-SNK* (*L225S*, *G241N*, *E244K*) allele, which inactivates RRM2, and the *npl3-LSNK* (*F160L*, *L225S*, *G241N*, *E244K*) allele, which disrupts both RRM domains [206,214]. Cells expressing the *npl3-F160L* allele were as sensitive as wild type to CPT *(Figure 14A)* and phosphorylated Rad53 similarly to wild type cells after HO-induction *(Figure 14B and loading control in Figure 15)*. By contrast, *npl3-SNK* and *npl3-LSNK* cells were more sensitive than wild type to CPT, although their hypersensitivity was less pronounced compared to *npl3Δ* cells *(Figure 14A)*. Furthermore, the HO-induced Rad53 phosphorylation was reduced in *npl3-SNK* and *npl3-LSNK* mutants, similar to *npl3Δ* cells *(Figure 14B)*.

We also analyzed whether the integrity of Npl3 RRM domains is required for resection by measuring ssDNA generation at the HO-induced DSB in *npl3-LSNK* mutant cells. Similar to the absence of Npl3, the *npl3-LSNK* allele impairs long-range resection. In fact, the r3–r7 resection fragments accumulated less efficiently in both *npl3Δ* and *npl3-LSNK* cells than in wild type *(Figure 14C and D)*. These results indicate that the RRM domains are required to support Npl3 functions in the DDR, with RRM2 playing a major role, suggesting that Npl3 regulates specific RNA molecules involved in the DDR.

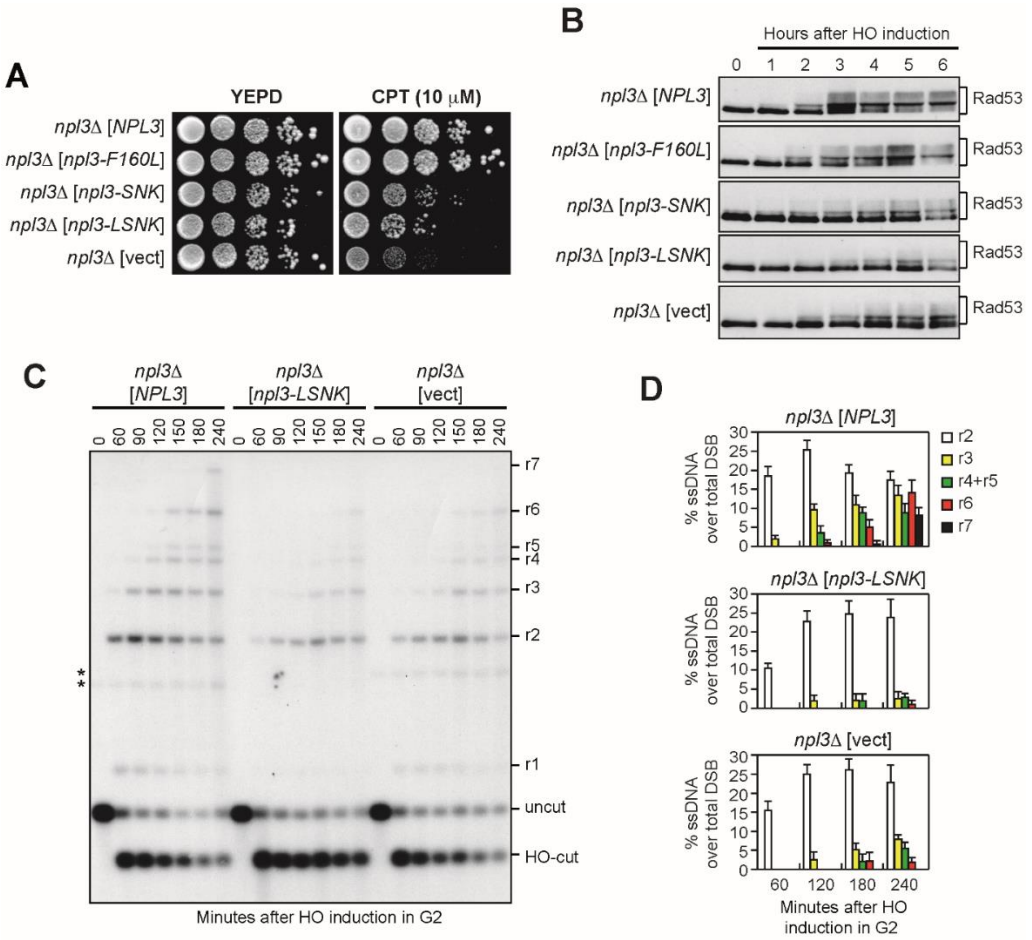


***Figure 14 - The Npl3 RNA binding domains are required for checkpoint and resection.***

**(A–D)** Exponentially growing cell cultures of a *npl3Δ* strain transformed with an empty centromeric vector (vect) or with the same vector carrying either the wild type *NPL3* gene or the indicated *npl3* mutant alleles were either spotted out onto YEPD plates with or without CPT **(A)**, or transferred to YEPRG to follow Rad53 phosphorylation by western blot **(B)**, or arrested in G2 and transferred to YEPRG (time zero) in the presence of nocodazole to monitor DSB resection as described in *Figure 12C* **(C)**. *indicates cross hybridization signals likely due to the presence of the plasmids. **(D)** Resection products in **(C)** were analyzed by densitometry. The mean values are represented with error bars denoting SD (n = 3).

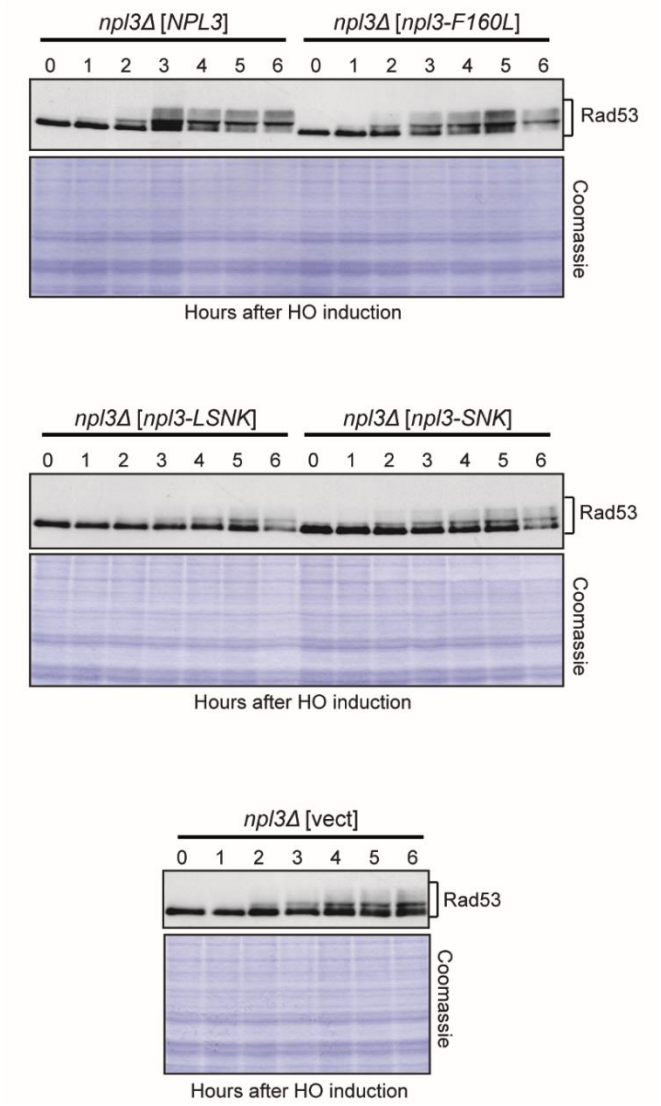


***Figure 15 - Loading control of western blot in Figure 14.***

Exponentially growing YEPR cell cultures were transferred to YEPRG at time zero. Protein extracts were subjected to western blot analysis with anti-Rad53 antibodies or stained with Coomassie as a loading control.

## The lack of Npl3 reduces Exo1 levels

Npl3 might either directly participate in resection or support DSB processing by promoting the expression of resection proteins. To discriminate between these two possibilities, we first evaluated whether Npl3 is recruited to DNA ends. Chromatin immunoprecipitation (ChIP) and real-time qPCR were performed after generation of an HO-induced DSB in G2-arrested cells expressing a fully functional Npl3-HA variant. Similar amounts of DNA at 0.6 or 5.4 kb from the HO-cut site were recovered in immunoprecipitates from cells expressing either the Npl3-HA variant or untagged Npl3 both before and after DSB formation *(Figure 16)*. This suggests that Npl3 is not bound/recruited to DSB ends and thus does not directly participate in resection.

Generation of ssDNA at DSBs is promoted by several proteins, which control either initiation (Mre11, Rad50, Xrs2 and Sae2) or extension (Dna2, Sgs1 and Exo1) of resection [32,224]. To assess whether Npl3 supports DSB processing by promoting the expression of resection factors, we measured the amount of the above proteins by western blot of protein extracts from wild type and *npl3Δ* cells expressing fully functional tagged versions of these proteins and treated with galactose to induce the HO cut. Similar amounts of Sgs1 *(Figure 17A)*, Mre11 and Xrs2 *(Figure 18A and B)* were detected in wild type and *npl3Δ* cells, indicating that Npl3 does not control the levels of these proteins. Consistent with the checkpoint defect of *npl3Δ* cells, Xrs2 and Sgs1, which are known to undergo DNA damage-induced phosphorylation [238,242], were less phosphorylated in *npl3Δ* cells compared to wild type *(Figure 17A and Figure 18B)*. The amount of Dna2 *(Figure 17B)*, Rad50 and Sae2 *(Figure 18C and D)* was higher in *npl3Δ* cells than in wild type. However, it is unlikely that these effects can account for the resection defect of *npl3Δ* cells. In fact, overexpression of neither *SAE2* nor *DNA2* affects ssDNA generation at DSB ends in wild type cells [66,243]. Furthermore, Rad50 forms the MRX complex together with Mre11 and Xrs2, and Mre11 was found to be limiting for the recruitment of the MRX complex to DSBs [52], suggesting that high Rad50 levels should not affect DSB resection because they do not increase MRX recruitment to DSBs.

Interestingly, the amount of Exo1 was strongly reduced in *npl3Δ* cells compared to wild type both in raffinose and after galactose addition *(Figure 17C)*. As Exo1 levels were not affected by treatment with the proteasome inhibitor MG132 of either wild type or *npl3Δ* cells exponentially growing in glucose *(Figure 19)*, altogether these data indicate that Npl3 promotes Exo1 production independently of both the DNA damage and the carbon source.

We investigated whether the integrity of the Npl3 RRM motifs is important to regulate Exo1 levels by evaluating the amount of MYC-tagged Exo1 in cells expressing RRM1 and/or RRM2 defective Npl3 variants. The amount of Exo1, quantified using Pgk1 as a normalization control, was reduced of ∼70% in YEPD exponentially growing *npl3Δ* cells compared to wild type *(Figure 17D)*. Npl3 interaction with RNA is important to regulate Exo1 levels, as we detected a similar reduction in *npl3-LSNK* and *npl3-SNK* mutant cells, although inactivation of only RRM1 did not affect Exo1 amount *(Figure 17D)*.

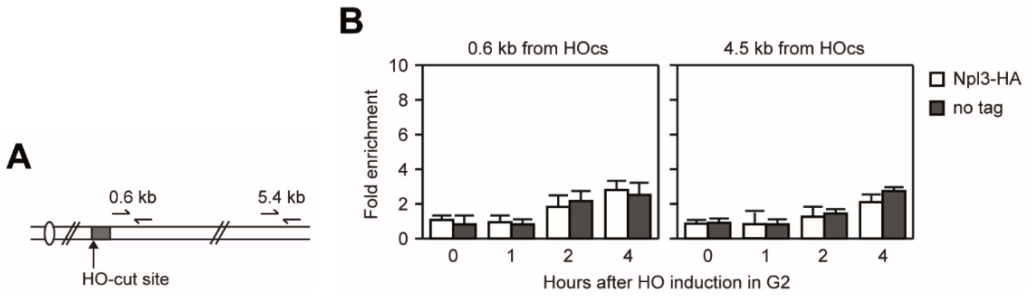


***Figure 16 - Npl3 is not enriched at an HO-induced DSB.***

**(A)** Schematic representation of *MAT* locus on chromosome III. The relative positions of the HO cleavage site and of primer pairs used for chromatin immunoprecipitation (ChIP) are shown. **(B)** G2-arrested YEPR wild type (no tag) and *NPL3-HA* cell cultures were transferred to YEPRG in the presence of nocodazole to maintain the G2 block and subjected to ChIP analysis with anti-HA antibodies and subsequent qPCR. Relative fold enrichment of the Npl3-HA fusion protein at the indicated distances from the HO cleavage site was determined. Plotted values are the mean values +SD (n=3).

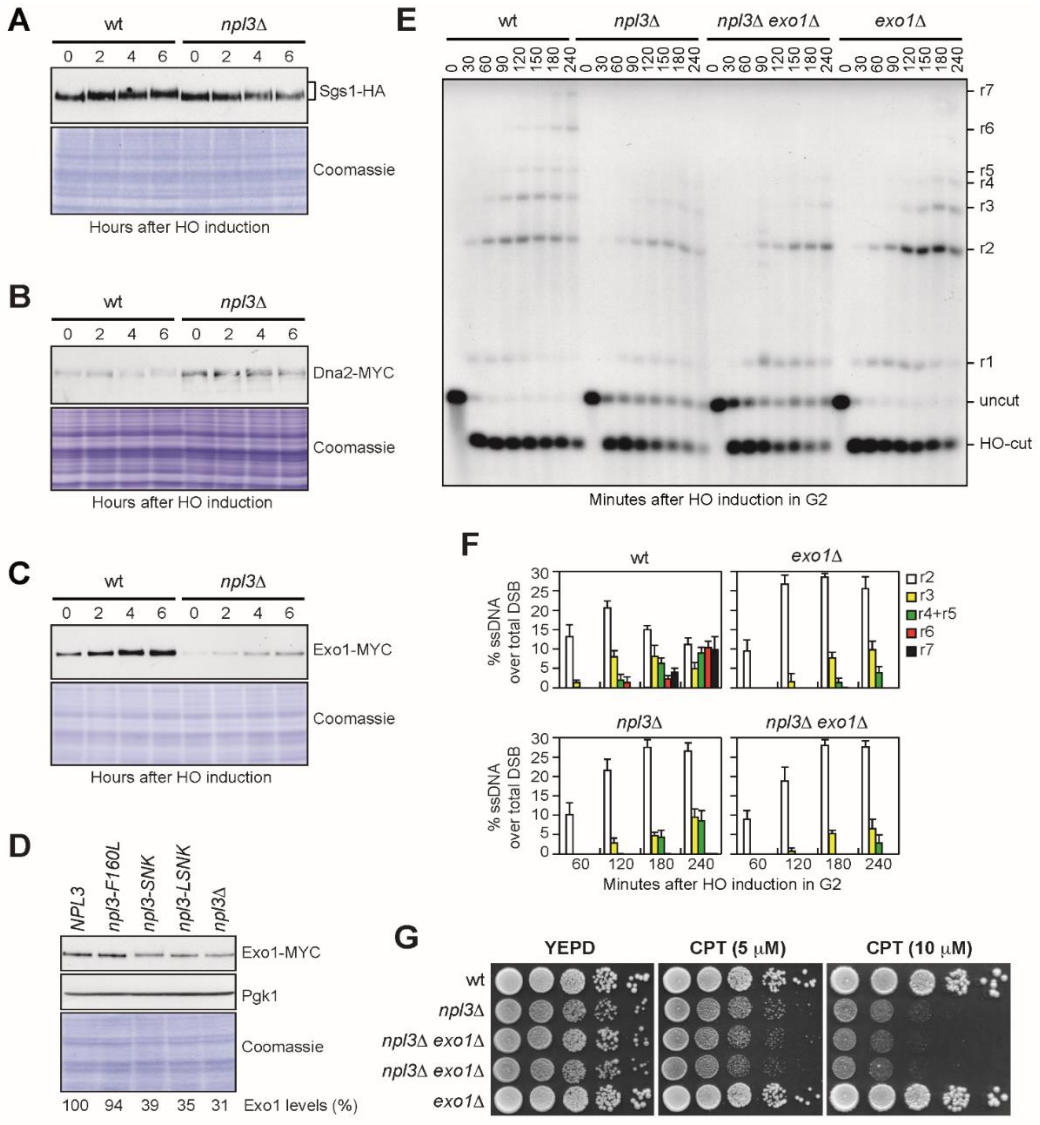


***Figure 17 - NPL3 and EXO1 belong to the same resection pathway.***

**(A–C)** Exponentially growing YEPR cell cultures of strains expressing the indicated tagged proteins were transferred to YEPRG (time zero). The same amounts of protein extracts were separated on SDS-PAGE and either subjected to western blot with antibodies specific for the indicated tags or stained with Coomassie as a loading control. **(D)** The same amounts of protein extracts prepared from exponentially growing YEPD cultures of strains as in *Figure 14*, all expressing the Exo1-MYC tagged protein, were either stained with Coomassie or subjected to western blot with anti-MYC and anti-Pgk1 (loading control) antibodies. The relative intensity of the Exo1-MYC signal compared to wild type (set to 100%) was estimated after normalization to the Pgk1 band. **(E and F)** G2-arrested cell cultures of the indicated strains were transferred to YEPRG (time zero) in the presence of nocodazole. **(E)** DSB resection as described in *Figure 12*C. **(F)** Resection products in **(E)** were analyzed by densitometry. The mean values are represented with error bars denoting SD (n = 3). **(G)** Exponentially growing cell cultures of the indicated strains were spotted out onto YEPD plates with or without CPT.

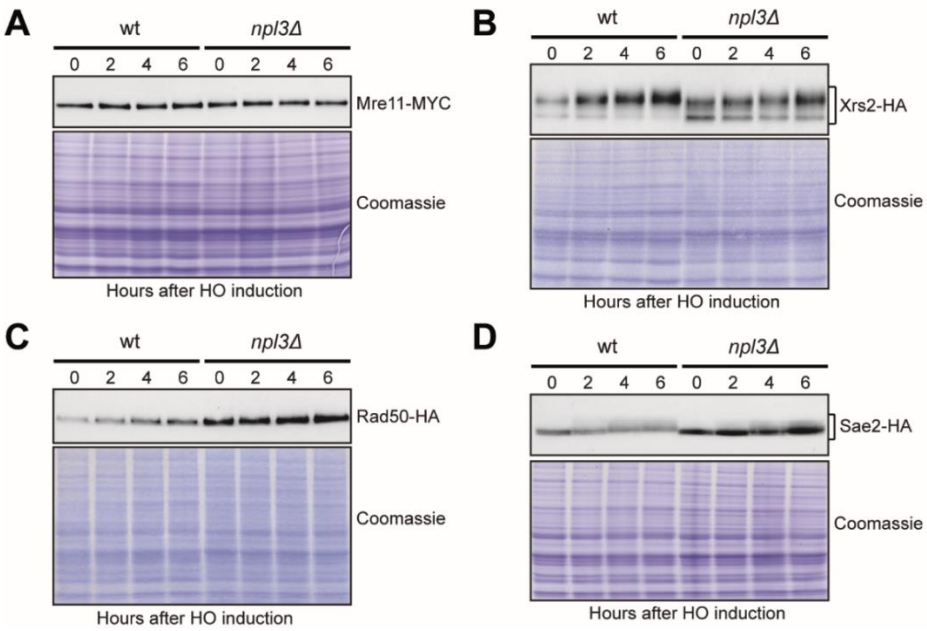


***Figure 18 - Levels of resection proteins in the absence of Npl3.***

Exponentially growing YEPR cell cultures of JKM139 derivative strains expressing the indicated tagged proteins were transferred in YEPRG at time zero. Protein extracts were subjected to western blot with antibodies specific for the indicated tags. The same amounts of protein extracts were separated on SDS-PAGE and stained with Coomassie as a loading control.

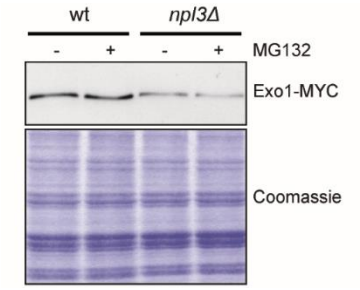


***Figure 19 - Exo1 is not degraded by proteasome in the absence of Npl3.***

Protein extracts prepared from exponentially growing YEPD cell cultures treated with the proteasome inhibitor MG132 (75 µM) for 3 hours (+) or untreated (-) were subjected to western blot analysis with anti-MYC antibodies. The same amounts of protein extracts were separated on SDS-PAGE and stained with Coomassie as a loading control.

### *NPL3* and *EXO1* belong to the same epistasis group for resection

As Exo1 is required for extensive resection of DNA ends [56,74], the low Exo1 levels in *npl3Δ* cells could be the cause of the resection defect of these cells. If this were the case, *npl3Δ* and *exo1Δ* cells should show a similar resection defect, and the lack of Exo1 should not increase the resection defect of *npl3Δ* cells. When we monitored ssDNA generation at the HO-induced DSB, both *exo1Δ* and *npl3Δ* single mutant cells efficiently initiated resection, but were impaired in the generation of the r3-r7 ssDNA products, and a similar defect in long-range resection was detectable in *npl3Δ exo1Δ* double mutant cells *(Figure 17E)*. Although the HO-cut is induced more efficiently in *exo1Δ* cells (98%) than in both *npl3Δ* and *npl3Δ exo1Δ* cells (83% and 79%, respectively), a quantitative analysis of the resection products normalized to the cleavage efficiency confirmed that the resection kinetics were similar in these three mutant strains *(Figure 17F)*.

The lack of Exo1 exacerbates the hypersensitivity to DNA damaging agents of mutants affecting other resection pathways, such as *sae2Δ* or *sgs1Δ* [74,132]. Similarly, *NPL3* deletion increased the hypersensitivity to CPT of *sae2Δ* cells *(Figure 20A)*. Furthermore, the *npl3Δ sgs1Δ* spores obtained by tetrad dissection of a sporulated *NPL3*/*npl3Δ SGS1*/*sgs1Δ* diploid strain generated very small colonies *(Figure 20B)*, suggesting that Npl3 and Sgs1 participate in different pathways to support cell viability. Conversely, *EXO1* deletion neither increased the growth defect nor the hypersensitivity to CPT of *npl3Δ* cells *(Figure 17G)*, indicating that Exo1 and Npl3 belong to the same resection pathway.

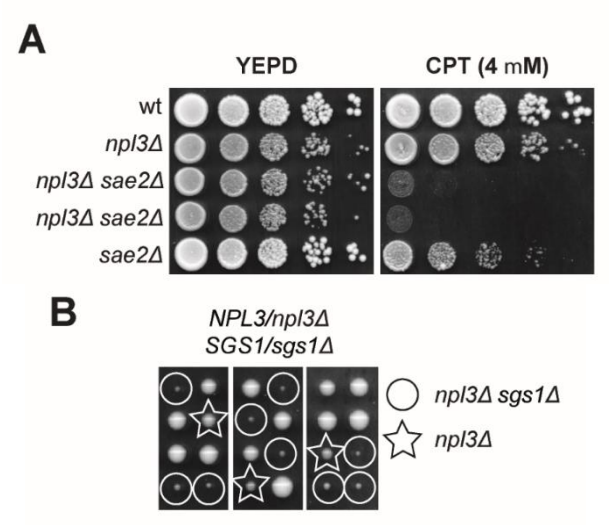


***Figure 20 - The lack of Npl3 increases the defects of cells lacking Sae2 or Sgs1.***

**(A)** Exponentially growing cell cultures of JKM139 derivative strains were serially diluted (1:10) before being spotted out onto YEPD plates with or without CPT. **(B)** Meiotic tetrads from diploid cells with the indicated genotype were dissected on YEPD plates that were incubated at 30°C for 3 days, followed by spore genotyping.

## Exo1 high levels partially restore resection in *npl3Δ* cells

If the low Exo1 amount causes the resection defect in *npl3Δ* cells, increased Exo1 levels are expected to restore resection in these cells. We therefore monitored the resection kinetics in wild type and *npl3Δ* cells carrying a high copy number 2µ plasmid with the *EXO1* gene [244]. The *EXO1* 2µ plasmid markedly increased the amount of long resection products in *npl3Δ* cells compared to the empty vector *(Figure 21A and B)*. In particular, *npl3Δ* cells with the empty vector were specifically impaired in the generation of resection fragments longer than 3.5 kb, while these longer ssDNA fragments appeared in *npl3Δ* cells carrying the *EXO1* 2µ plasmid. This indicates that Npl3 promotes the generation of long ssDNA tails by positively regulating Exo1 levels.

To verify that the *EXO1* 2µ plasmid increased Exo1 amount in the absence of Npl3, a 2µ plasmid either empty or carrying the *EXO1-MYC* allele was transformed into wild type and *npl3Δ* cells expressing the Exo1-Myc variant from the *EXO1* genomic locus.

Although the Exo1 levels were increased by the *EXO1-MYC* 2µ plasmid in both wild type and *npl3Δ* cells, some fast-migrating Exo1 forms appeared specifically in *npl3Δ* cells *(Figure 21C)*, suggesting that overproduced Exo1 may be unstable in the absence of Npl3. This might explain why the *EXO1-MYC* 2µ plasmid only partially restores resection in *npl3Δ* cells *(Figure 21A and B)*.

Interestingly, the *EXO1* 2µ plasmid partially suppressed the hypersensitivity to CPT of *npl3Δ* cells *(Figure 21D)*, indicating that the hypersensitivity of cells lacking Npl3 is at least partially due to the resection defect. Conversely, this plasmid did not suppress the hypersensitivity to MMS of *npl3Δ* cells *(Figure 21D)*, nor the elevated levels of spontaneous recombination caused by the Npl3 lack *(Figure 22)*. To measure mitotic recombination frequency, we used strains carrying the his3-513::TRP1::his3-537 heteroallelic duplication on chromosome XV [245] and transformed with either the *EXO1* 2µ plasmid or the empty vector. As expected [215], *NPL3* deletion increased 12.8-fold the recombination frequency at the *HIS3* locus compared to wild type cells *(Figure 22)*. The *EXO1* 2µ plasmid did not reduce, but rather slightly increased the recombination frequency in both wild type and *npl3Δ* cells *(Figure 22)*, indicating that the high recombination frequency in *npl3Δ* cells is not due to the low amount of Exo1.

The *EXO1* 2µ plasmid was also unable to restore the DSB-induced checkpoint in *npl3Δ* cells. In fact, HO-induced *npl3Δ* cells carrying either the empty vector or the *EXO1* 2µ plasmid showed similar defective Rad53 phosphorylation compared to wild type cells *(Figure 21E and loading control in Figure 23)*, indicating that the checkpoint defect of *npl3Δ* cells cannot be ascribed only to the resection defect. This result, together with the finding that the lack of Exo1 only very slightly affects the HO-induced Rad53 phosphorylation despite the resection defect [66,173], suggests that Npl3 might control the levels of other checkpoint proteins. However, we detected similar amounts of the three RPA subunits Rfa1, Rfa2 and Rfa3 in wild type and *npl3Δ* cells *(Figure 24A–C)*.

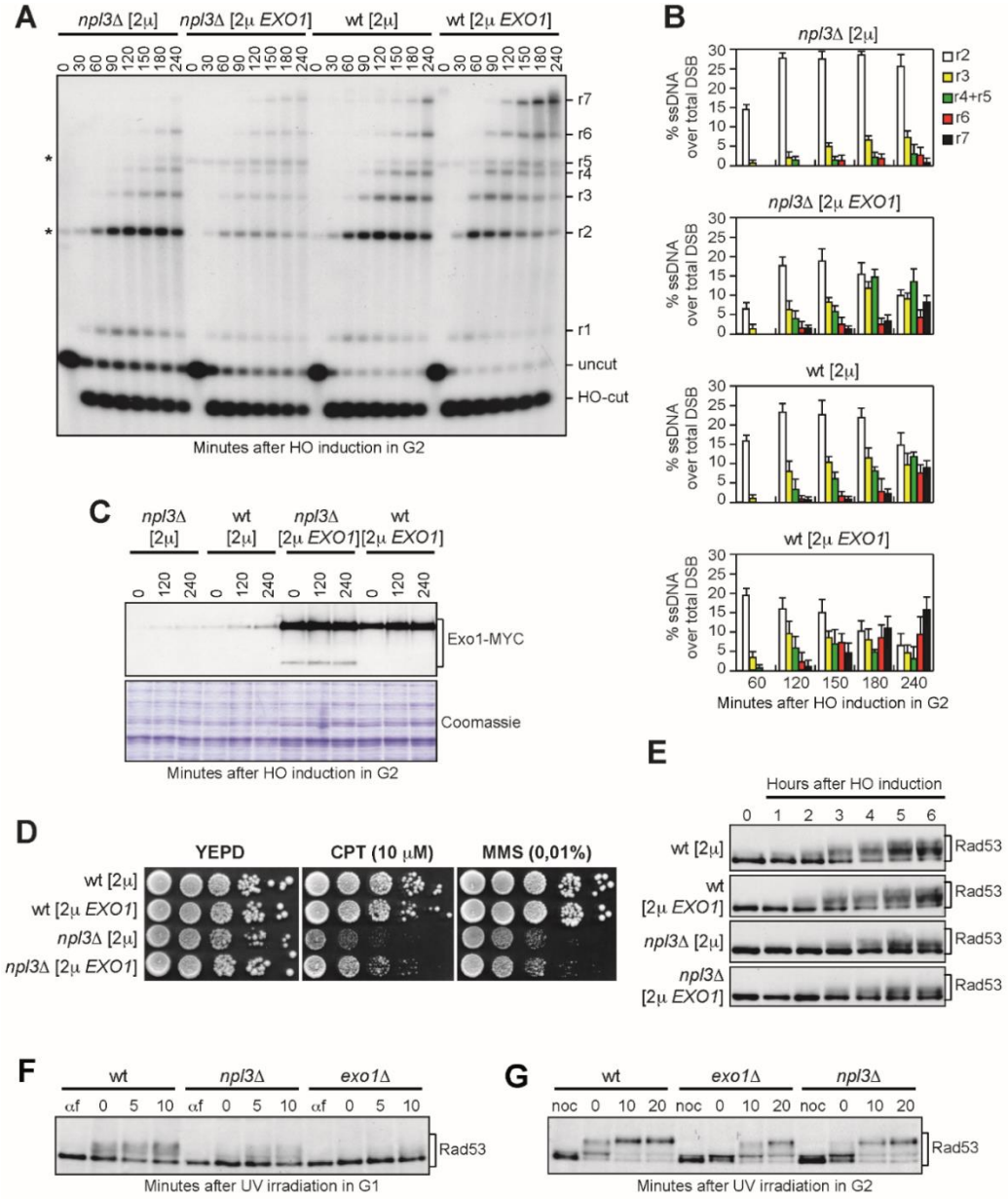


***Figure 21 - EXO1 overexpression partially suppresses both the resection defect and the hypersensitivity to CPT of npl3Δ cells.***

**(A and B)** G2-arrested YEPR cell cultures of wild type and *npl3Δ* strains, both transformed with a 2μ plasmid either carrying the *EXO1* gene or empty (2μ), were transferred to YEPRG (time zero) in the presence of nocodazole. **(A)** DSB resection as described in *Figure 12C*. *indicates cross hybridization signals that partially overlap the r2 or r5 bands, and are due to the presence of the 2μ plasmid. **(B)** Resection products in **(A)** were analyzed by densitometry. The mean values are represented with error bars denoting SD (n = 3). **(C)** G2-arrested cell cultures of wild type and *npl3Δ* strains, both expressing the Exo1-MYC tagged protein from the *EXO1* locus and transformed with a 2μ plasmid either carrying the *EXO1-MYC* gene or

empty (2μ), were transferred to YEPRG (time zero) in the presence of nocodazole. The same amounts of protein extracts were either subjected to western blot with anti-MYC antibodies or stained with Coomassie as a loading control. **(D and E)** Exponentially growing cell cultures of the strains described in **(A and B)** were either spotted out onto YEPD plates with or without CPT or MMS **(D)**, or transferred to YEPRG (time zero) to analyze Rad53 phosphorylation by western blot with anti-Rad53 antibodies **(E)**. **(F)** YEPD G1-arrested cell cultures (αf) of the indicated strains were UV irradiated (75 J/m$^2$) (time zero) and held in G1 in the presence of α-factor. Protein extracts were subjected to western blot with anti-Rad53 antibodies. **(G)** YEPD G2-arrested cell cultures (noc) of the strains in **(F)** were UV irradiated (75 J/m$^2$) (time zero) and held in G2 in the presence of nocodazole. Protein extracts were analyzed by western blot with anti-Rad53 antibodies.

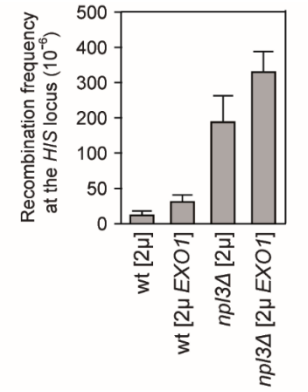


***Figure 22 -Exo1 high levels do not reduce the elevated frequency of mitotic recombination caused by Npl3 lack.***

Wild type and *npl3Δ* strains carrying the *his3-513::TRP1::his3-537* heteroallelic duplication on chromosome XV were transformed with either a *EXO1* 2μ plasmid or an empty vector (2μ). 10 independent clones for each strain were plated on complete medium plates to evaluate their viability and on plates lacking histidine to select the His+ recombinants generated by mitotic recombination at the *HIS3* locus. The number of the His+ colonies was evaluated and normalized to the viability of the strain to determine the recombination frequency.

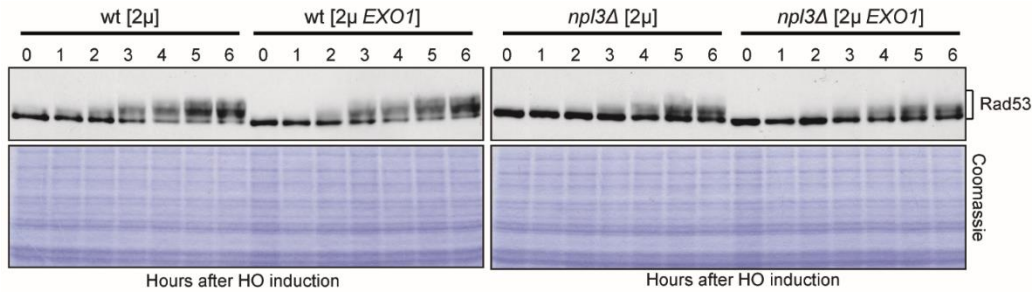


***Figure 23 - Loading control of western blot in Figure 21.***

Exponentially growing YEPR cell cultures were transferred in YEPRG at time zero. Protein extracts were subjected to western blot with anti-Rad53 antibodies or stained with Coomassie as a loading control.

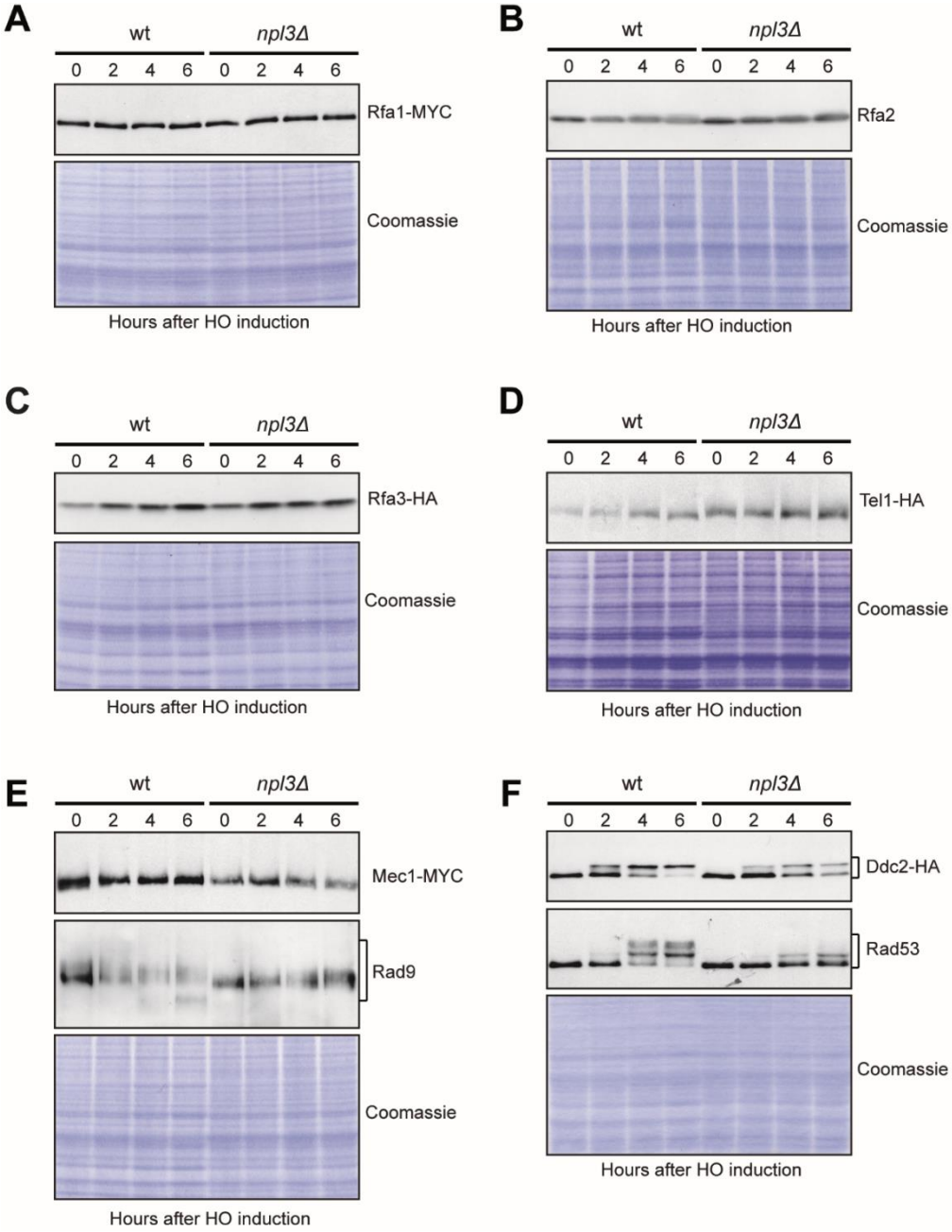


***Figure 24 - Levels of checkpoint proteins in the absence of Npl3.***

Exponentially growing YEPR cell cultures of JKM139 derivative strains expressing the indicated tagged proteins were transferred in YEPRG at time zero. Protein extracts prepared at different time points after HO induction were subjected to western blot analysis with antibodies specific for the indicated proteins or tags. The same amounts of protein extracts were separated on SDS-PAGE and stained with Coomassie as a loading control.

Furthermore, the abundance of the checkpoint proteins Tel1, Ddc2, Rad53, and Rad9 was unaffected by the absence of Npl3 *(Figure 24D-F)*. Conversely, the amount of Mec1 was slightly lower in *npl3Δ* cells than in wild type *(Figure 24E)*. However, a Mec1-dependent checkpoint is strongly activated in *npl3Δ* cells treated with phleomycin *(Figure 10G)*, suggesting that the slightly reduced amount of Mec1 detected in *npl3Δ* cells does not likely account for the checkpoint defect of the same cells. Altogether these results indicate that Npl3 plays two functions in the DDR: it promotes DSB resection by regulating Exo1 levels and it contributes to checkpoint activation by regulating some still unknown targets.

### Npl3 and Exo1 are required for checkpoint activation after UV irradiation

If the Npl3-mediated control of Exo1 protein levels is biologically relevant, we expect *exo1Δ* and *npl3Δ* cells to show some common phenotypes. Exo1 is required to activate the checkpoint after UV treatment in non-cycling cells by promoting the generation of large ssDNA gaps during nucleotide excision repair (NER) processing [246]. We then asked whether *npl3Δ* cells fail to activate the UV-induced checkpoint in G1- and G2-arrested cells, similarly to *exo1Δ* cells. Wild type, *npl3Δ* and *exo1Δ* cells were arrested either in G1 with α-factor or in G2 with nocodazole, UV irradiated, and transferred in fresh medium containing α-factor or nocodazole, respectively, to maintain the cell cycle arrests, as confirmed by FACS analyses *(Figure 25)*. As expected [246], Rad53 hyperphosphorylated forms appeared immediately after UV irradiation in wild type cells arrested either in G1 *(Figure 21F)* or in G2 *(Figure 21G)*, while they were strongly reduced in similarly treated *exo1Δ* cells *(Figure 21F and G)*. Also the lack of Npl3 impaired Rad53 phosphorylation in both G1 *(Figure 21F)* and G2 *(Figure 21G)*, although to a lesser extent than the absence of Exo1 *(Figure 21F and G)*, possibly because Exo1 is not totally absent in *npl3Δ* cells *(Figure 17C and D)*. Thus, similarly to Exo1, Npl3 is required for checkpoint activation after UV irradiation in G1 and in G2. As Npl3 is not required per se to activate the checkpoint, at least in G2-arrested cells *(Figure 10G)*,

these results suggest that the low Exo1 levels in *npl3Δ* cells are not sufficient to efficiently process the UV lesions and generate enough ssDNA to activate the checkpoint in non-cycling cells.

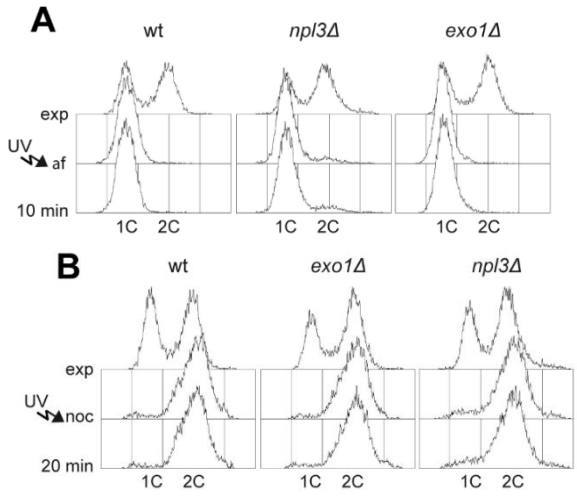


***Figure 25 - Cell cycle arrests of cells treated with UV.***

**(A)** Exponentially growing YEPD cell cultures of wild type JKM139 and otherwise isogenic *npl3Δ* and *exo1Δ* strains (exp) were arrested in G1 with α-factor (αf), UV irradiated (75 J/m$^2$), and held in G1 in the presence of α-factor. FACS analyses of DNA content to verify the cell cycle arrest in G1. **(B)** Exponentially growing YEPD cell cultures of the strains in **(A)** (exp) were arrested in G2 with nocodazole (noc), UV irradiated (75 J/m$^2$), and held in G2 in the presence of nocodazole. FACS analyses of DNA content to verify the cell cycle arrest in G2.

## Abnormal *EXO1* RNA species are produced in the absence of Npl3

Genome-wide analyses have shown that the absence of Npl3 results in either down- or up-regulation of many protein-coding genes [215,231,247]. These analyses did not show significant differences in *EXO1* expression in *npl3Δ* versus wild type cells, suggesting that Npl3 controls the abundance of the Exo1 protein by acting at post-transcriptional level. To verify this possibility, we first employed quantitative reverse transcriptase PCR (qRT-PCR) to measure the amount of *EXO1* RNA either in the presence or in the absence of Npl3. Total RNA was extracted from wild type, *npl3Δ* and *exo1Δ* cells exponentially

growing in YEPD and subjected to reverse transcription followed by quantitative real-time PCR with primer pairs located either inside the *EXO1* coding region (PP1 in *Figure 26A*) or the *ALG9* control gene. The amount of *EXO1* RNA was not diminished in the absence of Npl3 *(Figure 26B)*. Rather, we found a modest increase of *EXO1* RNA levels in *npl3Δ* cells compared to wild type *(Figure 26B)*. The levels of the Exo1 protein *(Figure 17C and D)* were monitored by using a tagged version of the protein generated by inserting a 18 MYC epitopes coding sequence just before the *EXO1* stop codon. Similarly to *EXO1* RNA, the *EXO1-MYC* RNA was slightly more abundant in *npl3Δ* cells than in wild type *(Figure 26B)*, indicating that neither Npl3 nor the insertion of the MYC coding sequence into the *EXO1* gene affects *EXO1* transcription.

If Npl3 promoted *EXO1* pre-mRNA processing, *npl3Δ* cells should accumulate aberrant RNA molecules. Thus, the same RNA extracts were analyzed by northern blot with a 1437 nt DNA probe complementary to the *EXO1* coding sequence *(Figure 26A)*. The probe was specific for the *EXO1* RNA species, as no signal was detected in RNA prepared from *exo1Δ* cells *(Figure 26C)*. In wild type RNA extracts this probe revealed a single band that migrated between the two ribosomal RNA (rRNA) species 25S (3392 nt) and 18S (1798 nt), as expected for the *EXO1* RNA, whose length should be approximately 2400 nt, considering that the average *S. cerevisiae* mRNA consists of the protein coding sequence (2109 nt for *EXO1*) plus 260 nt of 5′ and 3′ untranslated sequences [248]. The same probe detected at least 3 additional longer bands in the *npl3Δ* RNA preparation *(Figure 26C)*, indicating that the absence of Npl3 leads to the generation of longer than normal *EXO1* RNA molecules. Similarly, a single *EXO1* RNA species migrating just below the 3392 nt-long 25S rRNA was detected in cells carrying the *EXO1-MYC* construct, while at least an additional longer band was present in RNA extracts from *npl3Δ EXO1-MYC* cells *(Figure 26D)*. Furthermore, longer than normal *EXO1* RNA molecules were produced also in *npl3-LSNK* cells, where both Npl3 RRM domains were inactivated *(Figure 26E)*. Thus, extended *EXO1* RNA species are produced in the absence of Npl3 or of its RNA-binding capacity, suggesting that Npl3 might regulate initiation, termination or processing of the *EXO1* transcript.

In order to verify whether the abnormal *EXO1* transcripts in *npl3Δ* cells are extended at the 5′ end, we performed 5′ rapid amplification of cDNA ends (5′-RACE) on wild type and *npl3Δ* RNA extracts that were subjected to reverse transcription with an *EXO1* specific primer. A poly(A) tail was added to the resulting cDNA, which was then used as a template for two subsequent PCR reactions with primers annealing to the appended tail and to the *EXO1* coding sequence. A PCR with primers located at the 5′ tail and 248 bp downstream the *EXO1* initiation codon revealed a ∼400 bp abundant product and two weak smaller products in wild type extracts, while a single slightly bigger band was detected in *npl3Δ* *(Figure 26F)*. Although this result suggests that Npl3 influences the use of different transcription start sites in *EXO1* promoter, the small difference in length at the 5′ of the *EXO1* transcripts does not likely account for the extended RNA species observed by northern blot in *npl3Δ* cells *(Figure 26C and E)*.

We then evaluated whether these transcripts were extended at the 3′ end, as Npl3 was recently found to prevent transcriptional readthrough of both protein-coding and non-coding genes [231]. We therefore performed qRT-PCR analyses with different primer pairs located either internally to the *EXO1* coding sequence (PP1 and PP2), or 100, 300, 850, 1000 bp (PP3–PP6, respectively) downstream to the stop codon *(Figure 26A)*. The RNA levels estimated with the different primer pairs were normalized with respect to the RNA levels evaluated with the PP1 primer pair, which were set to 1.0 for each strain *(Figure 26G)*. The RNA levels estimated with the primer pair located immediately before the stop codon (PP2) were almost identical to those evaluated with the primer pair internal to the *EXO1* coding sequence (PP1) in both wild type and *npl3Δ* extracts *(Figure 26G)*. Strikingly, only *npl3Δ* extracts generated products with the primer pairs located downstream to the stop codon (PP3–PP6) *(Figure 26G)*, although the amount of these products was lower (almost 40%) than that of the products obtained with primer pairs internal to the *EXO1* coding sequence *(Figure 26G)*. These results indicate that a substantial fraction of *EXO1* RNA is not properly terminated in the absence of Npl3, thus generating RNA molecules with long 3′ tails that extend at least 1000 bp downstream to the *EXO1* stop codon.

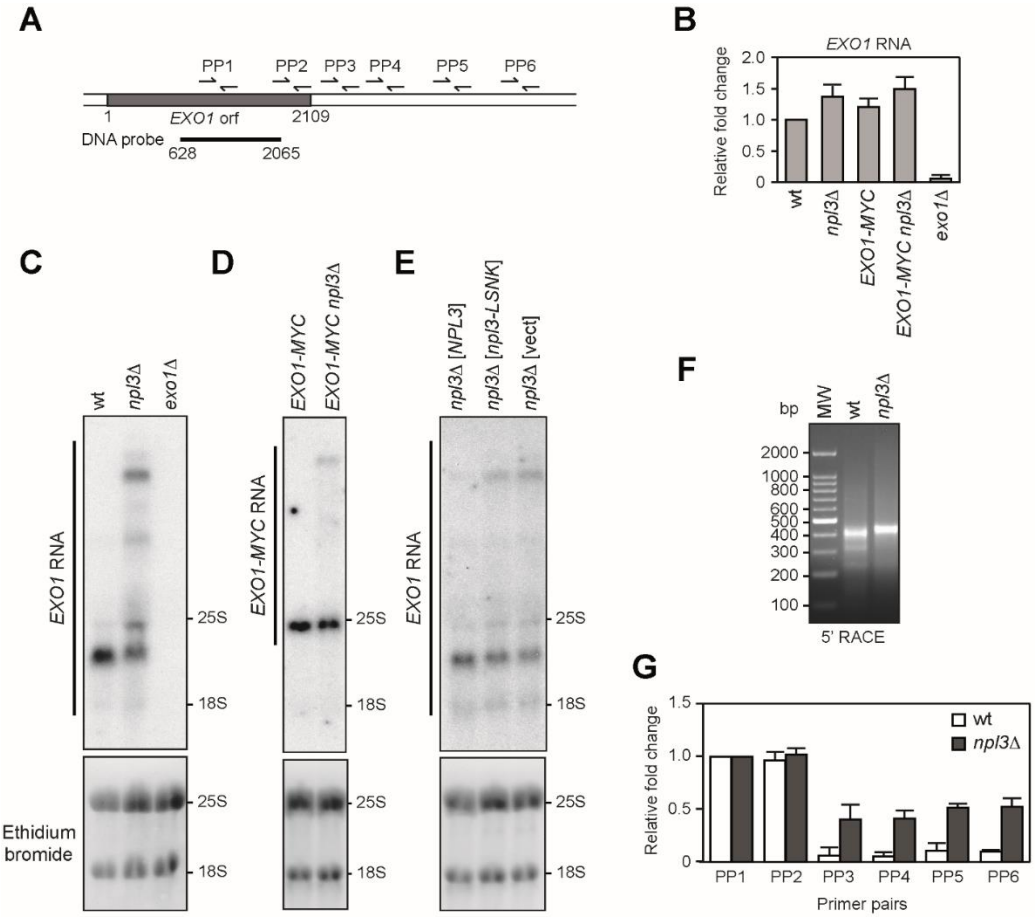


***Figure 26 - EXO1 RNA in the absence of Npl3.***

**(A)** Schematic representation of the *EXO1* locus. Primer pairs (PP1-PP6) used for qRT-PCR are indicated by arrows. A bar indicates the 1437 bp-DNA probe internal to the *EXO1* coding sequence (+628 to + 2065 from the ATG initiation codon) used for northern blot. **(B)** Total RNA was extracted from exponentially growing YEPD cell cultures of the indicated strains and subjected to quantitative reverse transcriptase PCR (qRT-PCR) with primer pairs located into the *EXO1* (PP1 in **(A)**) and *ALG9* coding sequences. The *EXO1* RNA levels relative to wild type (set to 1.0) were calculated using ΔΔCt method after normalization to the *ALG9* RNA levels for each sample. The mean values are represented with error bars denoting SD (n = 5). **(C–E)** Total RNA extracted from the indicated cell cultures was subjected to northern blot and hybridized with the probe as in **(A)**. The agarose gels were stained with ethidium bromide to detect 18S and 25S rRNAs (bottom). **(F)** Total RNA extracted from wild type and *npl3Δ* cells was subjected to 5′ RACE to visualize the *EXO1* 5′ partial cDNA ends. After reverse transcription with a *EXO1* specific primer and poly(A) tailing, two subsequent PCR reactions were performed with primers annealing to the appended tail and to the *EXO1* coding sequence 718 and 248 bp downstream the *EXO1* initiation codon. The final PCR products were separated on a 1.5% agarose gel and visualized with ethidium bromide. **(G)** Total RNA as in **(F)** was subjected to qRT-PCR with primer pairs depicted in **(A)**, or located in the *ALG9* coding sequence. The amount of products obtained with different *EXO1* primer pairs was normalized to the *ALG9* product using ΔΔCt method. Then, the normalized RNA levels estimated with the different primer pairs in the *EXO1* locus were normalized to the RNA levels evaluated with the PP1 primer pair and set to 1.0 for each strain. The mean values are represented with error bars denoting SD (n = 4).

### Rrp6 controls the levels of the *EXO1* RNA

It is known that 3′-extended RNAs might be unstable and targeted to degradation by the RNA decay systems. In particular, defects in 3′-end processing result in nuclear retention and degradation of faulty transcripts mainly by the nuclear exosome [227]. To test whether the nuclear exosome degrades the extended *EXO1* RNA molecules produced in the absence of Npl3, we checked if these abnormal *EXO1* RNAs further accumulate in *npl3Δ* cells lacking the exosome catalytic subunit Rrp6, whose lack was reported to impair viability of *npl3Δ* cells [249]. In our genetic background, *npl3Δ rrp6Δ* spores generated by sporulation and tetrad dissection of a *NPL3*/*npl3Δ RRP6*/*rrp6Δ* diploid gave rise to very small colonies, which could be further propagated in YEPD, despite their growth defect *(Figure 27A and E)*. We then subjected to both qRT-PCR and northern blot analysis the *EXO1* RNAs derived from exponentially growing wild type, *npl3Δ*, *rrp6Δ* and *npl3Δ rrp6Δ* cells. Both analyses revealed higher levels of *EXO1* RNA in *npl3Δ rrp6Δ* cells than in *npl3Δ* and *rrp6Δ* single mutants *(Figure 27B and C)*. The intensity of the bands detected by the *EXO1* probe in the northern blot, and in particular that of the slowest migrating band, was higher in *npl3Δ rrp6Δ* RNA extracts than in *npl3Δ (Figure 27C)*, suggesting that Rrp6 partially removes abnormal RNA intermediates that accumulate in the absence of Npl3.

As the amount of the 2400 nt-long *EXO1* RNA species was also higher in *npl3Δ rrp6Δ* cells compared to *npl3Δ* cells *(Figure 27C)*, we asked whether the absence of Rrp6 also increased the levels of Exo1 protein in cells lacking Npl3. Indeed, the amount of the Exo1-MYC tagged variant was slightly higher in exponentially growing *npl3Δ rrp6Δ* cells than in *npl3Δ* cells *(Figure 27D)*. This suggests that, in the presence of improperly processed transcripts, the exosome targets not only the faulty, but also some functional *EXO1* RNA molecules. Interestingly, although *npl3Δ rrp6Δ* cells grew poorly on YEPD plates *(Figure 27A and E)*, they formed colonies in the presence of CPT more efficiently than *npl3Δ* cells *(Figure 27E)*, similarly to what we observed with the overexpression of the *EXO1* gene *(Figure 21D)*. Taken together, these results indicate that Npl3 promotes

proper maturation of the *EXO1* RNA, thus preventing its degradation by the nuclear exosome.

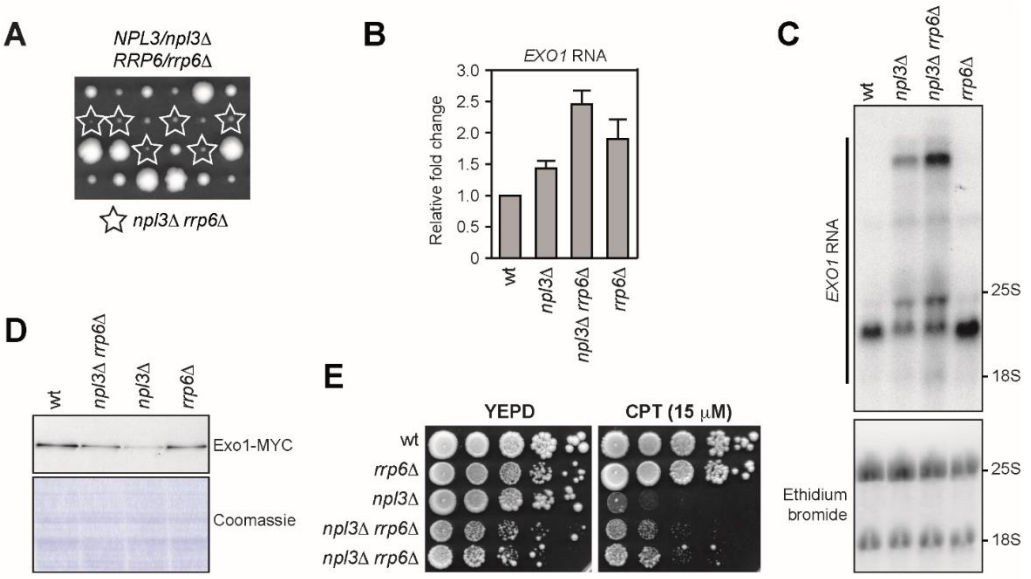


***Figure 27 - Rrp6 limits the accumulation of abnormal EXO1 RNAs in the absence of Npl3.***

**(A)** Meiotic tetrads from diploid cells with the indicated genotype were dissected on YEPD plates that were incubated at 30°C for 3 days, followed by spore genotyping. **(B, C)** Total RNA was extracted from exponentially growing YEPD cultures of the indicated strains and subjected to both qRT-PCR as in *Figure 26B* and northern blot as in *Figure 26C–E*. **(D)** The same amounts of protein extracts prepared from exponentially growing cell cultures with the indicated genotypes and expressing the Exo1-MYC tagged protein were either stained with Coomassie or subjected to western blot with anti-MYC antibodies. **(E)** Exponentially growing cell cultures of the indicated strains were spotted out onto YEPD plates with or without CPT.

**Genetics**
Early online December 11, 2018
doi: 10.1534/genetics.118.301830

GENETICS

# Uncoupling Sae2 functions in downregulation of Tel1 and Rad53 signalling activities

Chiara Vittoria Colombo, Luca Menin, Riccardo Ranieri, Diego Bonetti, Michela Clerici, and Maria Pia Longhese

Dipartimento di Biotecnologie e Bioscienze, Università di Milano-Bicocca, 20126 Milano, Italy

Mechanisms devoted to repair DNA lesions are essential for maintaining genome integrity. Their dysfunction is observed in many cancers and underlies the genomic instability that accompanies tumorigenesis. Among DNA lesions, DNA double strand breaks (DSBs) are the most severe ones because they have the potential to cause loss of genetic information and chromosomal rearrangements [9]. Mitotic DSBs can be repaired by homologous recombination (HR), which requires that the 5' strands at both DSB ends are nucleolytically degraded (resected) [136,224]. Then, the generated 3' single-stranded DNA (ssDNA) tails can invade an undamaged homologous DNA template, like the sister chromatid or the homologous chromosome [9].

In both yeast and mammals, DSB resection is initiated by the Mre11-Rad50-Xrs2 (MRX) complex (Mre11-Rad50-Nbs1, MRN, in mammals). MRX/MRN catalyzes an endonucleolytic cleavage of the 5' strands at both DSB ends, with the Sae2 protein (CtIP in mammals) promoting this endonucleolytic activity [40]. The MRX-Sae2 clipping activity is particularly important to eliminate proteins covalently attached to the 5' DNA ends and to generate an entry site for the long-range resection nucleases Exo1 and Dna2, the latter working in concert with the helicase Sgs1 (BLM in humans) [56,62,63,73,74,86,87]. Mre11 also has an exonuclease activity, which digests DNA ends in the 3'-5' direction towards the DSB end, while Exo1 and Dna2-Sgs1 take over resection in the 5'-3' direction from the gap [250,251].

DNA DSB generation triggers activation of the checkpoint protein kinases Mec1 (ATR in mammals) and Tel1 (ATM in mammals), which sense and signal the presence of DNA DSBs leading to arrest of cell cycle progression [41,224]. While Tel1/ATM is recruited on blunt DSB ends or DNA ends with short ssDNA tails [173,174], Mec1/ATR (in association with Ddc2/ATRIP) recognizes RPA-coated ssDNA that results from resection of DSB DNA ends [162,252,253]. Once activated by damaged DNA, Tel1 and Mec1 can propagate the checkpoint signals through the Rad53 and Chk1 effector kinases (Chk2 and Chk1 in mammals, respectively) [144]. Rad53 activation requires the BRCT-domain-containing protein Rad9 (53BP1 in mammals). Rad9 undergoes Mec1- and/or Tel1-dependent phosphorylation upon DNA damage [254,255], and these phosphorylation events create a

binding site for Rad53, thus allowing Rad53 in-trans autophosphorylation that leads to Rad53 full activation as a kinase [134,176–178,190,256,257].

MRX and Sae2 can modulate Tel1 activation in opposite manner. In fact, the lack of any MRX/MRN subunit abolishes Tel1/ATM activation by preventing its association to DSBs [156,157,258–260], indicating that MRX/MRN is required for Tel1/ATM recruitment to DSBs. By contrast, the lack of Sae2 enhances Tel1 signalling activity by increasing MRX, and therefore Tel1, persistence at the DSB ends [35,66,123,131,261]. This persistent MRX-Tel1 activation in *sae2Δ* cells is associated with enhanced activity of the downstream checkpoint kinase Rad53 that causes a permanent cell cycle arrest [66,261].

The enhanced MRX-Tel1-Rad53-mediated checkpoint activation has been proposed to account for the DNA damage hypersensitivity and the DSB resection defect of *sae2Δ* cells. In fact, *mre11* mutant alleles that reduce MRX binding to DSBs restore DNA damage resistance and resection in *sae2Δ* cells [67,68,262]. A similar effect also occurs when Tel1 function is compromised either by reducing its association to DSBs or by abrogating its kinase activity [132]. Moreover, impairment of Rad53 activity either by affecting its interaction with Rad9 or by abolishing its kinase activity suppresses both the hypersensitivity to DNA damage and the resection defect of *sae2Δ* cells [132]. The bypass of Sae2 function in DNA damage resistance and resection by Rad53 and Tel1 impairment is due to decreased amount of Rad9 bound at DSBs [132]. As Rad9 limits DSB resection by inhibiting Sgs1-Dna2 [107,108], reduced Rad9 association at DSBs relieves inhibition of Sgs1-Dna2 resection activity, thus increasing DSB resection even in the absence of Sae2. These findings lead to a model whereby Sae2 ensures DNA damage resistance and resection by negatively regulating MRX association to DNA DSBs and therefore Rad53 activation.

To better understand the contribution of MRX, Tel1 and Rad53 to the DNA damage hypersensitivity of Sae2 lacking cells and how Sae2 modulates the signalling activities of the above factors, we searched for *sae2* alleles that failed to inhibit Tel1 activation but retained Sae2 function in supporting DNA damage resistance. Here, we describe the hypomorphic *sae2-ms* allele that, similar to *sae2Δ*, enhances Tel1 signalling activity

by increasing MRX and Tel1 persistence at DSBs. However, unlike *SAE2* deletion, the Sae2-ms mutant variant is capable to support DNA damage resistance, indicating that MRX persistence at DSBs is not responsible for the increased DNA damage sensitivity of *sae2Δ* cells. Furthermore, Sae2-ms does not enhance Rad53 activation, indicating separable functions of Sae2 in downregulation of MRX-Tel1 and Rad53 signalling activities. Accordingly, the lack of Sae2, but not the presence of Sae2-ms, enhances Rad53 activation by increasing Rad53-Rad9 interaction even in the absence of DNA damage and this function occurs independently of MRX nuclease activity. Altogether, these data indicate that Sae2 function in controlling MRX removal from DSB is separable from that leading to Rad53 downregulation.

## Search for *sae2* alleles that hyperactivate Tel1 but do not cause DNA damage sensitivity

Cells lacking Sae2 show hypersensitivity to DNA damaging agents and persistent DNA damage-induced checkpoint activation that causes a prolonged cell cycle arrest [19,66,261]. This enhanced checkpoint signalling is due to increased MRX occupancy at DSBs, which activates a Tel1-dependent checkpoint that is accompanied by persistent Rad53 phosphorylation [35,66,261]. How Sae2 modulates MRX-Tel1 and Rad53 signalling activities at DSBs is poorly understood.

To gain insights into the role of Sae2 in DNA damage resistance and downregulation of the checkpoint response, we searched for separation-of-functions *sae2* mutants that hyperactivated Tel1, similar to *sae2Δ* cells, but conserved Sae2 function in DNA damage resistance. We took advantage of the finding that Tel1 hyperactivation allows *SAE2* deletion to suppress the hypersensitivity to hydroxyurea (HU) and methyl methanesulfonate (MMS) of Mec1 lacking cells kept viable by *SML1* deletion *(Figure 28A)* [261]. We random mutagenized the *SAE2* gene by low-fidelity PCR, followed by transformation of *mec1Δ sml1Δ* cells with the obtained linear *SAE2* PCR products, in

order to replace the corresponding *SAE2* wild type sequence with the mutagenized DNA fragments. Transformant clones were first chosen based on their increased viability in the presence of HU and MMS compared to *mec1Δ* cells. Among them, we selected for further characterization the clones that were more resistant to camptothecin (CPT) and phleomycin (phleo) compared to *sae2Δ* cells after transformation with a plasmid carrying the wild type *MEC1* gene.

By the above analysis we identified the *sae2-ms* allele, whose sequencing revealed three missense mutations leading to replacement of Ser134 with Leu, Pro217 with Thr and Ala230 with Val, respectively. Similar to *sae2Δ mec1Δ* cells, *sae2-ms mec1Δ* cells showed increased viability in the presence of HU or MMS compared to *mec1Δ* cells *(Figure 28A)*, indicating that the *sae2-ms* allele compensates for Mec1 deficiency under genotoxic treatments. Unlike *SAE2* deletion that, by itself, causes hypersensitivity to HU, MMS, CPT and phleomycin, *sae2-ms* cells did not lose viability in the presence of any of the above tested drugs *(Figure 28B)*, indicating that Sae2-ms mutant variant maintain Sae2 function in DNA damage resistance.

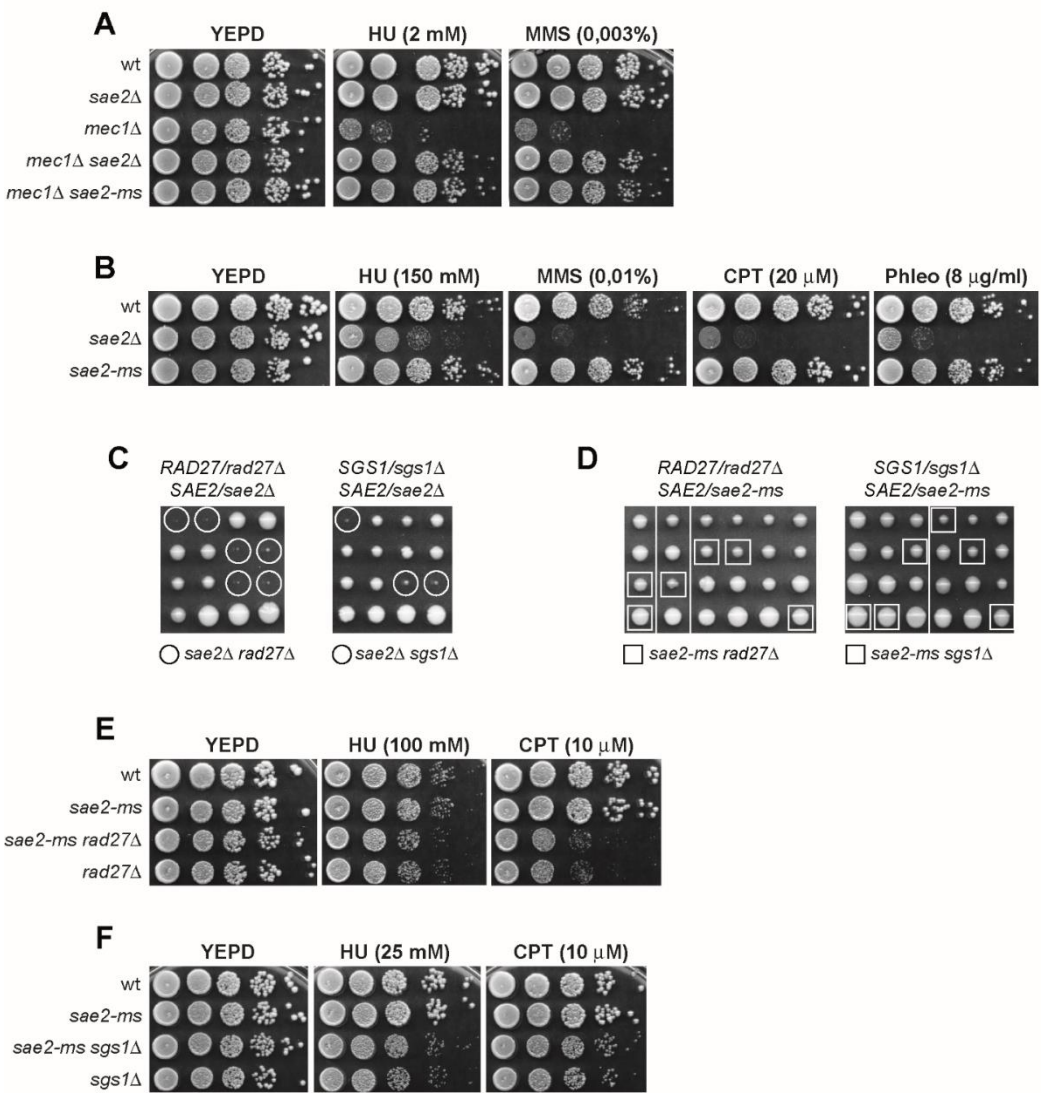


***Figure 28 - Sae2-ms suppresses the hypersensitivity to HU and MMS of mec1Δ cells.***

**(A,B)** Exponentially growing cells were serially diluted (1:10) and each dilution was spotted out onto YEPD plates with or without HU, MMS, CPT or phleomycin at the indicated concentrations. All strains in **(A)** carried *SML1* deletion. **(C,D)** Meiotic tetrads were dissected on YEPD plates that were incubated at 25°C, followed by spore genotyping. **(E,F)** Exponentially growing cells were serially diluted (1:10) and each dilution was spotted out onto YEPD plates with or without HU or CPT at the indicated concentrations.

## Sae2-ms supports viability of *rad27Δ* and *sgs1Δ* cells

Synthetic lethality/sickness is observed when deletion of *SAE2* is combined with deletion of *RAD27*, which encodes for a nuclease involved in Okazaki fragment processing during lagging strand DNA synthesis [263], suggesting that Sae2 is required to process lesions generated in a *rad27Δ* background [264,265]. A similar synthetic effect is also seen when *SAE2* is deleted in cells lacking the helicase Sgs1, possibly due to defective DSB resection and excessive telomere shortening [56,266].

To determine whether the Sae2-ms variant maintains the Sae2 functions mentioned above, diploid cells heterozygous for both *rad27Δ* and *sae2-ms* or *sgs1Δ* and *sae2-ms* were generated and, after sporulation, tetrads were dissected to determine whether viable *rad27Δ sae2-ms* or *sgs1Δ sae2-ms* spores could be obtained. As expected, *rad27Δ sae2Δ* and *sgs1Δ sae2Δ* spores were unviable or grew so slowly that could not be further propagated *(Figure 28C)*. By contrast, the *rad27Δ sae2-ms* and *sgs1Δ sae2-ms* spores grew remarkably well *(Figure 28D)*. Furthermore, *sae2-ms* did not exacerbate the hypersensitivity to HU and CPT of *rad27Δ (Figure 28E)* and *sgs1Δ* cells *(Figure 28F)*. These findings indicate that Sae2-ms maintains Sae2 function in supporting cell viability in the absence of Rad27 or Sgs1 both in the presence and in the absence of DNA damage.

## Sae2-ms maintains Sae2 functions in end-tethering and resection

Sae2 promotes DSB repair by supporting DNA-end resection and by maintaining the DSB ends adjacent to each other to facilitate DSB repair by both HR and NHEJ [57]. *SAE2* deletion was shown to severely impair DSB repair by single-strand annealing (SSA) [57]. This mechanism repairs a DSB flanked by direct DNA repeats when sufficient resection exposes the complementary DNA sequences that can then anneal to each other, resulting in deletion of the DNA region between the repeats [267–269]. We assessed whether Sae2-ms affects DSB repair by SSA by introducing the *sae2-ms* allele in the

YMV45 strain, which carries an HO endonuclease cleavage site flanked by two direct sequence repeats of the *LEU2* gene located 4.6 kb from each other on chromosome III [269]. This strain also carries a *GAL-HO* construct for galactose-inducible *HO* expression. Galactose was added to induce HO production and it was maintained in the medium so that continuously produced HO could re-cleave the HO sites eventually reconstituted by NHEJ. When kinetics of DSB repair was monitored by Southern blot analysis with a *LEU2* probe, accumulation of the SSA repair product after HO induction was reduced in *sae2Δ* cells compared to wild type, as expected, whereas it occurred with almost wild type kinetics in *sae2-ms* cells *(Figure 29A and B)*, indicating that Sae2-ms does not affect DSB repair by SSA.

The severe SSA-mediated DSB repair defect in *sae2Δ* cells has been attributed to the lack of Sae2 function in both DNA-end tethering and resection [57]. We then assessed more directly the ability of Sae2-ms to support end-tethering by using a strain where the DNA proximal to an irreparable HO-inducible DSB can be visualized by the binding of a LacI-GFP fusion protein to multiple repeats of the LacI repressor binding site, which is integrated at a distance of 50 kb on both sides of the HO cut site [270]. HO expression was induced by galactose addition to cell cultures that were arrested and kept blocked in G2 by nocodazole treatment to ensure that all cells would remain arrested in metaphase. Most wild type and *sae2-ms* cells showed a single LacI-GFP focus after HO induction, indicating their ability to maintain the broken DNA ends together, whereas *sae2Δ* cells showed an increase of cells with two LacI-GFP spots after HO induction, as expected *(Figure 29C)* [57].

We also tested more directly the ability of *sae2-ms* cells to resect a DSB by monitoring ssDNA formation after induction of a DSB at the *MAT* locus in JKM139 derivative strains expressing the *HO* gene from the galactose-inducible *GAL1* promoter [234]. The *HML* and *HMR* loci were deleted in these strains to prevent DSB repair by gene conversion. Resection of the HO-induced DSB renders the DNA sequence flanking the HO break resistant to cleavage by restriction enzymes, resulting in the appearance of resection intermediates that can be detected by Southern blot analysis with a probe that anneals

to the 3' end at one side of the break. As expected, *sae2Δ* cells showed a slight defect in DSB resection compared to wild type, whereas *sae2-ms* cells resected the DSB with wild type kinetics *(Figure 29D and E)*.

We proposed that the resection defect of *sae2Δ* cells is due to increased association at DSB ends of Rad9, which inhibits DSB resection [107,108,132]. Consistent with no DSB resection defects in *sae2-ms* cells, the amount of Rad9 bound at the HO-induced DSB in *sae2-ms* cells was similar to that detected in wild type cells, whereas it was higher in *sae2Δ* cells than in wild type, as expected *(Figure 29F)*. Furthermore, *SAE2* deletion exacerbated the DNA damage hypersensitivity of *exo1Δ* cells, possibly due to a more severe resection defect in the double mutant compared to each single mutant [74], while the *sae2-ms* mutation did not *(Figure 29G)*. Finally, *sae2-ms* cells did not increase the efficiency of ligation by NHEJ of a self-replicating plasmid *(Figure 29H)*, which was instead increased in *sae2Δ* cells likely because the reduced ssDNA generation increases the ability of NHEJ repair to occur. Altogether, these findings indicate that Sae2-ms does not impair either DNA end-tethering or resection.

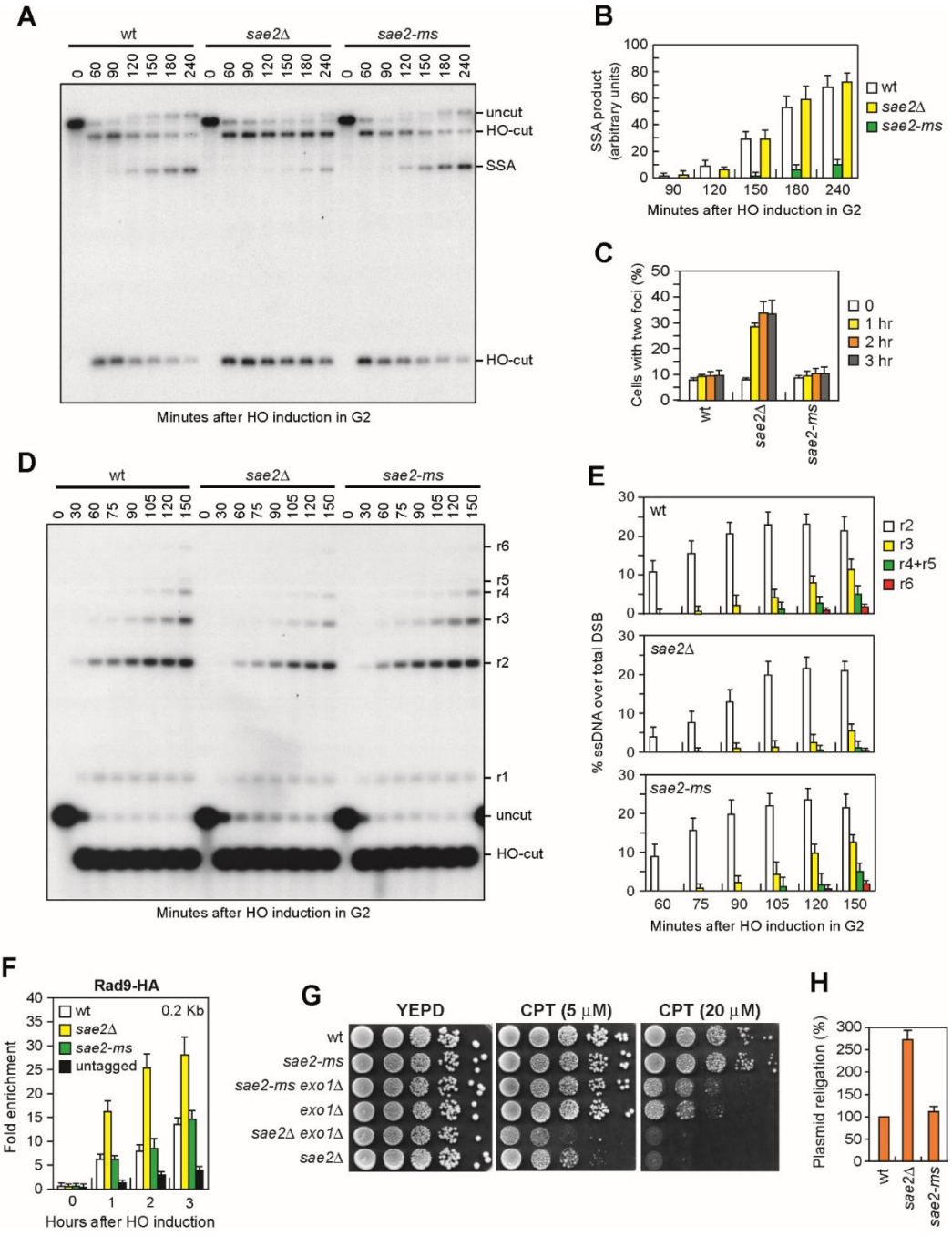


***Figure 29 - Sae2-ms is proficient in DSB resection and end-tethering.***

**(A)** Exponentially growing YEPR cell cultures were arrested in G2 with nocodazole and transferred to YEPRG in the presence of nocodazole at time zero to induce HO expression. Southern blot analysis of KpnI-digested genomic DNA with a *LEU2* probe. **(B)** Densitometric analysis. The experiment as in **(A)** was independently repeated and the mean values are represented with error bars denoting s.d. (n=3). **(C)** DSB

end-tethering. Exponentially growing YEPR cell cultures were arrested in G2 with nocodazole at time zero and transferred to YEPRG in the presence of nocodazole at time zero. 200 cells for each strain were analyzed to determine the percentage of cells showing two LacI-GFP foci. **(D)** DSB resection. YEPR exponentially growing cultures of JKM139 derivative strains were arrested in G2 with nocodazole and transferred to YEPRG in the presence of nocodazole at time zero to induce HO expression. SspI-digested genomic DNA was separated on alkaline agarose gel and hybridized with a single-stranded *MAT* probe that anneals to the unresected 3' end at one side of the break. 5'-3' resection progressively eliminates SspI sites, producing larger SspI fragments (r1 through r7) that can be detected by the probe. **(E)** Densitometric analysis. The experiment as in **(D)** was independently repeated and the mean values are represented with error bars denoting s.d. (n=3). **(F)** ChIP analysis. HO was induced at time zero in exponentially growing JKM139 derivative cells. Relative fold enrichment of Rad9-HA protein at the indicated distance from the HO cleavage site was determined after ChIP with anti-HA antibodies and qPCR analysis. Plotted values are the mean values with error bars denoting s.d. (n=3). **(G)** Exponentially growing cells were serially diluted (1:10) and spotted out onto YEPD plates with or without CPT at the indicated concentrations. **(H)** Plasmid re-ligation assay. The same amounts of BamHI-linearized pRS316 plasmid DNA were transformed into the cells. Data are expressed as percentage of re-ligation relative to wild type that was set up at 100% after normalization to the corresponding transformation efficiency of the uncut plasmid.

## Suppression of Mec1 deficiency by Sae2-ms requires Tel1, Rad9 and Rad53

Tel1 promotes activation of the downstream effector kinase Rad53 in response to DNA damage, and this activation requires Rad9 [41]. To assess whether suppression of the DNA damage hypersensitivity of *mec1Δ* cells by Sae2-ms is due to hyperactivation of a Tel1-mediated checkpoint response, we asked whether *mec1Δ* suppression by *sae2-ms* requires Tel1, Rad9 and/or Rad53. The *sae2-ms* allele failed to suppress the HU hypersensitivity of *tel1Δ mec1Δ* cells, which lose viability even in the absence of DNA damage compared to each single mutant *(Figure 30A)*, possibly due to premature senescence. Similarly, *sae2-ms* did not restore HU resistance of *mec1Δ* cells carrying either *RAD9* deletion *(Figure 30B)* or the kinase defective *rad53-K227A* allele *(Figure 30C)*. These findings indicate that the bypass of Mec1 function by Sae2-ms requires the Tel1, Rad9 and Rad53 checkpoint proteins. Consistent with the finding that this bypass requires Tel1, suppression of HU sensitivity in *mec1Δ sae2-ms* double mutant cells was unaffected by the lack of Ddc1 *(Figure 30D)*, which interacts with Mec3 and Rad17 to form a heterotrimeric complex that stimulates Mec1 kinase activity but not Tel1 kinase activity [41].

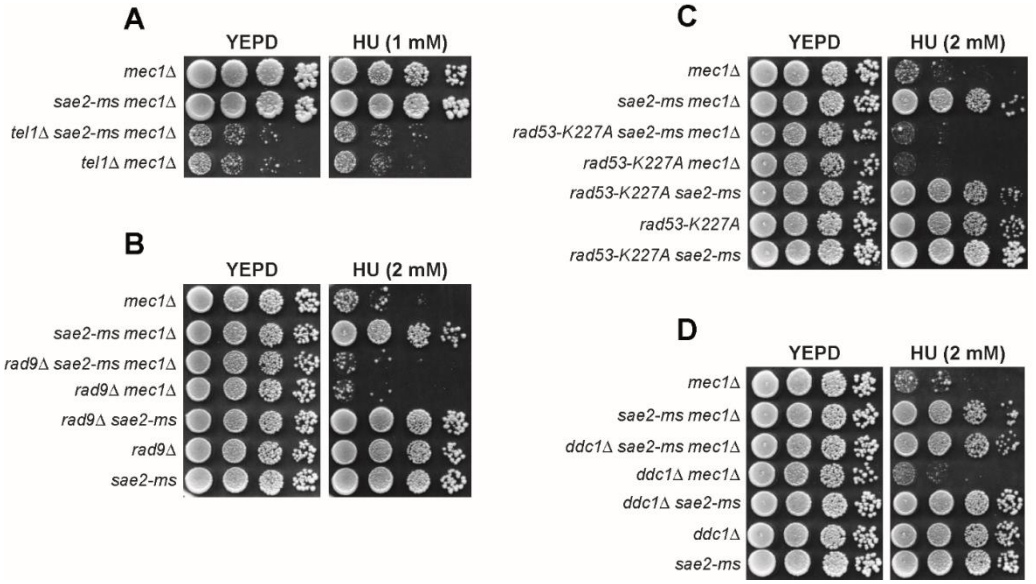


***Figure 30 - Sae2-ms requires Tel1, Rad53 and Rad9 for suppression of Mec1 deficiency.***

**(A-D)** Exponentially growing cells were serially diluted (1:10) and each dilution was spotted out onto YEPD plates with or without HU at the indicated concentrations.

## The sae2-S134L mutation is responsible for suppression of Mec1 deficiency

The Sae2-ms mutant variant carries the three aminoacidic substitutions S134L, P217T and A230V. We asked which substitution(s) was responsible for the suppression of *mec1Δ* hypersensitivity to DNA damage by constructing strains expressing *sae2-S134L* or *sae2-P217T, A230V* allele. Comparison analysis revealed that the *sae2-S134L* allele restored resistance of *mec1Δ* cells to HU and MMS to a level similar to that observed in *sae2-ms mec1Δ* cells, whereas the *sae2-P217T, A230V* allele did not *(Figure 31A)*. Thus, effective *mec1Δ* suppression appears to be exclusively due to the S134L aminoacid substitution. Similar to *sae2-ms* cells, *sae2-S134L* cells were not hypersensitive to DNA damaging agents *(Figure 32)*.

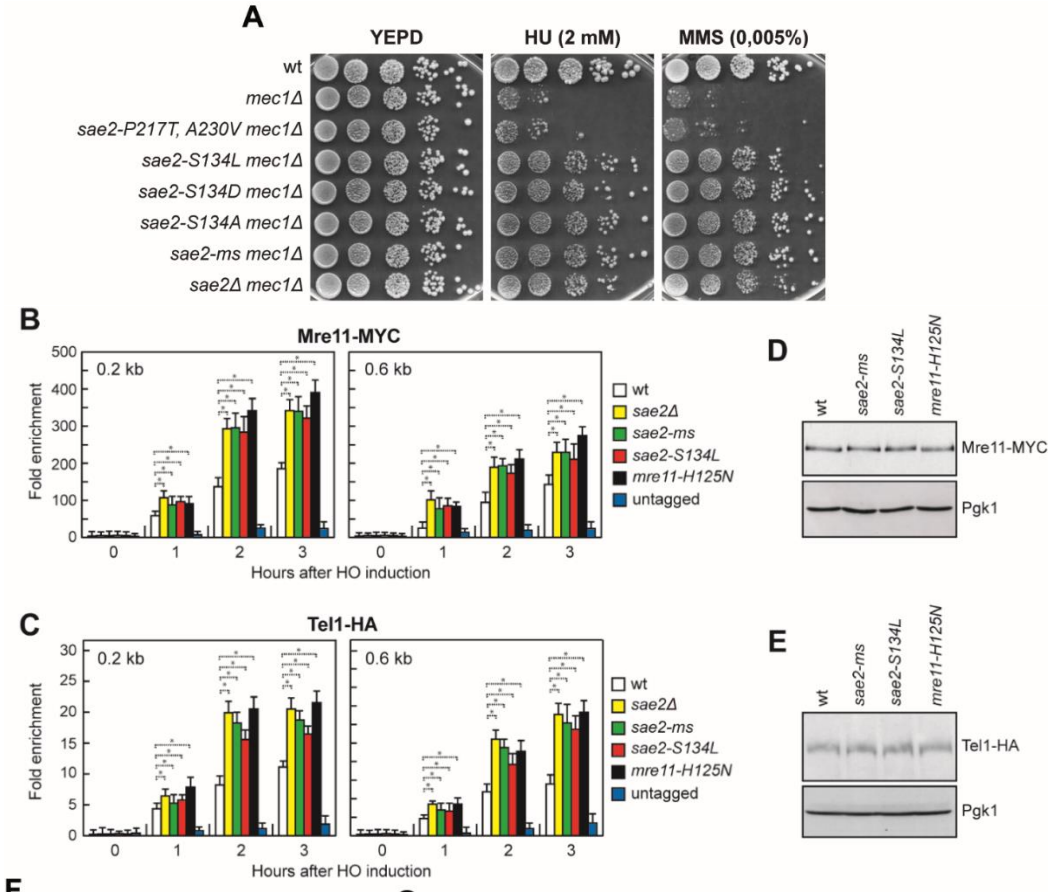


| | Recombination rate ($10^{-7}$) |
|---|---|
| wt | 1,708 (±238) |
| *mre11-H125N* | 14 (±5) |
| *sae2Δ* | 17 (±3) |
| *sae2-ms* | 157 (±10) |
| *sae2-S134L* | 188 (±34) |

***Figure 31 - Sae2-ms and Sae2-S134L enhance Mre11 and Tel1 association to DSBs and reduce hairpin cleavage.***

**(A)** Exponentially growing cells were serially diluted (1:10) and spotted out onto YEPD plates with or without HU or MMS at the indicated concentrations. **(B)** ChIP analysis. HO was induced at time zero in exponentially growing JKM139 derivative cells. Relative fold enrichment of Mre11-Myc protein at the indicated distances from the HO cleavage site was determined after ChIP with anti-Myc antibodies and subsequent qPCR analysis. Plotted values are the mean values with error bars denoting s.d. (n=3). *P<0.05 (Student's t-test). **(C)** As in **(B)**, but showing relative fold enrichment of Tel1-HA after ChIP with anti-HA antibodies. **(D,E)** Western blot analysis with anti-Myc or anti-HA antibodies of protein extracts prepared from exponentially growing cells. The same amount of extracts was probed with anti-Pgk1 antibodies as loading control. **(F)** Recombination frequency of strains with the *lys2-AluIR* and *lys2-Δ5'* ectopic

recombination system. The rate of Lys+ recombinants was derived from the median recombination frequency. Plotted values are the mean values with error bars denoting s.d. (n=3). **(G)** Exponentially growing cells were serially diluted (1:10) and spotted out onto YEPD plates with or without HU or MMS at the indicated concentrations.

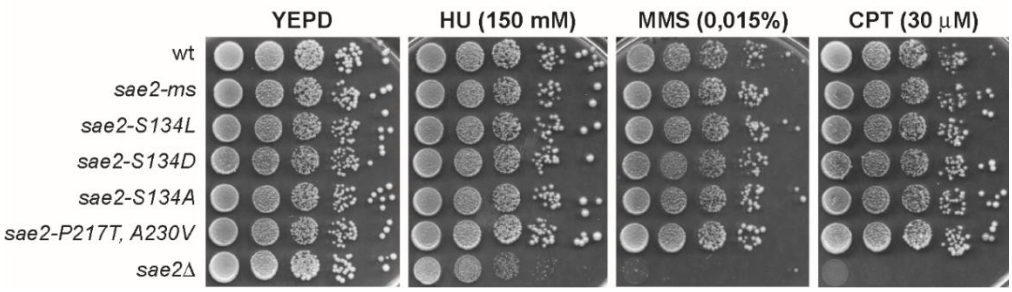


***Figure 32 - Sae2-ms and Sae2-S134L do not cause DNA damage sensitivity.***

Exponentially growing cells were serially diluted (1:10) and each dilution was spotted out onto YEPD plates with or without HU, MMS or CPT at the indicated concentrations.

The Sae2 S134 residue was shown to be phosphorylated by Cdk1 [58,61], prompting us to test the effect of substituting this residue with either the non phosphorylatable alanine residue or aspartic acid that mimics constitutive phosphorylation. We found that the *sae2-S134A* allele suppressed the HU and MMS sensitivity of *mec1Δ* cells as efficiently as *sae2-S134L* *(Figure 31A)*. However, also the S134D aminoacid substitution restored resistance of *mec1Δ* cells to HU and MMS *(Figure 31A)*, suggesting that the negative charge associated with the phosphorylation event of S134 is not relevant for Sae2 function in bypassing Mec1 deficiency. Consistent with this hypothesis, substitution with Valine of the E131 residue, which is located close to S134, suppressed the sensitivity to MMS of *mec1Δ* cells without causing DNA damage hypersensitivity [271], suggesting that the region of the protein surrounding these residues rather than S134 phosphorylation is important for the bypass of Mec1 function.

## Sae2-S134L and Sae2-ms reduce hairpin cleavage and increase MRX and Tel1 association at DNA DSBs

Previous work has established that *SAE2* deletion leads to increased MRX persistence at DSBs that can account for enhanced Tel1 activation and bypass of Mec1 deficiency [66,261]. Thus, we measured Mre11 and Tel1 association at DSBs by Chromatin Immunoprecipitation (ChIP) and quantitative PCR (qPCR). Association to DNA DSBs of both Mre11 *(Figure 31B)* and Tel1 *(Figure 31C)* was more robust and persisted longer not only in *sae2Δ* cells, but also in *sae2-ms* and *sae2-S134L* cells, indicating that Sae2-ms and Sae2-S134L increase the amount of MRX and Tel1 bound at DSBs. The increased Mre11 and Tel1 association was not due to increased Mre11 or Tel1 amounts, as similar levels of Mre11 *(Figure 31D)* and Tel1 *(Figure 31E)* proteins were detected in protein extracts from wild type, *sae2-ms* and *sae2-S134L* cells.

Sae2 is known to promote the Mre11 endonucleolytic activity within the MRX complex [40]. The *mre11-H125N* mutation, which specifically eliminates Mre11 nuclease activity, increases MRX and Tel1 persistence at DSBs *(Figure 31B and C)* [35,66], suggesting that this activity is responsible for MRX displacement from DSBs. Thus, we investigated whether the *sae2-ms* and *sae2-S134L* mutations might specifically affect it. As the Mre11 nuclease activity and Sae2 are required to open DNA hairpin structures both *in vitro* and *in vivo* [270,272], we used a genetic assay to measure hairpin resolution in *sae2-ms* and *sae2-S134L*. Inverted Alu elements inserted in the *lys2* gene on chromosome III form a hairpin-capped end whose opening by the MRX nuclease and Sae2 stimulates recombination with a truncated *lys2* gene on chromosome II to generate Lys+ cells [270]. As expected, *sae2Δ* and the nuclease defective *mre11-H125N* cells showed decreased rates of Lys+ cells generation compared to wild type cells *(Figure 31F)*. Interestingly, the generation rates of Lys+ prototrophs were reduced also in *sae2-ms* and *sae2-S134L* cells, although to lower extents than in *sae2Δ* cells *(Figure 31F)*. These findings suggest that Sae2-ms and Sae2-S134L can impair MRX removal from the sites of DNA damage by altering Mre11 nuclease activity.

However, although Mre11-H125N persisted longer at DNA DSBs *(Figure 31B)* and led to increased Tel1 association at DSBs *(Figure 31C)*, it did not suppress the hypersensitivity to HU of *mec1Δ* cells and only slightly suppressed their hypersensitivity to MMS *(Figure 31G)*. This finding suggests that upregulation of MRX and Tel1 is not sufficient to bypass Mec1 deficiency in the presence of the Mre11-H125N mutant variant.

## Sae2 plays distinct functions in downregulation of MRX-Tel1 and Rad53 activities

Activation of Rad53 requires its interaction with the adaptor Rad9 that is phosphorylated by Mec1/Tel1 [134,176–178,190,254–257]. To better understand the effects of Sae2-ms and Sae2-S134L on Tel1-mediated Rad53 activation, we analyzed Rad9 and Rad53 phosphorylation, detected as electrophoretic mobility shifts, in *mec1Δ*, *sae2Δ mec1Δ*, *sae2-ms mec1Δ* and *sae2-S134L mec1Δ* cells arrested in G1 and then released into the cell cycle in the presence of MMS. As expected, MMS-treated *mec1Δ* cells showed a decrease of both Rad9 *(Figure 33A)* and Rad53 phosphorylation *(Figure 33B)* compared to wild type cells. Consistent with the finding that the *sae2Δ*, *sae2-ms* and *sae2-S134L* alleles increase Tel1 signalling activity, Rad9 phosphorylation was increased in MMS-treated *sae2Δ mec1Δ*, *sae2-ms mec1Δ* and *sae2- S134L mec1Δ* cells compared to *mec1Δ* cells *(Figure 33A)*. However, while *sae2Δ mec1Δ* cells showed also enhanced Rad53 phosphorylation compared to *mec1Δ* cells, *sae2-ms mec1Δ* and *sae2-S134L mec1Δ* cells did not *(Figure 33B)*. The inability of *sae2-ms mec1Δ* and *sae2-S134L mec1Δ* cells to hyperactivate Rad53 compared to *sae2Δ mec1Δ* cells is not due to a more efficient DNA repair, as *sae2-ms* and *sae2-S134L* cells did not show Rad53 hyperactivation also in response to a single irreparable DSB *(Figure 33C)*. In fact, when cultures of JKM139 derivative strains were transferred to galactose to induce HO, *sae2Δ mec1Δ* cells showed increased amount of Rad53 phosphorylation compared to *mec1Δ* cells, while neither *sae2-ms mec1Δ* nor *sae2-S134L mec1Δ* cells did it *(Figure 33C)*.

These findings indicate that Sae2-ms and Sae2-S134L mutant variants are defective in downregulating MRX-Tel1 signalling, but not Rad53 signalling.

Cells carrying a single irreparable DSB undergo checkpoint-mediated cell cycle arrest, but then they adapt to this checkpoint, decreasing Rad53 activation and re-entering the cell cycle [235,273]. The heightened Rad53 activation in *sae2Δ* cells prevents the turning off of the checkpoint triggered by a single irreparable DSB [66]. To assess further that Tel1/MRX upregulation by Sae2-ms and Sae2-S134L does not increase Rad53 activation, we analysed the ability of *sae2-ms* and *sae2-S134L* cells to adapt to a single irreparable DSB. When G1-arrested cell cultures of JKM139 derivative strains were spotted on galactose-containing plates to induce HO, most *sae2Δ* cells were still arrested at the two-cell dumbbell stage after 20 hours, whereas wild type, *sae2-ms* and *sae2-S134L* cells overrode the checkpoint-mediated cell cycle arrest within 16 hours, producing microcolonies with four or more cells *(Figure 33D)*. Moreover, when galactose was added to exponentially growing cell cultures of the same strains, Rad53 phosphorylation decreased in wild type, *sae2-ms* and *sae2-S134L* cells 12-14 hours after galactose addition, while it persisted throughout the experiment in *sae2Δ* cells *(Figure 33E)*. Altogether, these findings indicate that Sae2-ms and Sae2-S134L mutant variants are specifically defective in downregulating MRX-Tel1 activation but not Rad53 activation, indicating that Sae2 plays distinct functions in the inhibition of MRX-Tel1 and Rad53 activities.

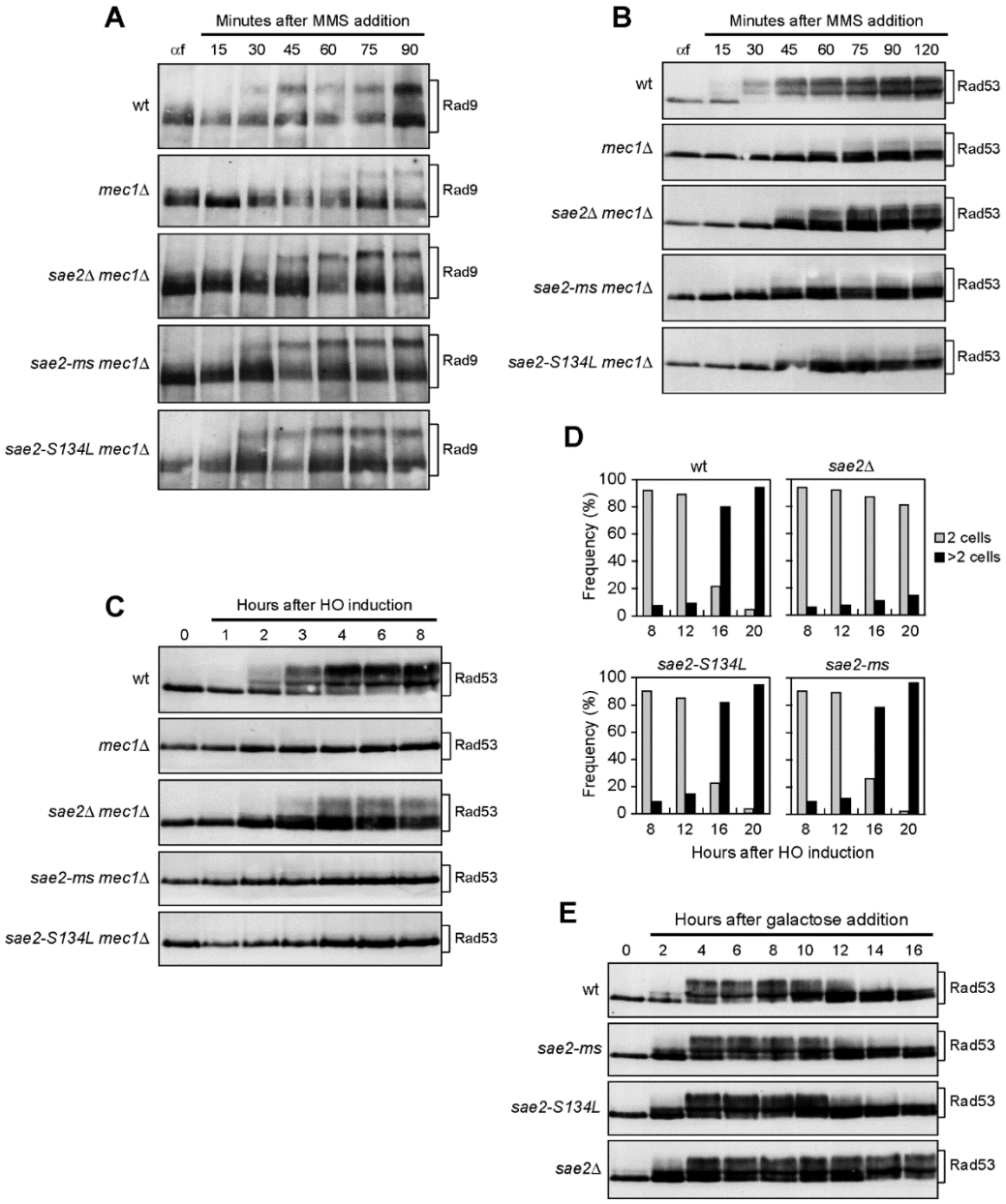


***Figure 33 - Sae2-ms and Sae2-S134L do not enhance Rad53 phosphorylation.***

**(A,B)** Exponentially growing cells were arrested in G1 with α-factor (αf) and released into the cell cycle in the presence of MMS (0,03%). Western blot analysis with anti-Rad9 **(A)** and anti- Rad53 antibodies **(B)**. **(C)** Exponentially growing YEPR cultures of JKM139 derivative strains were transferred to YEPRG at time zero to induce HO. Western blot analysis with anti-Rad53 antibodies. **(D)** Adaptation assay. YEPR G1-arrested cell cultures were plated on galactose-containing plates (time zero). At the indicated time points, 200 cells for each strain were analyzed to determine the frequency of large budded cells (2 cells) and of cells forming microcolonies of more than 2 cells. **(E)** Exponentially growing YEPR cell cultures were transferred to YEPRG at time zero to induce HO. Western blot analysis with anti-Rad53 antibodies.

## Sae2 inhibits the interaction between Rad9 and Rad53

Rad9 phosphorylation by Mec1/Tel1 creates a binding site for Rad53 interaction [176,190,256]. Mec1 and Tel1 subsequently phosphorylate Rad53 that is associated with Rad9 [134,177], followed by Rad53 in trans autophosphorylation and full activation of the kinase [178,257]. Interestingly, Sae2 was shown to physically interact with Rad53 [47]. The finding that Sae2-ms and Sae2-S134L increase Rad9 phosphorylation but not Rad53 phosphorylation suggests that Sae2 may limit Rad53 activation by inhibiting Rad9-Rad53 interaction. We therefore immunoprecipitated HA epitope-tagged Rad9 from cell extracts prepared from undamaged exponentially growing cells. As shown in *Figure 34A*, a basal level of Rad53 binding to Rad9 was detected in wild type cells even in the absence of DNA damage and this interaction increased when Rad9 was immunoprecipitated from *sae2Δ* cells. By contrast, both *sae2-ms* and *sae2-S134L* cells showed a level of Rad53 binding to Rad9 similar to that observed in wild type cells *(Figure 34B)*. This finding indicates that Sae2 inhibits Rad53-Rad9 interaction independently of its role in downregulation of MRX-Tel1. The inhibition of Rad9-Rad53 interaction does not depend on Sae2 stimulation of MRX nuclease activity, as Rad53 binding to Rad9 in *mre11-H125N* cells was similar to that of wild type cells *(Figure 34A)*. Sae2 overproduction was shown to decrease Rad53 phosphorylation and activation independently of DSB repair [66]. The ability of Sae2-ms and Sae2-S134L to downregulate Rad53 activation is not due either to increased production or to increased binding to the sites of damage of the corresponding mutant proteins. In fact, similar amounts of Sae2, Sae2-ms and Sae2-S134L were detected in protein extracts from wild type, *sae2-ms* and *sae2-S134L* cells *(Figure 34C)*. Furthermore, the amount of Sae2-ms and Sae2-S134L bound at an HO-induced DSB was similar or even lower than that of wild type Sae2 *(Figure 34D)*.

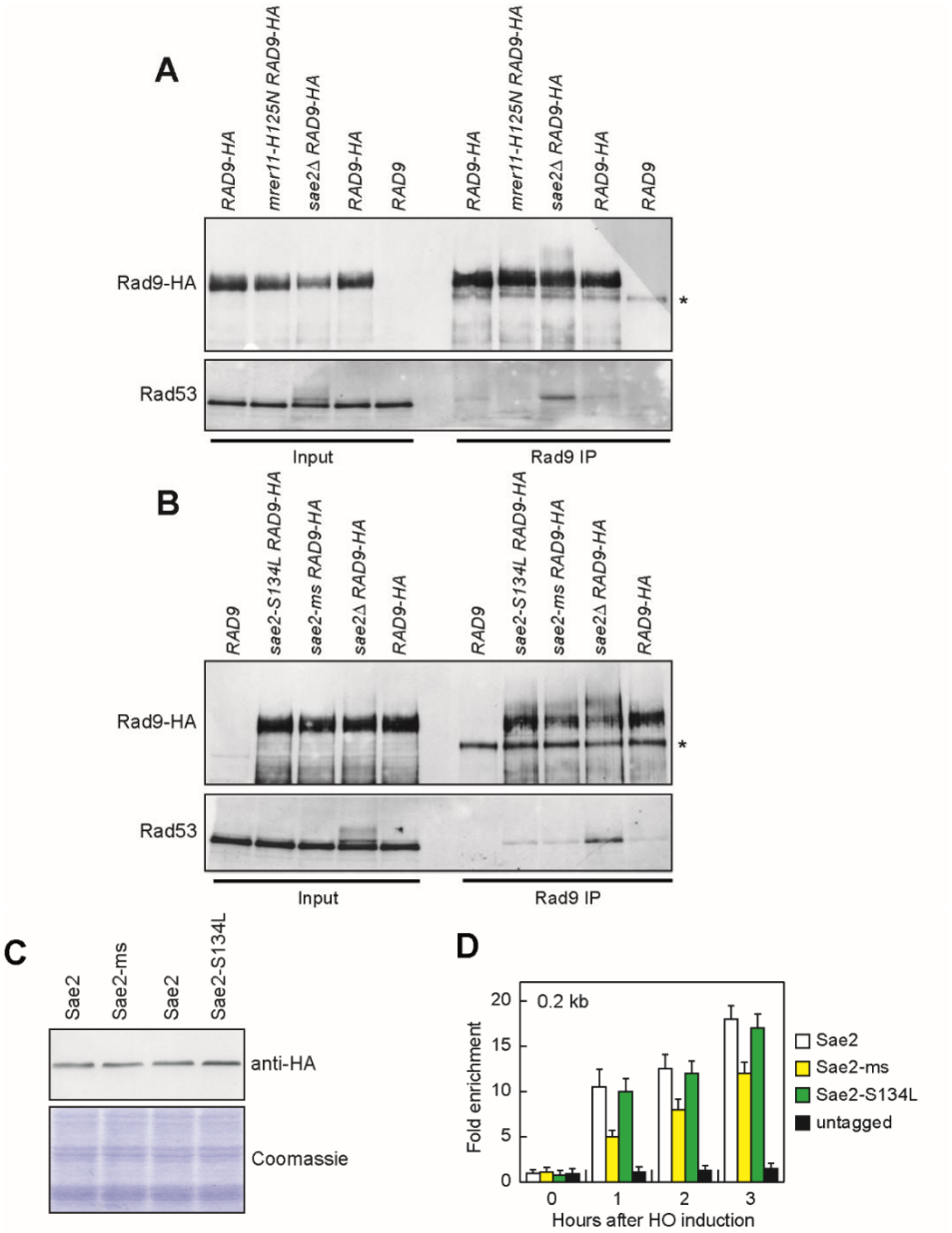


**Figure 34 - Sae2 inhibits Rad9-Rad53 interaction.**

**(A,B)** Protein extracts prepared from exponentially growing cells were analyzed by western blotting with anti-HA (Rad9) and anti- Rad53 antibodies either directly (Input) or after immunoprecipitation (Rad9 IP) with anti-HA antibodies. * indicates a cross-hybridization signal. **(C)** Western blot analysis with anti-HA antibodies of extracts prepared from exponentially growing cells. The same amount of extracts was stained with Coomassie as loading control. **(D)** ChIP analysis. HO was induced at time zero in exponentially growing JKM139 derivative cells. Relative fold enrichment of Sae2-HA protein at the indicated distances from the HO cleavage site was determined after ChIP with anti-HA antibodies and subsequent qPCR analysis. Plotted values are the mean values with error bars denoting s.d. (n=3).

# *DISCUSSION*

DNA double strand breaks are among the most dangerous lesions for cells, as they can lead to genomic instability. Since genome instability is among the main features of cancer cells, an efficient response to DNA damage is essential to ensure the transmission of a faithful genetic inheritance to the progeny and to prevent cancer transformation [1,4,8].

Cells respond to DNA damage by activating both repair and checkpoint mechanisms. DNA damage checkpoint is a transduction cascade, activated by the highly conserved kinases Tel1/ATM and Mec1/ATR, which induces a temporary cell cycle arrest, in order to give cells sufficient time to repair the lesion [149]. The main DSB repair mechanism in *S. cerevisiae* is the homologous recombination, which uses the intact information on the homologous chromosome or on the sister chromatid to fix the damage. HR requires the nucleolytic degradation of DSB ends (resection), a two-step process initiated by MRX and Sae2 that catalyse an endonucleolytic cleavage of the 5'-ends. This cleavage creates an entry point for Exo1 and Dna2 nucleases, the latter working in concert with Sgs1 helicase, which extend resection generating long ssDNA tails [32,40,56,74].

Both resection and checkpoint mechanisms need to be tightly regulated in order to avoid excessive ssDNA generation and to achieve efficient DNA damage repair. Indeed, several factors have been implicated in the regulation of these processes. Some of these factors directly localize to the damage site and participate to repair/checkpoint, while others control the expression of the above factors at different levels, from transcription to translation. Among these factors, in the last years, several RNA binding proteins have been found to participate in the control of the levels of different DDR proteins [200,225].

Moreover, DSB end resection and DNA damage checkpoint are strongly connected to each other, in order to guarantee a fine coordination between DNA repair and cell cycle progression. For this reason, different factors are involved in both repair and checkpoint mechanisms. For example, Sae2 protein promotes DSB end resection and negatively regulates Tel1 and Rad53 checkpoint signalling activities [35,66,261]. Indeed, in the absence of Sae2, an increased MRX association at DSBs, which in turn corresponds

to an increased Tel1 recruitment at the site of damage, causes persistent Tel1- and Rad53-mediated checkpoint activation [35,66]. Reducing either MRX association to DSBs or Rad53/Tel1 signalling restores DNA damage resistance in Sae2-deficient cells [67,68,132,262], suggesting that the DNA damage hypersensitivity of *sae2Δ* cells is due to a failure to downregulate MRX/Tel1 and/or Rad53 activities, thus highlighting the strong relation between repair and checkpoint.

In the first part of this thesis, I have contributed to elucidate a new level of resection regulation, based on the control of Exo1 exonuclease expression by the RNA binding protein Npl3. Indeed, we have shown that the lack of the RBP Npl3 impairs the generation of long stretches of ssDNA at DSB ends and decreases the amount of the exonuclease Exo1. Furthermore, the lack of Exo1 does not exacerbate the resection defect of *npl3Δ* cells, while high Exo1 levels partially restore resection in these cells, indicating that Npl3 supports long-range resection by ensuring the production of a sufficient amount of Exo1.

We have also found that Npl3 is required to activate a Mec1-dependent checkpoint in response to different kinds of DNA damage, but it is dispensable for checkpoint activation after phleomycin treatment in G2 *(Figure 10 and Figure 21)*. As Exo1 is required to generate long stretches of ssDNA [173,246,274], which are the signals that activate Mec1 at least in response to both DSBs and UV-induced DNA lesions [162,173,235,274,275], the reduced Exo1 amount in *npl3Δ* cells could account for the checkpoint defect of the same cells. However, *EXO1* overexpression does not alleviate the checkpoint defect of *npl3Δ* cells experiencing a single DSB. This result, together with the finding that the lack of Exo1 causes a very mild, if any, checkpoint defect in response to a single DSB [66,173], suggests that Npl3 regulates the functions of other proteins involved in checkpoint activation besides Exo1. Although genome-wide transcription analyses showed that most checkpoint genes are not significantly downregulated in the absence of Npl3 [215], a very mild decrease of *MEC1* gene expression was reported in *npl3Δ* cells [231], which also show a slight reduction in Mec1 protein abundance *(Figure*

*24E)*. Furthermore, *npl3Δ* cells show increased amounts of *SAE2* mRNA [231] that correlate with increased levels of the Sae2 protein *(Figure 18D)*. As high Sae2 levels have been shown to counteract Mec1-dependent checkpoint activation [66], the checkpoint defect of *npl3Δ* cells might be due to the high Sae2 levels. Thus, we speculate that the checkpoint defect of *npl3Δ* cells may result both from a defect in ssDNA generation due to low Exo1 levels and from a mild deregulation of factors involved in checkpoint signaling, such as Sae2 and Mec1. These Mec1 and Sae2 misregulations are likely not sufficient to impair checkpoint activation by themselves, as the checkpoint is strongly activated in *npl3Δ* cells treated with phleomycin. However, they might impair Mec1 recruitment/activation in response to DNA lesions that require extensive nucleolytic processing to be detected by Mec1, such as DSBs or UV-induced DNA lesions.

The idea that Npl3 regulates other DDR factors besides Exo1 is also supported by the observation that the lack of Npl3 causes hypersensitivity to DSB-inducing agents, whereas *EXO1* deletion does not [74,274]. Accordingly, *EXO1* overexpression partially rescues the hypersensitivity to CPT of *npl3Δ* cells, while it does not affect the hypersensitivity of the same cells to MMS. This result also suggests that Exo1 is important to repair the damage induced by CPT, while other defects can contribute to the hypersensitivity to MMS of *npl3Δ* cells. One of these defects might be the replication stress caused by the accumulation of transcription-dependent DNA:RNA hybrids in the absence of Npl3. In fact, overproduction of RNaseH1, which removes these hybrids *in vivo* [215,241], suppresses the hypersensitivity to MMS *(Figure 12A)* and reduces the high levels of spontaneous mitotic recombination caused by the lack of Npl3 [215]. On the contrary, *EXO1* overexpression does not reduce the recombination frequency in *npl3Δ* cells *(Figure 22)*.

How does Npl3 control the abundance of the Exo1 protein? As the low Exo1 amount in *npl3Δ* cells does not correlate with a decrease in total *EXO1* RNA levels *(Figure 26)* [215,231], we exclude that Npl3 promotes *EXO1* transcription. Rather, the extended *EXO1* RNA species detected in the absence of Npl3 may be due to termination defects and

transcription readthrough. In fact, defects in transcription termination were seen for approximately 30% of protein-coding genes in *npl3Δ* cells [231], and we found that a region 1000 bp downstream to the *EXO1* stop codon was transcribed in *npl3Δ* cells but not in wild type, while we did not find a significant extension of the *EXO1* RNA 5′ end in the absence of Npl3. Furthermore, Npl3 was found to be co-transcriptionally recruited to DNA at highly transcribed genes (among which *EXO1*), where it distributes in a gradient that increases toward the 3′ end of the coding region [215], and to bind both the 5′ [231,247] and the 3′ ends of mRNAs [247]. Npl3 inactivation is also known to impair mRNA export and to cause the accumulation of transcripts in the nucleus [221]. Taken together, these results suggest that, in the absence of Npl3, some *EXO1* nascent transcripts are not appropriately packaged, thus possibly interfering with the transcription termination process and forming abnormal *EXO1* RNA species that are not exported to the cytoplasm and/or not efficiently translated. Furthermore these abnormal *EXO1* RNA species could compete with the canonical transcripts for the export from the nucleus to the cytoplasm, thus allowing less wild type *EXO1* mRNA molecules to reach the cytoplasm and be translated into proteins. It would be interesting to analyse the nuclear and cytoplasmic fractions of *EXO1* mRNAs to validate this hypothesis.

Moreover, the aberrant *EXO1* transcripts could promote the RNA degradative systems. The abnormal *EXO1* RNAs are likely degraded, at least in part, by the nuclear exosome, as the lack of Rrp6 in *npl3Δ* cells results in a further accumulation of extended *EXO1* RNA species. Accordingly, the exosome was found to degrade transcripts that are not co-transcriptionally packaged because of mutations in the THO complex, which, similarly to Npl3, is required for pre-mRNA processing and export [276]. The lack of Rrp6 slightly increases Exo1 protein levels in *npl3Δ* cells, suggesting that in the presence of faulty transcripts Rrp6 can sequester and/or degrade also functional RNAs. Rrp6 was found to prevent chromatin release of aberrant transcripts when co-transcriptional pre-mRNA processing fails, thus eventually providing these transcripts with additional time to complete their maturation [277,278]. Furthermore, Rrp6 was recently reported to

participate in mRNA nuclear retention caused by Npl3 inactivation. In fact, while *npl3* temperature-sensitive mutant cells accumulate mRNAs in the nucleus at the restrictive temperature, mRNAs are partially released in the cytoplasm in *npl3 rrp6* double mutant cells [279]. Interestingly, Rrp6 deletion also partially suppresses the temperature sensitivity of these *npl3* mutant cells, suggesting that part of the improperly packaged mRNAs produced in the absence of Npl3 may be functional, although incompetent for export [279].

Exo1 is an evolutionarily conserved processive exonuclease that can degrade several kilobases of DNA [77,80] and is implicated in a variety of DNA metabolic processes including DNA repair as well as processing of both stalled replication forks and uncapped telomeres [76,108,223,280,281]. Exo1 action is modulated by both positive and negative regulators, which control Exo1 access to DNA and limit excessive DNA degradation [32,77,129,224,282]. Exo1 expression is also induced during yeast meiosis to promote meiotic DSB processing and crossing over [283]. In mammals, splicing of *EXO1* transcripts is facilitated after DNA damage by a splicing complex that contains the DDR protein BRCA1 [284]. The Npl3-mediated regulation of Exo1 amount that we have shown here represents another level of control of Exo1 activity that guarantees the availability of suitable amounts of Exo1 to respond to DNA damage and maintain genome integrity.

In the second part of this thesis, I have contributed to elucidate the mechanism of Sae2-mediated DNA damage checkpoint regulation, focusing on Sae2 capability to inhibit Tel1 and Rad53 signalling activities. Indeed, to better understand the function of Sae2 in supporting DNA damage resistance and in dampening MRX, Tel1 and Rad53 activation, we searched for *sae2* alleles that hyperactivate Tel1 but that do not cause DNA damage hypersensitivity by themselves. This screen allowed us to identify the Sae2-ms mutant variant, which restores resistance of *mec1Δ* cells to HU and MMS in a Tel1-, Rad9- and Rad53-dependent manner. Sae2-ms carries three amino acid substitutions, with S134L being responsible for *mec1Δ* suppression.

Similar to *SAE2* deletion, both Sae2-ms and Sae2-S134L increase Tel1 signalling activity by enhancing MRX and Tel1 association to DNA ends. Upregulation of MRX-Tel1 in *sae2Δ* cells is accompanied by enhanced DSB-induced Rad53 phosphorylation and activation. Although *sae2Δ*, *sae2-ms* and *sae2-S134L* cells show equivalent increase in MRX and Tel1 association to DSBs, Sae2-ms and Sae2-S134L do not lead to persistent Rad53 phosphorylation and activation as the absence of Sae2. These findings indicate that Sae2 plays distinct functions in dampening Tel1 and Rad53 signalling activities.

Rad9 phosphorylation by Mec1/Tel1 creates a binding site for Rad53 interaction [176,190,256]. Mec1 and Tel1 subsequently phosphorylate Rad53 that is associated with Rad9 [134,177], and this event is followed by Rad53 in trans autophosphorylation and activation [178,257]. Consistent with an upregulation of Tel1 activity, both the lack of Sae2 and the presence of Sae2-ms or Sae2-S134L increase DSB-induced Rad9 phosphorylation. However, the lack of Sae2, but neither Sae2-ms nor Sae2-S134L presence, increases the interaction between Rad53 and Rad9 even in the absence of DNA lesions, indicating that Sae2 limits Rad53 activation by inhibiting Rad53-Rad9 interaction and that Sae2-ms and Sae2-S134L maintain this function.

How does Sae2 regulate the interaction between Rad9 and Rad53? The Sae2-mediated inhibition of Rad53-Rad9 interaction does not require Sae2 function in promoting MRX nuclease activity, as Rad53-Rad9 interaction was not enhanced in *mre11-H125N* cells. We have previously shown that *SAE2* deletion increases the amount of Rad9 bound at DSBs and this Rad9 persistence is the primary cause of the DNA damage hypersensitivity and the resection defect of *sae2Δ* cells [132]. Interestingly, Sae2-ms does not increase Rad9 persistence at DSBs. This finding suggests that the Mre11 nuclease activity does not limit Rad9 accumulation at DSBs and that Sae2 by itself can directly interfere with Rad9 persistence at DNA ends. As Rad9 is required to activate Rad53, the robust Rad9 accumulation at DSBs in *sae2Δ* cells could be responsible for the increased Rad9-Rad53 interaction and therefore Rad53 hyperactivation. However, since defective Rad53 kinase activity bypasses Sae2 function in DNA damage resistance and resection by decreasing the amount of Rad9 bound at DSBs [132], it is also possible that

Sae2 directly inhibits Rad9-Rad53 interaction and the lack of this function leads to Rad53 hyperactivation, which in turn increases Rad9 association to DSBs in a positive feedback loop. In any case, the finding that *sae2-ms* and *sae2-S134L* are proficient in long-range resection and are DNA damage resistant indicates that the increased Rad9 accumulation at DSBs is responsible for the DNA damage hypersensitivity and the impaired long-range resection of *sae2Δ* cells.

Both Sae2-ms and Sae2-S134L appear to be specifically defective in hairpin cleavage, which is known to depend on Mre11 endonucleolytic activity [270,271], suggesting that the MRX-Sae2-mediated DNA clipping contributes to eliminate MRX bound to DNA ends. Consistent with a role of Mre11 endonuclease in MRX removal, abolition of Mre11 nuclease activity by the H125N substitution increases the amount of MRX and Tel1 bound at DSBs to extents similar to those caused by *SAE2* deletion. However, Mre11-H125N does not compensate for Mec1 deficiency as it does *SAE2* deletion. Interestingly, the Mre11-H125N mutant variant was shown to increase the amount of Sae2 bound at DSBs [35]. As Sae2 overproduction decreases Rad53 phosphorylation and activation [66], the increased Sae2 persistence at DSBs in *mre11-H125N* cells may not allow to reach a sufficient level of Rad53 activation to compensate for Mec1 deficiency despite an increased MRX-Tel1 signalling. As Rad53 limits DSB resection by inhibiting Exo1 [129], downregulation of Rad53 activity by Sae2 in *mre11- H125N* mutant cells can also explain why these cells are not resection defective and are considerably less sensitive to DNA damaging agents than *sae2Δ* cells.

By contrast, association of Sae2-ms and Sae2-S134L to DSBs was similar to that of wild type Sae2 or even lower. The finding that suppression of Mec1 deficiency by Sae2-ms and Sae2- S134L still requires Rad53 indicates that upregulation of MRX/Tel1 signalling by these two mutant variants increases Rad53 activation to a level that is sufficient to compensate for Mec1 deficiency, although it is lower than in *sae2Δ* cells because Sae2-ms and Sae2-S134L maintain the ability to limit Rad9-Rad53 interaction.

In summary, our findings support a model whereby Sae2 has two distinct functions in DNA damage signalling. On one hand, it removes MRX and Tel1 from DNA ends possibly

by promoting Mre11 endonuclease activity. On the other hand, it inhibits Rad53 activation by limiting its interaction with Rad9. These two functions provide different layers of regulation of the checkpoint response in the maintenance of genome stability.

In conclusion, in this thesis we have demonstrated that multiple levels of regulation orchestrate both DSB end resection and DNA damage checkpoint activation. Since these pathways are highly conserved from yeast to humans, investigating their molecular mechanisms could provide new strategies for the clinical treatment of cancer-related genomic instability.

# *MATERIALS AND METHODS*

# Yeast and bacterial strains

## Yeast strains and plasmids

The *Saccharomyces cerevisiae* strains used in this study are listed in ***Table 1*** and are derivatives of W303 (*MATa/α ade2-1 can1-100 his3-11,15 leu2-3,112 trp1-1 ura3-1 rad5-535*), JKM139 (*MATa ho hmlΔ::ADE1 hmrΔ::ADE1 ade1-100 leu2-3,112 lys5 trp1::hisG ura3-52 ade3::GAL-HO*), YMV45 (*ho hml::ADE1 mata::hisG hmr::ADE1 leu2::leu2(Asp718-SalI)-URA3-pBR332-MATa ade3::GAL::HO ade1 lys5 ura3-52 trp1::hisG*), YJK40.6 (*MATΔ hmlΔ hmrΔ can1 lys5 ade2 leu2 trp1 ura3 his3 ade3::GAL-HO VII::TRP1-HO LacI-GFP::URA3 LacO::LYS5 LacO::KanR*), 344-115B2 (*MATα his3-513::TRP1::his3-537 ura3-52 trp1 leu2*) and HS21 (*MATα ade5-1 his7-2 ura3Δ trp1-289 leu2-3,112::p305L3 LEU2 lys2::AluIR*) strains. Strains JKM139 and YMV45 were kindly provided by J. Haber (Brandeis University, Waltham, USA), strain YJK40.6 was kindly provided by D.P. Toczyski (University of California, San Francisco, USA), strain HS21 was kindly provided by M. A. Resnick (Research Triangle Park, N.C.). Deletions were generated by one-step PCR disruption method. PCR one-step tagging methods was used to obtain strains carrying fully functional MYC-tagged or HA-tagged alleles. The accuracy of all gene replacement and integrations was verified by PCR or southern blot analyses. The centromeric plasmid carrying the *tetO-RNH1* allele [241] and the control vector were kindly provided by A. Aguilera (University of Seville, Sevilla, Spain), the *EXO1* 2µ plasmid [244] and the control vector were kindly provided by E. Alani (Cornell University, New York, NY, USA), the control vector and the centromeric plasmids carrying the wild type *NPL3* or the mutant alleles *npl3-F160L*, *npl3-SNK* (*L225S*, *G241N*, *E244K*), and *npl3-LSNK* (*F160L*, *L225S*, *G241N*, *E244K*) [214] were kindly provided by J. Lee-Soety (Saint Joseph's University, Philadelphia, PA, USA).

*Table 1 – Saccharomyces cerevisiae strains used in this study*

| Strain | Relevant genotype | Source |
|---|---|---|
| JKM139 | *MATa ho hmlΔ::ADE1 hmrΔ::ADE1 ade1-100 leu2-3,112 lys5 trp1::hisG ura3-52 ade3::GAL-HO* | [234] |
| YLL3466.1 | JKM139 *MATa npl3Δ::NATMX* | This study |
| 184-10A | JKM139 *MATa mec1Δ::HIS3 sml1Δ::KANMX* | [173] |
| YLL1854.2 | JKM139 *MATa MRE11-18MYC::TRP1* | [66] |
| DMP6178/9B | JKM139 *MATa MRE11-18MYC::TRP1 npl3Δ::NATMX* | This study |
| YLL3187.1 | JKM139 *MATa XRS2-3HA::URA3* | [243] |
| DMP6195/2A | JKM139 *MATa XRS2-3HA::URA3 npl3Δ::NATMX* | This study |
| YLL3501.1 | JKM139 *MATa RAD50-3HA::URA3* | [128] |
| DMP6196/1B | JKM139 *MATa RAD50-3HA::URA3 npl3Δ::NATMX* | This study |
| YLL3101.5 | JKM139 *MATa SAE2-3HA::TRP1* | This study |
| DMP6179/8C | JKM139 *MATa SAE2-3HA::TRP1 npl3Δ::NATMX* | This study |
| DMP6030/3A | JKM139 *MATa SGS1-3HA::URA3* | This study |
| DMP6182/7B | JKM139 *MATa SGS1-3HA::URA3 npl3Δ::NATMX* | This study |
| DMP5923/6A | JKM139 *MATa DNA2-18MYC::TRP1* | [243] |
| DMP6180/3A | JKM139 *MATa DNA2-18MYC::TRP1 npl3Δ::NATMX* | This study |
| YLL1959.2 | JKM139 *MATa EXO1-18MYC::TRP1* | [243] |
| DMP6010/3B | JKM139 *MATa EXO1-18MYC::TRP1 npl3Δ::NATMX* | This study |
| DMP6010/6C | JKM139 *MATa EXO1-18MYC::TRP1 npl3Δ::NATMX* | This study |
| YLL1540.4 | JKM139 *MATa exo1Δ::LEU2* | [66] |
| YLL3287.5 | JKM139 *MATa rrp6Δ::NATMX* | [243] |
| DMP6293/25D | JKM139 *MATa rrp6Δ::NATMX npl3Δ::NATMX* | This study |
| DMP6293/30A | JKM139 *MATa rrp6Δ::NATMX npl3Δ::NATMX* | This study |
| YLL3695.1 | JKM139 *MATa rrp6Δ::NATMX EXO1-18MYC::TRP1* | This study |
| DMP6293/37C | JKM139 *MATa rrp6Δ::NATMX EXO1-18MYC::TRP1 npl3Δ::NATMX* | This study |
| YLL3467.6 | JKM139 *NPL3-3HA::TRP1* | This study |
| YLL3012.1 | JKM139 *MATa DDC2-3HA::URA3* | [243] |
| DMP6009/5A | JKM139 *MATa DDC2-3HA::URA3 npl3Δ::NATMX* | This study |
| DMP5991/13A | JKM139 *MATa RFA1-18MYC::TRP1* | This study |
| DMP5991/3A | JKM139 *MATa RFA1-18MYC::TRP1 npl3Δ::NATMX* | This study |
| YLL3096.8 | JKM139 *MATa MEC1-9MYC::TRP1* | [131] |
| DMP6238/5C | JKM139 *MATa MEC1-9MYC::TRP1 npl3Δ::NATMX* | This study |
| YLL3526.20 | JKM139 *MATa RFA3-3HA::TRP1* | [243] |
| DMP6181/4A | JKM139 *MATa RFA3-3HA::TRP1 npl3Δ::NATMX* | This study |
| YLL3222.6 | JKM139 *MATa TEL1-3HA::NAT* | [131] |
| DMP6590/19C | JKM139 *MATa TEL1-3HA::NAT npl3Δ::NAT* | This study |
| YLL1523.3 | JKM139 *MATa sae2Δ::KANMX* | [132] |

| | | |
|---|---|---|
| YLL3941.2 | JKM139 *MATa sae2-ms::LEU2* | This study |
| YLL3421.2 | JKM139 *MATa RAD9-3HA::TRP1* | [131] |
| DMP6911/4B | JKM139 *MATa sae2Δ::KANMX RAD9-3HA::TRP1* | This study |
| DMP6911/1C | JKM139 *MATa sae2-ms::LEU2 RAD9-3HA::TRP1* | This study |
| DMP6859/1C | JKM139 *MATa MRE11-18MYC::TRP1 sae2Δ::KANMX* | This study |
| DMP6878/5B | JKM139 *MATa MRE11-18MYC::TRP1 sae2-ms::LEU2* | This study |
| DMP6879/1B | JKM139 *MATa MRE11-18MYC::TRP1 sae2-S134L::LEU2* | This study |
| YLL4104.2 | JKM139 *MATa MRE11-H125N-18MYC::TRP1* | This study |
| DMP6860/2B | JKM139 *MATa TEL1-3HA::NAT sae2Δ::KANMX* | This study |
| DMP6874/9D | JKM139 *MATa TEL1-3HA::NAT sae2-ms::LEU2* | This study |
| DMP6875/5C | JKM139 *MATa TEL1-3HA::NAT sae2-S134L::LEU2* | This study |
| DMP6870/8B | JKM139 *MATa TEL1-3HA::NAT mre11Δ::NAT::mre11-H125N::URA3* | This study |
| YLL2841.1 | JKM139 *MATa sml1Δ::NATMX* | [131] |
| DMP6910/6A | JKM139 *MATa mre11Δ::NAT::mre11-H125N::URA3 mec1Δ::HIS3 sml1Δ::KANMX* | This study |
| DMP6910/8C | JKM139 *MATa mre11Δ::NAT::mre11-H125N::URA3 mec1Δ::HIS3 sml1Δ::KANMX* | This study |
| DMP6910/12D | JKM139 *MATα mre11Δ::NAT::mre11-H125N::URA3 mec1Δ::HIS3 sml1Δ::KANMX* | This study |
| DMP6910/13C | JKM139 *MATa mre11Δ::NAT::mre11-H125N::URA3 sml1Δ::KANMX* | This study |
| YLL2769.9 | JKM139 *MATa sae2Δ::KANMX mec1Δ::HIS3 sml1Δ::KANMX* | This study |
| YLL3940.1 | JKM139 *MATa sae2-ms::LEU2 mec1Δ::HIS3 sml1Δ::KANMX* | This study |
| DMP6872/2B | JKM139 *MATa sae2-S134L::LEU2 mec1Δ::HIS3 sml1Δ::KANMX* | This study |
| YLL4081.9 | JKM139 *MATa sae2-S134L::LEU2* | This study |
| DMP6912/1A | JKM139 *MATa sae2-S134L::LEU2 RAD9-3HA::TRP1* | This study |
| YLL4102.9 | JKM139 *MATa sae2-ms-3HA::TRP1::LEU2* | This study |
| YLL4103.1 | JKM139 *MATa sae2-S134L-3HA::TRP1::LEU2* | This study |
| 344-115B2 | *MATα his3-513::TRP1::his3-537 ura3-52 trp1 leu2* | [245] |
| YLL3873 | *MATα his3-513::TRP1::his3-537 ura3-52 trp1 leu2 npl3Δ::KAN* | This study |

| | | |
|---|---|---|
| W303 | *MAT*a/α *ade2-1 can1-100 his3-11,15 leu2-3,112 trp1-1 ura3-1 rad5-535* | [285] |
| DMP2818/1D | W303 *MATa sml1Δ::KANMX* | [286] |
| DMP4243/15A | W303 *MATa sae2Δ::KANMX sml1Δ::KANMX* | This study |
| YLL 490.4 | W303 *MATa mec1Δ::HIS3 sml1Δ::KANMX* | [286] |
| DMP4243/4C | W303 *MATa mec1Δ::HIS3 sae2Δ::KANMX sml1Δ::KANMX* | This study |
| YLL3939.1 | W303 *MATa mec1Δ::HIS3 sae2-ms::LEU2 sml1Δ::KANMX* | This study |
| YLL1070.1 | W303 *MATa sae2Δ::HIS3* | [262] |
| YLL3942.1 | W303 *MATa sae2-ms::LEU2* | This study |
| YLL254.1 | W303 *MATa rad27Δ::KANMX* | [59] |
| DMP5671/4C | W303 *MATα sae2Δ::KANMX* | This study |
| DMP6398/2A | W303 *MATα sae2-ms::LEU2* | This study |
| YLL2415.1 | W303 *MATa sgs1Δ::URA3* | This study |
| DMP6715/7B | W303 *MATa sae2-ms::LEU2 rad27Δ::KANMX* | This study |
| DMP6716/1D | W303 *MATa sae2-ms::LEU2 sgs1Δ::URA3* | This study |
| DMP6725/11D | W303 *MATa sae2-ms::LEU2 exo1Δ::LEU2* | This study |
| YLL2402.1 | W303 *MATa exo1Δ::LEU2* | [285] |
| YLL2403.7 | W303 *MATa sae2Δ::KANMX exo1Δ::LEU2* | [285] |
| DMP6727/20B | W303 *MATa tel1Δ::HIS mec1Δ::HIS3 sae2-ms::LEU2 sml1Δ::KANMX* | This study |
| DMP6727/15B | W303 *MATa tel1Δ::HIS mec1Δ::HIS3 sml1Δ::KANMX* | This study |
| DMP6719/10C | W303 *MATa rad9Δ::URA3 mec1Δ::HIS3 sae2-ms::LEU2 sml1Δ::KANMX* | This study |
| DMP4726/6C | W303 *MATa rad9Δ::URA3 mec1Δ::HIS3 sml1Δ::KANMX* | [287] |
| DMP6719/7B | W303 *MATa rad9Δ::URA3 sae2-ms::LEU2 sml1Δ::KANMX* | This study |
| DMP4726/15A | W303 *MATa rad9Δ::URA3 sml1Δ::KANMX* | This study |
| DMP6713/4D | W303 *MATa sae2-ms::LEU2 sml1Δ::KANMX* | This study |
| DMP6721/20C | W303 *MATa rad53-K227A::KANMX mec1Δ::HIS3 sae2-ms::LEU2 sml1Δ::KANMX* | This study |
| DMP6721/20B | W303 *MATa rad53-K227A::KANMX mec1Δ::HIS3 sml1Δ::KANMX* | This study |
| DMP6721/14C | W303 *MATa rad53-K227A::KANMX sae2-ms::LEU2 sml1Δ::KANMX* | This study |

| | | |
|---|---|---|
| YLL590.3 | W303 *MATa rad53-K227A::KANMX sml1Δ::KANMX* | [286] |
| DMP6724/32D | W303 *MATa ddc1Δ::KANMX mec1Δ::HIS3 sae2-ms::LEU2 sml1Δ::KANMX* | This study |
| DMP6724/33D | W303 *MATa ddc1Δ::KANMX mec1Δ::HIS3 sml1Δ::KANMX* | This study |
| DMP6724/29C | W303 *MATa ddc1Δ::KANMX sae2-ms::LEU2 sml1Δ::KANMX* | This study |
| DMP6724/14B | W303 *MATa ddc1Δ::KANMX sml1Δ::KANMX* | This study |
| DMP6732/20C | W303 *MATa mec1Δ::HIS3 sae2-P217T,A230V::LEU2 sml1Δ::KANMX* | This study |
| DMP6731/7A | W303 *MATa mec1Δ::HIS3 sae2-S134L::LEU2 sml1Δ::KANMX* | This study |
| DMP6730/11D | W303 *MATa mec1Δ::HIS3 sae2Δ::KANMX::sae2-S134D::LEU2 sml1Δ::KANMX* | This study |
| DMP6729/2D | W303 *MATa mec1Δ::HIS3 sae2Δ::KANMX::sae2-S134A::LEU2 sml1Δ::KANMX* | This study |
| DMP6731/15A | W303 *MATa sae2-S134L::LEU2* | This study |
| DMP6730/4D | W303 *MATa sae2Δ::KANMX::sae2-S134D::LEU2* | This study |
| DMP6729/9D | W303 *MATa sae2Δ::KANMX::sae2-S134A::LEU2* | This study |
| DMP6732/19B | W303 *MATa sae2-P217T,A230V::LEU2* | This study |
| YMV45 | *ho hml::ADE1 mata::hisG hmr::ADE1 leu2::leu2(Asp718-SalI)- URA3-pBR332-MATa ade3::GAL::HO ade1 lys5 ura3-52 trp1::hisG* | [269] |
| YLL1621.9 | YMV45 *sae2Δ::KANMX* | [132] |
| YLL3956.1 | YMV45 *sae2-ms::HPHMX* | This study |
| YJK40.6 | *MATΔ hmlΔ hmrΔ can1 lys5 ade2 leu2 trp1 ura3 his3 ade3*::*GAL-HO VII*::*TRP1-HO LacI-GFP*::*URA3 LacO*::*LYS5 LacO*::*KanR* | [288] |
| YLL1709.11 | YJK40.6 *sae2Δ::NATMX* | [57] |
| YLL3945.3 | YJK40.6 *sae2-ms::LEU2* | This study |
| HS21 | *MATα ade5-1 his7-2 ura3Δ trp1-289 leu2-3,112::p305L3 LEU2 lys2::AluIR* | [270] |
| YLL1357 | HS21 *MATα sae2Δ::KANMX* | [59] |
| YLL3944.1 | HS21 *MATα sae2-ms::HPHMX* | This study |
| YLL4000.1 | HS21 *MATα sae2-S134L::HPHMX* | This study |

### *E. coli* strain

*E. coli* DH5αTM strain (*F-, φ80 dlacZM15, D(lacZTA-argF) U169, deoR, recA1, endA1, hsdR17, (rK-, mK+) phoA supE44, λ−, thi-1, gyrA96, relA1*) was used as bacterial host for plasmid manipulation and amplification. *E. coli* DH5αTM competent cells to transformation are purchased from Invitrogen.

## Growth media

### *S. cerevisiae* media

YEP (Yeast-Extract Peptone) is the standard rich medium for *S. cerevisiae* and contains 10 g/L yeast extract, 20 g/L peptone and 50 mg/L adenine. YEP must be supplemented with 2% glucose (YEPD), 2% raffinose (YEP+raf) or 2% raffinose and 3% galactose (YEP+raf+gal) as carbon source. YEP-based selective media are obtained including 400 µg/mL G418, 300 µg/mL hygromicin-B (HPH) or 100 µg/mL nourseotricin (NAT). Solid media are obtained including 2% agar. Stock solutions are 50% glucose, 30% raffinose, 30% galactose, 80 mg/mL G418, 50 mg/mL hygromicin-B and 50 mg/mL nourseotricin. YEP and glucose stock solution are autoclave-sterilized and stored at RT. Sugars and antibiotics stock solutions are sterilized by microfiltration and stored at RT and 4°C, respectively. S.C. (Synthetic Complete) is the minimal growth medium for *S. cerevisiae* and contains 1.7 g/L YNB (Yeast Nitrogen Base) without amino acids, 5 g/L ammonium sulphate, 200 µM inositol, 25 mg/L uracil, 25 mg/L adenine, 25 mg/L hystidine, 25 mg/L leucine, 25 mg/L tryptophan. S.C. can be supplemented with drop-out solution (20 mg/L arginine, 60 mg/L isoleucine, 40 mg/L lysine, 10 mg/L methionine, 60 mg/L phenylalanine, 50 mg/L tyrosine), based on yeast strains requirements. One or more amino acid/base can be omitted to have S.C.-base selective media (e.g. S.C.-ura is S.C. lacking uracil). To obtain G418 or NAT S.C. selective medium the 5 g/L ammonium sulphate is replaced with 1 g/L monosodic glutamic acid. Solid media are obtained by

including 2% agar. Stock solutions are 17 g/L YNB + 50 g/L ammonium sulphate (or 10 g/L monosodic glutamic acid), 5 g/L uracil, 5 g/L adenine, 5 g/L hystidine, 5 g/L leucine, 5 g/L tryptophan, 100X drop out solution (2 g/L arginine, 6 g/L isoleucine, 4 g/L lysine, 1 g/L methionine, 6 g/L phenylalanine, 5 g/L tyrosine), 20 mM inositol. All these solutions are sterilized by micro-filtration and stored at 4°C. VB sporulation medium contains 13.6 g/L sodium acetate, 1.9 g/L KCl, 0.35 g/L $MgSO_4$, 1.2 g/L NaCl and pH is adjusted to 7.0. To obtain solid medium include 2% agar. Sterilization is obtained by autoclavation.

### *E. coli* media

LD is the standard growth medium for *E. coli*. LD medium contains 10 g/L tryptone, 5 g/L yeast extract and 5 g/L NaCl. Solid medium is obtained by including 1% agar. LD+Amp selective medium is obtained including 50 µg/mL Ampicillin. LD is autoclave-sterilized and stored at RT. Ampicillin stock solution (2.5 g/L) is sterilized by micro-filtration and stored at 4°C.

## Synchronization of yeast cells

### Synchronization of yeast cells with α-factor

α-factor allows to synchronize a population of yeast cells in G1 phase. This pheromone activates a signal transduction cascade that arrests the cell cycle in G1 phase. Only *MATa* cells are responsive to α-factor. To synchronize a population of exponentially growing yeast cells in YEPD, 2 µg/mL α-factor are added to cell cultures at the concentration of $6x10^6$ cells/mL. If the percentage of budded cells falls below 5%, cells are considered to be G1-arrested. Cells are then washed and resuspended in fresh

medium with or without 5 µg/mL α-factor, to maintain G1-arrest or release cells into the cell cycle, respectively.

### Synchronization of yeast cells with nocodazole

Nocodazole allows to synchronize a population of yeast cells in G2 phase. This drug causes the depolimerization of microtubules, thus activating the mitotic checkpoint which arrests cell cycle at the metaphase to anaphase transition. To synchronize a population of exponentially growing yeast cells in YEPD, 5 µg/mL nocodazole, together with DMSO at a final concentration of 1% (use a stock solution of nocodazole 0,5 mg/mL in 100% DMSO), are added to cell cultures at the concentration of $6x10^6$ cells/mL. If the percentage of dumbbell cells reaches 95%, cells are considered to be G2-arrested. Cells are then washed and resuspended in fresh medium with or without 15 µg/mL nocodazole, to maintain G2-arrest or release cells into the cell cycle, respectively.

## Molecular biology techniques

### Transformation of *E. coli* DH5α cells

DH5α competent cells are thawed on ice. 50-100 µL cells are incubated 30 minutes in ice with 1 µL plasmid DNA. Cells are then subjected to heat shock at 37°C for 30 seconds and after that they are incubated on ice for 2 minutes. Finally, 900 µL LD are added and cells are incubated 30 minutes at 37°C to allow the expression of ampicillin resistance marker gene. Cells are then plated on LD+Amp and incubated overnight at 37°C.

### Transformation of *S. cerevisiae* cells

YEPD exponentially growing yeast cells are harvested by centrifugation and washed with 1 mL 1 M lithium acetate (LiAc) pH 7.5. Cells are then resuspended in 1 M LiAc pH 7.5 to obtain a cells/LiAc 1:1 solution. 12 µL cells/LiAc are incubated 30 minutes at RT with 45 µL 50% PEG (PolyEthylene Glycol) 3350, 4 µL carrier DNA (salmon sperm DNA) and 1-4 µL DNA of interest (double these quantities for transformation with PCR products). After the addition of 6 µL 60% glycerol, cells are incubated at RT for 30 minutes, heat-shocked at 42°C for 10-20 minutes and plated on appropriate selective medium.

### Plasmid DNA extraction from *E. coli* - Minipreps with QIAGEN columns

This protocol allows the purification of up to 20 µg high copy plasmid DNA from 1-5 mL overnight *E. coli* culture in LD medium. Cells are pelleted by centrifugation and resuspended in 250 µL buffer P1 (100 µg/mL RNase, 50 mM Tris-HCl pH 8, 10 mM EDTA pH 8). After the addition of 250 µL buffer P2 (200 mM NaOH, 1% SDS), the solution is mixed thoroughly by inverting the tube 2-3 times, and the lysis reaction occurs in maximum 5 minutes at RT. 350 µL N3 buffer (QIAGEN) are added to the solution, which is then centrifuged at 13000 rpm for 10 minutes. The supernatant is applied to a QIAprep spin column which is washed once with 500 µL PB buffer (QIAGEN) and once with 750 µL PE buffer (QIAGEN). Finally, the DNA is eluted in 30 µL EB buffer (10 mM Tris HCl pH 8.5) pre-heated at 70°C.

### Extraction of yeast genomic DNA (Teeny yeast DNA preps)

About $5x10^8$ yeast cells from overnight exponentially growing cultures (or cultures treated to induce damage) are harvested by centrifugation and washed with 1 mL of a 0.9 M sorbitol, 0.1 M EDTA pH 7.5 solution. Dried pellet can eventually be stored at

-20°C or it can be resuspended in 400 µL of the previous solution supplemented with 14mM β-mercaptoethanol. Yeast cells wall is digested by 40 minutes incubation at 37°C with 0.4 mg/mL 20T zymolyase. Spheroplasts are harvested by 1 minute centrifugation and resuspended in 400 µL 1X TE (10 mM Tris-HCl pH 7.5, 1 mM EDTA pH 7.5). After addition of 90 µL of a solution containing 278 mM EDTA pH 8.5, 445 mM Tris-base and 2.2% SDS, spheroplasts are incubated 30 minutes at 65°C. Following the addition of 80 µL 5M potassium acetate, samples are kept on ice for 1 hour. Cell residues are eliminated by 20 minutes centrifugation at 4°C. DNA is then precipitated with chilled 100% ethanol, resuspended in 500 µL 1X TE and incubated 1 hour with 25 µL 1 mg/mL RNase to eliminate RNA. DNA is then precipitated with 500 µL isopropanol and resuspended in the appropriate volume (typically 40 µL) of 1X TE.

**Polymerase Chain Reaction (PCR)**

PCR allows to obtain high copy number of a specific DNA fragment starting from a very low quantity of DNA. The reaction is directed to the DNA fragment of interest, by using a couple of oligonucleotides flanking the specific DNA sequence. These oligonucleotides work as primers for the DNA polymerase. The reaction consists of a number of polymerization cycles, based on 3 main temperature-dependent steps: denaturation of DNA (which occurs over 90°C), primer annealing to the DNA (it typically takes place at 45- 55°C depending on primers features), synthesis of the sequence of interest by a thermophilic DNA polymerase (which usually works at 72°C). Different polymerases with different properties (processivity, fidelity, working temperature) are commercially available and suitable for different purposes. Taq polymerase is generally used for analytical or mutagenic PCR. High-fidelity polymerases, like Phusion and VENT polymerases, are generally employed when 100% polymerization accuracy is required. The typical 50 µL PCR mixture contains 1µL template DNA, 0.5 µM primers, 200 µM dNTPs, 5 µL 10X Reaction Buffer, 1 mM $MgCl_2$, 1-2 U DNA polymerase and water to 50 µL. The

typical cycle-program for a reaction is as follows: step 1, 2 minutes denaturation at 94-95°C; step 2, 30 seconds denaturation at 94-95°C; step 3, 1 minute annealing at primers Tm (melting temperature); step 4, 1 minute polymerization per kb at 72°C; step 5, return to step 2 and repeat 30 times; step 6, 10 minutes polymerization at 72°C. The choice of primers sequences determines the working Tm, which depends on the length (L) and GC% content of the oligonucleotides and can be calculated as follows: Tm = 59.9 + 0.41(GC%) – 675/L.

## Agarose gel electrophoresis

Agarose gel electrophoresis is the easiest and most common way to separate and analyze DNA molecules. This technique allows the separation of DNA fragments based on their different molecular weight (or length in kb). The purpose of this technique might be to visualize the DNA, to quantify it or to isolate a particular DNA fragment. The DNA is visualized by the addition in the gel of ethidium bromide, a fluorescent dye that intercalates between the bases of nucleic acids. Ethidium bromide absorbs UV light and emits the energy as visible orange light, revealing the DNA molecules to which it is bound. To pour a gel, agarose powder is mixed with 1X TAE (0.04 M Tris-Acetate, 0.001 M EDTA) to the desired concentration, and the solution is heated until it is completely melted. Most gels are between 0.8% and 2% agarose. A 0.8% gel displays good resolution of large DNA fragments (5-10 Kb), while a 2% gel shows good resolution of small fragments (0.2-1 Kb). Ethidium bromide is added to the gel at a final concentration of 1 µg/mL to facilitate visualization of the DNA after electrophoresis. After cooling the gel solution to about 60°C, it is poured into a casting tray containing a sample comb and it is allowed to solidify at RT or at 4°C. Then, the gel is placed into an electrophoresis chamber, it is covered with 1X TAE buffer and the comb is removed. Samples containing DNA mixed with loading buffer are pipetted into the sample wells. The loading buffer contains 0.05% bromophenol blue and 5% glycerol, which give

colour and density to the sample. A marker containing DNA fragments of known length and concentration is loaded in parallel to determine the size and the quantity of DNA fragments in the samples. Current is applied and DNA migrates toward the positive electrode. When adequate migration has occurred, DNA fragments are visualized by placing the gel under an UV transilluminator.

### DNA extraction from agarose gel - Paper strip method

This method allows to isolate a single DNA fragment from an agarose gel. By using a scalpel blade, cut a slit immediately ahead of the band to be extracted. Cut a piece of GF-C filter and place it in the slit. Switch on the current for 1-2 minutes at 150 V. The DNA runs onward into the paper and it is delayed by the smaller mesh size of the paper. Remove the strip of paper from the gel and place it into a 0.5 mL micro-centrifuge tube. Make a tiny hole in the bottom of the tube using a syringe needle, place the 0.5 mL tube inside a 1.5 mL tube and spin for 30 seconds. Buffer and DNA are transferred from the 0.5 mL tube to the 1.5 mL tube. Extract the DNA with 1 volume of phenol/chloroform and precipitate the DNA with 100 mM sodium acetate and 3 volumes of 100% ethanol. After centrifugation re-dissolve DNA in an appropriate volume of 1X TE buffer.

### Southern blot analysis to visualize single strand annealing (SSA) repair

DSB formation and repair by SSA in YMV45 strain can be detected by southern blot analysis. Yeast genomic DNA prepared with standard methods (Teeny yeast DNA preps) is digested with KpnI restriction enzyme. The resulting DNA fragments are separated by agarose gel electrophoresis on a 0.8% agarose gel in 1X TAE buffer. When adequate migration has occurred, gel is washed 1 hour with denaturation buffer (0.2 N NaOH, 0.6 M NaCl), and 1 hour with neutralization buffer (1.5 M NaCl, 1 M Tris-HCl pH 7.4). DNA is blotted onto

a GeneScreen neutral nylon membrane (New England Nuclear, Boston) by overnight capillary transfer with 10X SSC buffer (20X SSC: 3 M NaCl, 0.3 M sodium citrate pH 7.5). Membrane is then UV-crosslinked. Hybridization is carried out by incubating the membrane for 5 hours at 55°C with pre-hybridization buffer (0.5 M sodium phosphate buffer pH 7.2, 7% SDS, 1 mM EDTA pH 7.5, 0,5% BSA), followed by overnight incubation at 55°C with pre-hybridization buffer supplemented with the probe. The probe is obtained by random priming method (DECAprimeTM kit by Ambion), by using an *Asp718-SalI* fragment containing part of the *LEU2* gene as a template, and labelling it with [α-32P]-dATP. Filter is then washed (45 minutes + 45 minutes) at 55°C with a washing solution (0.1 M sodium phosphate buffer pH 7.2, 1%SDS), air dried and then exposed to an autoradiography film. Quantitative analysis of the repair product is performed by calculating the ratio of band intensities for SSA product with respect to a loading control.

**Southern blot analysis to visualize ssDNA derived from DSB end resection**

DSB end resection at the *MAT* locus in JKM139 derivative strains can be analysed by alkaline denaturing southern blot analysis. SspI-digested genomic DNA is precipitated by adding 0.3 M NaAc pH 5.2, 5 mM EDTA pH 8 and 2 volumes EtOH 100%. After chilling overnight, samples are centrifuged 30 minutes at 4°C and pellet is resuspended in alkaline gel loading buffer (50 mM NaOH, 1 mM EDTA pH 8, 2.5% Ficoll (type 400) and 0.025% bromophenol blue). Denatured DNA is loaded onto a 0.8% agarose gel, previously equilibrated in alkaline electrophoresis buffer (50 mM NaOH, 1 mM EDTA pH 8), and a glass plate is placed on the gel to prevent the dye from diffusing from the agarose during the run. Denaturing gel is run slowly, at low voltages (e.g. 30 V overnight). After the DNA has migrated far enough, the gel can be stained with 0.5 µg/mL ethidium bromide in 1X TAE buffer for 1 hour. Gel is then soaked in 0.25 N HCl for 7 minutes with gentle agitation, rinsed with water for 10 minutes, soaked in 0.5 N

NaOH, 1.5 M NaCl for 30 minutes and rinsed again with water for 10 minutes. DNA is blotted overnight by capillary transfer onto neutral nylon membrane using 10X SSC. Membrane is then neutralized in 0.5 M Tris-HCl pH 7.5, 1 M NaCl, air dried and UV-crosslinked. Hybridization is carried out by incubating the membrane for 5 hours at 42°C with pre-hybridization buffer (5X SSPE, 50% formamide, 4X denhardt's solution + BSA, 6% destran sulphate, 100 µg/mL salmon sperm DNA, 200 µg/mL tRNA carrier), followed by overnight incubation at 42°C with pre-hybridization buffer supplemented with single-stranded RNA (ssRNA) probe. The ssRNA probe is obtained by *in vitro* transcription using Promega Riboprobe System-T7 and a pGEM-7Zf-based plasmid (pML514) containing a 900-bp fragment of the *MAT* locus as a template and labelling it with [α-32P]-UTP. Following hybridization, membrane is washed twice with 5X SSPE (20X SSPE = 3 M NaCl, 200 mM $NaH_2PO_4$, 20mM EDTA, pH 7.4) at 42°C for 15 minutes, 30 minutes with 1X SSPE 0.1% SDS at 42°C, 30 minutes with 0.1X SSPE 0.1% SDS at 42°C, twice with 0.2X SSPE 0.1% SDS at 68°C for 15 minutes and 5 minutes with 0.2X SSPE at RT. Finally, membrane is air dried exposed to an autoradiography film. Quantitative analysis of DSB resection is performed by calculating the ratio of band intensities for ssDNA to total amount of DSB products. The resection efficiency is normalized with respect to the HO cleavage efficiency by subtracting the value of the uncut band from the total amount of DSB products for each time point.

### Total protein extracts – TCA precipitation method

Total protein extracts are prepared from $10^8$ cells, collected from exponentially growing yeast cultures (or cultures treated to induce damage). Cells are harvested by centrifugation, washed with 1 mL 20% trichloracetic acid (TCA), in order to prevent proteolysis, and then resuspended in 50 µL 20% TCA. After addition of 200 µL of glass beads, cells are disrupted by vortexing for 8 minutes. Glass beads are washed with 400 µL 5% TCA and the resulting extracts, once separated from the beads, are centrifuged at

3000 rpm for 10 minutes. The pellet is resuspended in 70 µL Laemmli buffer (0.62 M Tris, 2% SDS, 10% glycine, 0.001% bromophenol blue, 100 mM DTT), neutralized with 30 µL 1M Tris-base and boiled for 2 minutes. Protein extracts are finally clarified by centrifugation at 3000 rpm for 10 minutes.

## SDS-PAGE and western blot analysis

Protein extracts for western blot analysis, prepared by TCA precipitation, are loaded onto 10% polyacrylamide gels (10% Running gel: 375 mM Tris-HCl pH 8.8, 0,1% SDS, 10% Acrylamide, 0,13% Bisacrylamide, 0,1% APS, 0.001% Temed – Stacking gel: 125 mM Tris-HCl pH 6.8, 0,1% SDS, 5% Acrylamide, 0,14% Bisacrylamide, 0,1% APS, 0.001% Temed). Less concentrated gels are used to separate big proteins (e.g. 7% polyacrylamide gels are employed to visualize Tel1), while more concentrated gels are used to separate very small proteins (e.g. 15% polyacrylamide gels are employed to visualize Rfa3). Proteins are separated based on their molecular weight by polyacrylamide gel electrophoresis in the presence of sodium dodecyl sulphate (SDS-PAGE). When adequate migration has occurred, proteins are blotted onto nitrocellulose membrane. Membrane is usually saturated by 1-hour incubation in 1X TBS (150 mM NaCl, 50 mM Tris-HCl pH 8) supplemented with 4% milk and 0.2% triton X-100. In the case of some antibodies (e.g. anti-PGK1), milk is substituted with Bovine Serum Albumin (BSA) and triton is substituted with Tween-20. Membranes are then incubated for 2 hours with primary antibodies (in 1X TBS + 4% milk + 0.2% triton) and washed three times for 10 minutes with 1X TBS. Subsequently membranes are incubated for 1 hour with secondary antibodies (in 1X TBS + 4% milk + 0,2% triton) and again washed three times with 1X TBS. Detection is performed with ECL (Enhanced ChemiLuminescence - Genespin) and autoradiography films according to the manufacturer. Primary monoclonal 12CA5 anti-HA antibodies, used to detect HA-tagged proteins, are purchased at GE Healthcare, as well as peroxidase conjugated IgG anti-rabbit and anti-mouse secondary antibodies.

Anti-Rad53 (AB104232) polyclonal antibodies, used to detect Rad53 in the first paper of the results *(The RNA binding protein Npl3 promotes resection of DNA double-strand breaks by regulating the levels of Exo1)*, are purchased from Abcam, as well as 9E10 anti-MYC antibodies (Ab32), used to detect MYC-tagged proteins. Rad53 detection in the second paper of the results *(Uncoupling Sae2 functions in downregulation of Tel1 and Rad53 signalling activities)* is carried out by using anti-Rad53 polyclonal antibodies kindly provided by J. Diffley (The Francis Crick Institute, London, UK). Anti-Rfa2 and anti-Rad9 polyclonal antibodies are kindly provided by B. Stillman (Cold Spring Harbor Laboratory, Cold Spring Harbor, NY, USA) and N. Lowndes (University of Ireland, Galway, Ireland), respectively. Quantitative analysis of phosphorylation normalized to the cut efficiency is performed by calculating the ratio of band intensities for slowly-migrating bands to the total amount of protein, and dividing the obtained values by the cleavage efficiency evaluated by qPCR

**Chromatin ImmunoPrecipitation (ChIP) analysis**

50 mL of exponentially growing cell cultures (or cultures treated to induce the single DSB) at the concentration of $8x10^6$ cells/mL are treated with 1.4 mL of 37% formaldehyde for 5-15 minutes (depending on the strength of the binding between the specific protein and the DNA) while shaking, in order to create DNA-protein covalent bonds (crosslink). Then 2.5 mL of 2.5 M glycine are added for 5 minutes while shaking, in order to stop the crosslink. Treated cells are kept on ice until centrifugation at 3000 rpm for 5 minutes at 4°C. Cell pellet is washed with 30 mL HBS buffer (50 mM HEPES pH 7.5, 140 mM NaCl) and then with 25 mL ChIP lysis buffer (50 mM HEPES pH 7.5, 140 mM NaCl, 1 mM EDTA pH 8, 1% IGEPAL CA-630, 0.1% Sodium deoxycholate, 1 mM phenylmethylsulfonyl fluoride (PMSF)). After centrifugation at 3000 rpm for 5 minutes, the supernatant is carefully and completely removed. Then 0.4 mL of ChIP lysis buffer, supplemented with complete anti-proteolitic tablets (Roche), is added and samples are

resuspended and stored at -80°C. The following day, cells are broken at 4°C with glass beads by using a FastPrep-24 cell disruptor. Four breakage cycles of 30 seconds at 6.5 m/s speed with 1 minute interval-time are performed. After breaking cells the glass beads are eliminated. This passage is followed by centrifugation at 4°C at 14000 rpm for 30 minutes. Pellet is resuspended in 0.5 mL ChIP lysis buffer + antiproteolitics and then sonicated (5 cycles of 25 seconds at 40% power output), in order to share DNA in fragments of 500-1000 bp. After centrifugation at 4°C at 10000 rcf for 5 minutes 460 µL supernatant are retained and further clarified by centrifugation at 4°C at 10000 rcf for 15 minutes. 400 µL of clarified supernatant are immunoprecipitated with Dynabeads coated with specific antibodies, while 5 µL supernatant are kept as "input DNA". MYC-tagged and HA-tagged proteins are immunoprecipitated with Abcam anti-MYC (Ab32) and anti-HA (12CA5) antibodies, respectively. After 2 hours incubation with the desired antibodies, dynabeads are washed RT as follow: twice with SDS buffer (50 mM HEPES pH 7.5, 1 mM EDTA pH 8, 140 mM NaCl, 0.025% SDS), once with High-salt buffer (50 mM HEPES pH 7.5, 1 mM EDTA pH 8, 1 M NaCl), once with T/L buffer (20 mM Tris-HCl pH 7.5, 250 mM LiCl, 1 mM EDTA pH 8, 0.05% sodium deoxycholate, 0.5% IGEPAL CA-630), and finally twice with T/E buffer (20 mM Tris-HCl pH 7.5, 0.1 mM EDTA pH 8). All the washes are done by pulling down Dynabeads for 2 minutes and then nutating them for 4 minutes with the specific washing buffer. After the last wash Dynabeads are resuspended in 145 µL 1X TE + 1% SDS, shaked on a vortex, kept at 65°C for 2 minutes, shaked on vortex again and then pulled down. Then, 120 µL of the supernatant are put at 65°C overnight for reverse cross-linking. Also the previously taken input DNA samples must be put at 65°C overnight after the addition of 115 µL of 1X TE + 1% SDS buffer. The next day DNA is purified by using QIAGEN QIAquick PCR purification kit. 550 µL PB buffer are added to each sample and, after vortexing, the sample is loaded onto spin columns, followed by centrifugation at 14000 rpm for 1 minute. 400 µL PE buffer are added to the columns, followed by centrifugation at 14000 rpm for 30 seconds, then 300 µL PE buffer are added to the columns again and, after 5 minutes waiting, columns are centrifuged at 14000 rpm for 2 minutes. Finally, 25 µL EB buffer are added in the

columns and, after 1 minute incubation, DNA is eluted by centrifuging at 14000 rpm for 1 minute. Elution is repeated a second time in the same way, then input DNA is diluted 1:50 in EB buffer. Quantification of immunoprecipitated DNA is achieved by quantitative real-time PCR (qPCR) on a Bio-Rad MiniOpticon apparatus, using primer pairs located at different distances from the HO-induced DSB and at the *ARO1* locus of chromosome IV. Triplicate samples in 20 µL reaction mixture containing 10 ng of template DNA, 300 nM of each primer, 2X SsoFast™ EvaGreen® supermix (Bio-Rad #1725201) (2X reaction buffer with dNTPs, Sso7d-fusion polymerase, $MgCl_2$, EvaGreen dye, and stabilizers) are run in white 48-well PCR plates Multiplate™ (Bio-Rad #MLL4851). The qPCR program is as follows: step 1, 98°C for 2 minutes; step 2, 98°C for 5 seconds; step 3, 60°C for 10 seconds; step 4, return to step 2 and repeat 30 times. At the end of the cycling program, a melting program (from 65°C to 95°C with a 0.5°C increment every 5 seconds) is run to test the specificity of each qPCR. Data are expressed as fold enrichment at the HO-induced DSB over that at the non-cleaved *ARO1* locus, after normalization of each ChIP signal to the corresponding input for each time point. Fold enrichment is then normalized to the efficiency of DSB induction.

**co-Immunoprecipitation (co-IP)**

$2x10^9$ exponentially growing cells are collected by centrifugation, washed with water and put on ice. Cell pellet is then resuspended in 200 µL cold breaking buffer (1X PBS, 10% Glycerol, 1% Triton X-100, 1 mM EDTA pH 7.5, 10 mM NaF, 20 mM β-Glycerophosphate, 5 mM Sodium Orthovanadate, 1 mM PMSF) supplemented with complete anti-proteolitic tablets (Roche). 200 µL glass beads are added and cells are mechanically disrupted by 14 breakage cycles composed by 30 seconds vortexing and 30 seconds interval each. Glass beads are then washed with 200 µL cold breaking buffer and the resulting extracts, once separated from the beads, are centrifuged at 4°C at 14000 rpm for 20 minutes. The clarified supernatant is transferred in new tubes, it is

quantified at the spectrophotometer by direct UV A280 measurement and all the extracts are normalized to O.D. = 30 in 500 µL with breaking buffer + antiproteolitics. 15 µL normalized extracts are kept as "input", mixed with 15 µL of Laemmli buffer and boiled for 3 minutes. 12CA5 anti-HA monoclonal antibodies are added to the rest of the normalized extracts and incubated at 4°C with gentle mixing for 1 hour. Then 50 µL of a 50% (vol/vol) Protein A-Sepharose resin is added to the samples and they are incubated at 4°C with gentle mixing for 1 hour again. After centrifugation at 4°C at 800 rpm for 2 minutes, the resin is washed three times with cold breaking buffer and three times with cold 1X PBS (137 mM NaCl, 2.7 mM KCl, 10 mM $Na_2HPO_4$, 1.8 mM $KH_2PO_4$). After the last wash, the resin is resuspended in 40 µL 2X Laemmli buffer and boiled for 3 minutes. Finally, the proteins of interest in the supernatant, as well as the inputs, are separated by SDS-PAGE and detected by western blot analysis, by hybridizing with 12CA5 anti-HA antibodies and with Abcam anti-Rad53 antibodies.

## Total RNA extraction from yeast

Total RNA can be extracted from cells by using the Bio-Rad Aurum total RNA mini kit. Before the extraction, all the autoclavable solutions not provided by the kit have to be DEPC-treated. $5x10^7$ cells from exponentially growing cell cultures are harvested by centrifugation and washed with 1 mL of a 1 M sorbitol, 0.1 M EDTA pH 7.5 solution. Dried pellet can be stored at -80°C or it can be resuspended in 1 mL of the previous solution supplemented with 14mM β-mercaptoethanol and with 2.5 mg/mL (50 U/mL) zymolyase. Yeast cells wall is digested by 10 minutes incubation at 37°C, followed by centrifugation at 5000 rpm for 5 minutes and subsequent supernatant elimination. 350 µL lysis buffer (Bio-Rad) supplemented with 1% β-mercaptoethanol are added to the pellet, which is then resuspended by pipetting up and down in order to mix thoroughly. After the addition of 350 µL of 70% ethanol, samples are mix thoroughly again and then the homogenized lysate is loaded onto the RNA binding columns. After 30 seconds

centrifugation at 14000 rpm, 700 µL of low stringency wash solution are added into the columns, followed by centrifugation for 30 seconds again. For each column, 5 µL of reconstituted DNase I are mixed with 75 µL of DNase dilution solution. 80 µL of diluted DNase I are added into the columns, which are then incubated at RT for 45 minutes. 700 µL of high stringency wash solution are added into the columns, followed by centrifugation at 14000 rpm for 30 seconds and by a wash in 700 µL of low stringency wash solution. After 3 minutes centrifugation, 80 µL of elution solution, pre-heated at 70°C, are added to each column. After 1 minute incubation, total RNA is eluted by centrifuging for 2 minutes at 14000 rpm.

**Quantitative reverse transcriptase PCR (qRT-PCR)**

After extraction with Bio-Rad Aurum total RNA mini kit, total RNA is quantified at the spectrophotometer by direct UV A260 measurement. First strand cDNA is synthetized with the Bio-Rad iScript™ cDNA Synthesis Kit. A 20 µL reaction mixture containing 1 µg of template RNA, 1X iSCRIPT reaction mix and 1 µL iSCRIPT reverse transcriptase is assembled. The reaction mix is incubated in a thermal cycler using the following protocol: step 1, 25°C for 5 minutes; step 2, 42°C for 30 minutes; step 3, 85°C for 5 minutes. A negative control without reverse transcriptase is assembled for each RNA sample, in order to detect genomic DNA contaminations. qRT-PCR is performed on a MiniOpticon Real-time PCR system (Bio-Rad), by using primer pairs located in the *EXO1* or *ALG9* coding sequence or downstream from the *EXO1* stop codon. Triplicate samples in 20 µL reaction mixture containing 1 µL of template cDNA, 300 nM of each primer, 2X SsoFast™ EvaGreen® supermix (Bio-Rad #1725201) are run in white 48-well PCR plates Multiplate™ (Bio-Rad #MLL4851). The qPCR program is as follows: step 1, 98°C for 2 minutes; step 2, 98°C for 5 seconds; step 3, 60°C for 10 seconds; step 4, return to step 2 and repeat 30 times. At the end of the cycling program, a melting program (from 65°C to 95°C with a 0.5°C increment every 5 seconds) is run to test the specificity of each

qPCR. *EXO1* RNA levels are quantified using the ΔΔCt method and normalized to *ALG9* RNA levels. The normalized RNA levels are compared with the RNA levels evaluated with the PP1 primer pair, which are set to 1 for each strain.

**Northern blot**

After extraction with Bio-Rad Aurum total RNA mini kit, total RNA is quantified at the spectrophotometer by direct UV A260 measurement. Equal amounts of total RNA for each sample are prepared for loading by the addition of 2 µL 5X gel running buffer (100 mM MOPS pH 7, 40 mM sodium acetate, 5 mM EDTA pH 8), 3.5 µL of 37% formaldehyde, 10 µL of formamide. After heating at 70°C for 5 minutes, 1 µL of 1 mg/mL ethidium bromide and 2 µL of gel loading buffer (50% glycerol, 1 mM EDTA pH 8, 0.25 % bromophenol blue, 0.25 % xylene cyanol) are added to each sample. Samples are then loaded onto a 1% agarose gel supplemented with 1X gel running buffer and 2.2 M formaldehyde and submerged with 1X gel running buffer. After adequate run at 50 V, the ribosomal RNAs 18S and 25S, which are used as loading controls, are visualized by placing the gel under an UV transilluminator. The gel is then washed three times for 5 minutes in water, followed by a wash of 45 minutes in 20X SSC, before transferring the RNA on a nitrocellulose filter by overnight capillary transfer with 20X SSC buffer. All the autoclavable solutions used until this step of the protocol are DEPC-treated. After the transfer the filter is washed for 5 minutes in 6X SSC, air dried and the RNA is UV-crosslinked on the membrane. Hybridization is carried out by incubating the membrane for 5 hours at 42°C with pre-hybridization buffer (5X SSC, 50% formamide, 1X denhardt's solution + BSA, 200 µg/mL salmon sperm DNA, 50 mM phosphate buffer pH 6.5), followed by overnight incubation at 42°C with pre-hybridization buffer supplemented with 10% dextran sulphate and with the probe. The probe is obtained by random priming method (DECAprimeTM kit by Ambion), by using a BamHI–BglII DNA fragment (1437 bp) internal to the *EXO1* coding sequence (+628 to + 2065 from the

ATG initiation codon), extracted from pML546 plasmid, as a template and labelling it with [α-32P]-dATP. pML546 was constructed by inserting a 3109 bp XhoI–NotI blunt fragment containing the *EXO1* gene from pEAm67 2µ plasmid into the SalI-SmaI YEpLac195 vector. Filter is then washed four times with 2X SSC and 0.1% SDS at 42°C for 10 minutes, twice with 0.2X SSC and 0.1% SDS at 50°C for 20 minutes and once with 0.2X SSC at RT for 5 minutes. Lastly the filter is air dried and exposed to an autoradiography film.

### 5′ rapid amplification of cDNA ends (RACE)

After extraction with Bio-Rad Aurum total RNA mini kit, total RNA is quantified at the spectrophotometer by direct UV A260 measurement. 5 µg of total RNA are subjected to reverse transcription by using SuperScript™ II (Invitrogen) and an *EXO1* specific primer to obtain the *EXO1* 5′ partial cDNA ends. After RNA degradation with RNaseH1 and poly(A) tailing of the ss-cDNA, a second DNA strand is synthetized starting from a $Q_T$ ($Q_{TOTAL}$) primer, containing both an oligo-dT sequence capable of annealing with the appended poly(A) tail and a unique sequence. The resulting cDNA is used as a template for two subsequent rounds of amplification using primers that anneal to the $Q_T$ sequence and *EXO1* specific primers. The PCR products are run on 1.5% agarose gel and visualized with ethidium bromide.

## Other techniques

### FACS analysis of DNA content

FACS (Fluorescence-Activated Cell Sorting) analysis allows to determine the DNA content of every single cell of a given population of yeast cells. $6x10^6$ cells are harvested by centrifugation, resuspended in 1 mL 70% ethanol and incubated at RT for at least 30 minutes. Cells are then washed with 1 mL 50 mM Tris pH 7.5 and incubated overnight

at 37°C in 500 µL of the same solution supplemented with 1 mg/mL RNase. Samples are then centrifuged and cells are washed with 1 mL FACS Buffer and stained with 500 µL FACS buffer supplemented with 50 µg/mL propidium iodide. After sonicating for 10-15 seconds at 40% power output, 50 µL of each sample are diluted in 1 mL 50 mM Tris pH 7.5 and analysed with a Becton-Dickinson FACS Scan.

### Drop test

Overnight-grown saturated cultures of the indicated strains are counted and serially diluted (10 fold) in water, after normalization to the same concentration. 7 µl drops of each dilution are deposited on plates with the indicated media (with or without genotoxic agents at the indicated concentrations). Images are scanned 2-3 days after plating and growth at 30°C.

### Search for *sae2* mutations that suppress *mec1Δ* sensitivity to HU and MMS

To search for *sae2* alleles that suppress *mec1Δ* sensitivity to HU and MMS, but that do not impair Sae2 function in DSB repair, we used low-fidelity PCR to random mutagenize the *SAE2* gene. Linear *SAE2* PCR products were then transformed into *mec1Δ sml1Δ* cells in order to replace the corresponding *SAE2* wild type sequence with the mutagenized DNA fragments. Transformant clones were screened for increased viability in the presence of HU and MMS compared to *mec1Δ*. Among them, the clones that, after transformation with a plasmid carrying wild type *MEC1* gene, showed CPT resistance compared to *sae2Δ* cells were chosen for further characterization.

## Plasmid religation assay

The centromeric pRS316 plasmid is digested with the BamHI restriction enzyme before being transformed into exponentially growing *S. cerevisiae* cells. Parallel transformation with undigested pRS316 DNA is used to determine the transformation efficiency. Efficiency of re-ligation is determined by counting the number of colonies that are able to grow on medium selective for the plasmid marker and is normalized respect to the transformation efficiency for each sample. The re-ligation efficiency in mutant cells is then compared to that of wild type cells that is set up to 100%.

## Hairpin opening assay

This method allows to evaluate the rate of mitotic ectopic recombination between two *lys2* alleles. An *Alu*-IR, formed between identical 320 bp inverted *Alu*s separated by a 12 bp spacer, is inserted into the *LYS2* gene on chromosome II. Recombination between *lys2*::*Alu* and the *lys2-Δ5'* allele located at the *LEU2* locus of chromosome III can generate $Lys^+$ prototrophs through simple gene conversion or gene conversion associated with crossing-over. After plating exponentially growing cell cultures on selective medium without lysine, the rate of Lys+ recombinants is derived from the median recombination frequency determined from ten different isolates of each strain as previously described [270]. The mean recombination rate among three independent trials is calculated.

# *REFERENCES*

1. Giglia-Mari, G., Zotter, A. & Vermeulen, W. DNA Damage Response. *Cold Spring Harb. Perspect. Biol.* **3**, a000745 (2011).

2. Friedberg, E. C., Walker, G. C., Siede, W. & Wood, R. D. *DNA Repair and Mutagenesis*. American Society for Microbiology Press, (2005).

3. Friedberg, E. C. DNA damage and repair. *Nature* **421**, 436–440 (2003).

4. Hanahan, D. & Weinberg, R. A. Hallmarks of Cancer: The Next Generation. *Cell* **144**, 646–674 (2011).

5. Negrini, S., Gorgoulis, V. G. & Halazonetis, T. D. Genomic instability — an evolving hallmark of cancer. *Nat. Rev. Mol. Cell Biol.* **11**, 220–228 (2010).

6. Stratton, M. R., Campbell, P. J. & Futreal, P. A. The cancer genome. *Nature* **458**, 719–724 (2009).

7. Bartkova, J. *et al.* DNA damage response as a candidate anti-cancer barrier in early human tumorigenesis. *Nature* **434**, 864–870 (2005).

8. Aparicio, T., Baer, R. & Gautier, J. DNA double-strand break repair pathway choice and cancer. *DNA Repair* **19**, 169–175 (2014).

9. Mehta, A. & Haber, J. E. Sources of DNA double-strand breaks and models of recombinational DNA repair. *Cold Spring Harb. Perspect. Biol.* **6**, a016428 (2014).

10. O'Driscoll, M. & Jeggo, P. A. The role of double-strand break repair — insights from human genetics. *Nat. Rev. Genet.* **7**, 45–54 (2006).

11. Bassing, C. H. & Alt, F. W. The cellular response to general and programmed DNA double strand breaks. *DNA Repair* **3**, 781–796 (2004).

12. Longhese, M. P., Bonetti, D., Guerini, I., Manfrini, N. & Clerici, M. DNA double-strand breaks in meiosis: Checking their formation, processing and repair. *DNA Repair* **8**, 1127–1138 (2009).

13. Hefferin, M. L. & Tomkinson, A. E. Mechanism of DNA double-strand break repair by non-homologous end joining. *DNA Repair* **4**, 639–648 (2005).

14. Lieber, M. R. The Mechanism of Double-Strand DNA Break Repair by the Nonhomologous DNA End Joining Pathway. *Annu. Rev. Biochem.* **79**, 181–211 (2010).

15. Huertas, P. DNA resection in eukaryotes: deciding how to fix the break. *Nat. Struct. Mol. Biol.* **17**, 11–16 (2010).

16. Daley, J. M., Palmbos, P. L., Wu, D. & Wilson, T. E. Nonhomologous End Joining in Yeast. *Annu. Rev. Genet.* **39**, 431–451 (2005).

17. Hopfner, K.-P. *et al.* The Rad50 zinc-hook is a structure joining Mre11 complexes in DNA recombination and repair. *Nature* **418**, 562–566 (2002).

18. He, J. *et al.* Rad50 Zinc Hook Is Important for the Mre11 Complex to Bind Chromosomal DNA Double-stranded Breaks and Initiate Various DNA Damage Responses. *J. Biol. Chem.* **287**, 31747–31756 (2012).

19. Clerici, M., Mantiero, D., Lucchini, G. & Longhese, M. P. The Saccharomyces cerevisiae Sae2 Protein Promotes Resection and Bridging of Double Strand Break Ends. *J. Biol. Chem.* **280**, 38631–38638 (2005).

20. Davis, A. J. & Chen, D. J. DNA double strand break repair via non-homologous end-joining. *Transl. Cancer Res.* **2**, 130–143 (2013).

21. Dudášová, Z., Dudáš, A. & Chovanec, M. Non-homologous end-joining factors of Saccharomyces cerevisiae. *FEMS Microbiol. Rev.* **28**, 581–601 (2004).

22. Mathiasen, D. P. & Lisby, M. Cell cycle regulation of homologous recombination in Saccharomyces cerevisiae. *FEMS Microbiol. Rev.* **38**, 172–184 (2014).

23. Ferretti, L. P., Lafranchi, L. & Sartori, A. A. Controlling DNA-end resection: a new task for CDKs. *Front. Genet.* **4**, 99 (2013).

24. San Filippo, J., Sung, P. & Klein, H. Mechanism of Eukaryotic Homologous Recombination. *Annu. Rev. Biochem.* **77**, 229–257 (2008).

25. Symington, L. S. & Gautier, J. Double-Strand Break End Resection and Repair Pathway Choice. *Annu. Rev. Genet.* **45**, 247–271 (2011).

26. Ip, S. C. Y. *et al.* Identification of Holliday junction resolvases from humans and yeast. *Nature* **456**, 357–361 (2008).

27. Bartek, J. & Lukas, J. DNA damage checkpoints: from initiation to recovery or adaptation. *Curr. Opin. Cell Biol.* **19**, 238–245 (2007).

28. Cejka, P. DNA End Resection: Nucleases Team Up with the Right Partners to Initiate Homologous Recombination. *J. Biol. Chem.* **290**, 22931–22938 (2015).

29. Niu, H., Raynard, S. & Sung, P. Multiplicity of DNA end resection machineries in chromosome break repair. *Genes Dev.* **23**, 1481–1486 (2009).

30. Mimitou, E. P. & Symington, L. S. DNA end resection: Many nucleases make light work. *DNA Repair* **8**, 983–995 (2009).

31. You, Z. & Bailis, J. M. DNA damage and decisions: CtIP coordinates DNA repair and cell cycle checkpoints. *Trends Cell Biol.* **20**, 402–409 (2010).

32. Daley, J. M., Niu, H., Miller, A. S. & Sung, P. Biochemical mechanism of DSB end resection and its regulation. *DNA Repair* **32**, 66–74 (2015).

33. Bonetti, D., Colombo, C. V., Clerici, M. & Longhese, M. P. Processing of DNA Ends in the Maintenance of Genome Stability. *Front. Genet.* **9**, 390 (2018).

34. Stark, J. M. & Shen, B. Examining the roles of DNA2 during mammalian end resection. *Cell Cycle* **11**, 4111 (2012).

35. Lisby, M., Barlow, J. H., Burgess, R. C. & Rothstein, R. Choreography of the DNA Damage Response: Spatiotemporal Relationships among Checkpoint and Repair Proteins. *Cell* **118**, 699–713 (2004).

36. Lamarche, B. J., Orazio, N. I. & Weitzman, M. D. The MRN complex in double-strand break repair and telomere maintenance. *FEBS Lett.* **584**, 3682–3695 (2010).

37. Rupnik, A., Lowndes, N. F. & Grenon, M. MRN and the race to the break. *Chromosoma* **119**, 115–135 (2010).

38. Stracker, T. H. & Petrini, J. H. J. The MRE11 complex: starting from the ends. *Nat. Rev. Mol. Cell Biol.* **12**, 90–103 (2011).

39. Paull, T. T. & Deshpande, R. A. The Mre11/Rad50/Nbs1 complex: Recent insights into catalytic activities and ATP-driven conformational changes. *Exp. Cell Res.* **329**, 139–147 (2014).

40. Cannavo, E. & Cejka, P. Sae2 promotes dsDNA endonuclease activity within Mre11–Rad50–Xrs2 to resect DNA breaks. *Nature* **514**, 122–125 (2014).

41. Gobbini, E., Cesena, D., Galbiati, A., Lockhart, A. & Longhese, M. P. Interplays between ATM/Tel1 and ATR/Mec1 in sensing and signaling DNA double-strand breaks. *DNA Repair* **12**, 791–799 (2013).

42. Hopfner, K.-P. *et al.* Structural Biology of Rad50 ATPase: ATP-Driven Conformational Control in DNA Double-Strand Break Repair and the ABC-ATPase Superfamily. *Cell* **101**, 789–800 (2000).

43. Lammens, K. *et al.* The Mre11:Rad50 Structure Shows an ATP-Dependent Molecular Clamp in DNA Double-Strand Break Repair. *Cell* **145**, 54–66 (2011).

44. Deshpande, R. A. *et al.* ATP-driven Rad50 conformations regulate DNA tethering, end resection, and ATM checkpoint signaling. *EMBO J.* **33**, 482–500 (2014).

45. Lim, H. S., Kim, J. S., Park, Y. B., Gwon, G. H. & Cho, Y. Crystal structure of the Mre11–Rad50–ATPγS complex: understanding the interplay between Mre11 and Rad50. *Genes Dev.* **25**, 1091–1104 (2011).

46. Oh, J., Al-Zain, A., Cannavo, E., Cejka, P. & Symington, L. S. Xrs2 Dependent and Independent Functions of the Mre11-Rad50 Complex. *Mol. Cell* **64**, 405–415 (2016).

47. Liang, J., Suhandynata, R. T. & Zhou, H. Phosphorylation of Sae2 Mediates Forkhead-associated (FHA) Domain-specific Interaction and Regulates Its DNA Repair Function. *J. Biol. Chem.* **290**, 10751–10763 (2015).

48. Wang, H. *et al.* The Interaction of CtIP and Nbs1 Connects CDK and ATM to Regulate HR–Mediated Double-Strand Break Repair. *PLOS Genet.* **9**, e1003277 (2013).

49. Chen, L., Trujillo, K., Ramos, W., Sung, P. & Tomkinson, A. E. Promotion of Dnl4-Catalyzed DNA End-Joining by the Rad50/Mre11/Xrs2 and Hdf1/Hdf2 Complexes. *Mol. Cell* **8**, 1105–1115 (2001).

50. Becker, E., Meyer, V., Madaoui, H. & Guerois, R. Detection of a tandem BRCT in Nbs1 and Xrs2 with functional implications in the DNA damage response. *Bioinformatics* **22**, 1289–1292 (2006).

51. Tsukamoto, Y., Mitsuoka, C., Terasawa, M., Ogawa, H. & Ogawa, T. Xrs2p regulates Mre11p translocation to the nucleus and plays a role in telomere elongation and meiotic recombination. *Mol. Biol. Cell* **16**, 597–608 (2005).

52. Shima, H., Suzuki, M. & Shinohara, M. Isolation and Characterization of Novel xrs2 Mutations in Saccharomyces cerevisiae. *Genetics* **170**, 71–85 (2005).

53. Lee, J.-H. *et al.* Regulation of Mre11/Rad50 by Nbs1 EFFECTS ON NUCLEOTIDE-DEPENDENT DNA BINDING AND ASSOCIATION WITH ATAXIA-TELANGIECTASIA-LIKE DISORDER MUTANT COMPLEXES. *J. Biol. Chem.* **278**, 45171–45181 (2003).

54. Trujillo, K. M. *et al.* Yeast xrs2 binds DNA and helps target rad50 and mre11 to DNA ends. *J. Biol. Chem.* **278**, 48957–48964 (2003).

55. Andres, S. N. & Williams, R. S. CtIP/Ctp1/Sae2, molecular form fit for function. *DNA Repair* **56**, 109–117 (2017).

56. Mimitou, E. P. & Symington, L. S. Sae2, Exo1 and Sgs1 collaborate in DNA double-strand break processing. *Nature* **455**, 770–774 (2008).

57. Nicolette, M. L. *et al.* Mre11–Rad50–Xrs2 and Sae2 promote 5' strand resection of DNA double-strand breaks. *Nat. Struct. Mol. Biol.* **17**, 1478–1485 (2010).

58. Fu, Q. *et al.* Phosphorylation-Regulated Transitions in an Oligomeric State Control the Activity of the Sae2 DNA Repair Enzyme. *Mol. Cell. Biol.* **34**, 778–793 (2014).

59. Baroni, E., Viscardi, V., Cartagena-Lirola, H., Lucchini, G. & Longhese, M. P. The Functions of Budding Yeast Sae2 in the DNA Damage Response Require Mec1- and Tel1-Dependent Phosphorylation. *Mol. Cell. Biol.* **24**, 4151–4165 (2004).

60. Anand, R., Ranjha, L., Cannavo, E. & Cejka, P. Phosphorylated CtIP Functions as a Co-factor of the MRE11-RAD50-NBS1 Endonuclease in DNA End Resection. *Mol. Cell* **64**, 940–950 (2016).

61. Huertas, P., Cortés-Ledesma, F., Sartori, A. A., Aguilera, A. & Jackson, S. P. CDK targets Sae2 to control DNA-end resection and homologous recombination. *Nature* **455**, 689–692 (2008).

62. Wang, W., Daley, J. M., Kwon, Y., Krasner, D. S. & Sung, P. Plasticity of the Mre11–Rad50–Xrs2–Sae2 nuclease ensemble in the processing of DNA-bound obstacles. *Genes Dev.* **31**, 2331–2336 (2017).

63. Reginato, G., Cannavo, E. & Cejka, P. Physiological protein blocks direct the Mre11–Rad50–Xrs2 and Sae2 nuclease complex to initiate DNA end resection. *Genes Dev.* **31**, 2325–2330 (2017).

64. Lengsfeld, B. M., Rattray, A. J., Bhaskara, V., Ghirlando, R. & Paull, T. T. Sae2 is an endonuclease that processes hairpin DNA cooperatively with the Mre11/Rad50/Xrs2 complex. *Mol. Cell* **28**, 638–651 (2007).

65. Arora, S. *et al.* Genetic Separation of Sae2 Nuclease Activity from Mre11 Nuclease Functions in Budding Yeast. *Mol. Cell. Biol.* **37**, e00156-17 (2017).

66. Clerici, M., Mantiero, D., Lucchini, G. & Longhese, M. P. The Saccharomyces cerevisiae Sae2 protein negatively regulates DNA damage checkpoint signalling. *EMBO Rep.* **7**, 212–218 (2006).

67. Puddu, F. *et al.* Synthetic viability genomic screening defines Sae2 function in DNA repair. *EMBO J.* **34**, 1509–1522 (2015).

68. Chen, H. *et al.* Sae2 promotes DNA damage resistance by removing the Mre11–Rad50–Xrs2 complex from DNA and attenuating Rad53 signaling. *Proc. Natl. Acad. Sci. U. S. A.* **112**, E1880–E1887 (2015).

69. Sartori, A. A. *et al.* Human CtIP promotes DNA end resection. *Nature* **450**, 509–514 (2007).

70. Makharashvili, N. *et al.* Catalytic and Noncatalytic Roles of the CtIP Endonuclease in Double-Strand Break End Resection. *Mol. Cell* **54**, 1022–1033 (2014).

71. Cruz-García, A., López-Saavedra, A. & Huertas, P. BRCA1 Accelerates CtIP-Mediated DNA-End Resection. *Cell Rep.* **9**, 451–459 (2014).

72. Daley, J. M. *et al.* Enhancement of BLM-DNA2-Mediated Long-Range DNA End Resection by CtIP. *Cell Rep.* **21**, 324–332 (2017).

73. Nimonkar, A. V. *et al.* BLM–DNA2–RPA–MRN and EXO1–BLM–RPA–MRN constitute two DNA end resection machineries for human DNA break repair. *Genes Dev.* **25**, 350–362 (2011).

74. Zhu, Z., Chung, W.-H., Shim, E. Y., Lee, S. E. & Ira, G. Sgs1 Helicase and Two Nucleases Dna2 and Exo1 Resect DNA Double-Strand Break Ends. *Cell* **134**, 981–994 (2008).

75. Symington, L. S. End Resection at Double-Strand Breaks: Mechanism and Regulation. *Cold Spring Harb. Perspect. Biol.* **6**, a016436 (2014).

76. Tran, P. T., Erdeniz, N., Dudley, S. & Liskay, R. M. Characterization of nuclease-dependent functions of Exo1p in Saccharomyces cerevisiae. *DNA Repair* **1**, 895–912 (2002).

77. Cannavo, E., Cejka, P. & Kowalczykowski, S. C. Relationship of DNA degradation by Saccharomyces cerevisiae Exonuclease 1 and its stimulation by RPA and Mre11-Rad50-Xrs2 to DNA end resection. *Proc. Natl. Acad. Sci.* **110**, E1661–E1668 (2013).

78. Shim, E. Y. *et al.* Saccharomyces cerevisiae Mre11/Rad50/Xrs2 and Ku proteins regulate association of Exo1 and Dna2 with DNA breaks. *EMBO J.* **29**, 3370–3380 (2010).

79. Gobbini, E. *et al.* The MRX complex regulates Exo1 resection activity by altering DNA end structure. *EMBO J.* **37**, e98588 (2018).

80. Myler, L. R. *et al.* Single-Molecule Imaging Reveals How Mre11-Rad50-Nbs1 Initiates DNA Break Repair. *Mol. Cell* **67**, 891-898.e4 (2017).

81. Eid, W. *et al.* DNA end resection by CtIP and exonuclease 1 prevents genomic instability. *EMBO Rep.* **11**, 962–968 (2010).

82. Tomimatsu, N. *et al.* Phosphorylation of EXO1 by CDKs 1 and 2 regulates DNA end resection and repair pathway choice. *Nat. Commun.* **5**, 3561 (2014).

83. Tomimatsu, N. *et al.* DNA-damage-induced degradation of EXO1 exonuclease limits DNA end resection to ensure accurate DNA repair. *J. Biol. Chem.* **292**, 10779–10790 (2017).

84. Bae, S.-H. & Seo, Y.-S. Characterization of the Enzymatic Properties of the Yeast Dna2 Helicase/Endonuclease Suggests a New Model for Okazaki Fragment Processing. *J. Biol. Chem.* **275**, 38022–38031 (2000).

85. Kao, H.-I., Campbell, J. L. & Bambara, R. A. Dna2p Helicase/Nuclease Is a Tracking Protein, Like FEN1, for Flap Cleavage during Okazaki Fragment Maturation. *J. Biol. Chem.* **279**, 50840–50849 (2004).

86. Niu, H. *et al.* Mechanism of the ATP-dependent DNA End Resection Machinery from S. cerevisiae. *Nature* **467**, 108–111 (2010).

87. Cejka, P. *et al.* DNA end resection by Dna2-Sgs1-RPA and its stimulation by Top3-Rmi1 and Mre11-Rad50-Xrs2. *Nature* **467**, 112–116 (2010).

88. Sturzenegger, A. *et al.* DNA2 Cooperates with the WRN and BLM RecQ Helicases to Mediate Long-range DNA End Resection in Human Cells. *J. Biol. Chem.* **289**, 27314–27326 (2014).

89. Pinto, C., Kasaciunaite, K., Seidel, R. & Cejka, P. Human DNA2 possesses a cryptic DNA unwinding activity that functionally integrates with BLM or WRN helicases. *eLife* **5**, e18574 (2016)

90. Levikova, M., Pinto, C. & Cejka, P. The motor activity of DNA2 functions as an ssDNA translocase to promote DNA end resection. *Genes Dev.* **31**, 493–502 (2017).

91. Miller, A. S. *et al.* A novel role of the Dna2 translocase function in DNA break resection. *Genes Dev.* **31**, 503–510 (2017).

92. Rezazadeh, S. RecQ helicases; at the crossroad of genome replication, repair, and recombination. *Mol. Biol. Rep.* **39**, 4527–4543 (2012).

93. Bernstein, K. A., Gangloff, S. & Rothstein, R. The RecQ DNA helicases in DNA Repair. *Annu. Rev. Genet.* **44**, 393–417 (2010).

94. Daley, J. M., Chiba, T., Xue, X., Niu, H. & Sung, P. Multifaceted role of the Topo IIIα–RMI1-RMI2 complex and DNA2 in the BLM-dependent pathway of DNA break end resection. *Nucleic Acids Res.* **42**, 11083–11091 (2014).

95. Morgan, D. O. CYCLIN-DEPENDENT KINASES: Engines, Clocks, and Microprocessors. *Annu. Rev. Cell Dev. Biol.* **13**, 261–291 (1997).

96. Ira, G. *et al.* DNA end resection, homologous recombination and DNA damage checkpoint activation require CDK1. *Nature* **431**, 1011–1017 (2004).

97. Chen, X. *et al.* Cell cycle regulation of DNA double-strand break end resection by Cdk1-dependent Dna2 phosphorylation. *Nat. Struct. Mol. Biol.* **18**, 1015–1019 (2011).

98. Manfrini, N., Guerini, I., Citterio, A., Lucchini, G. & Longhese, M. P. Processing of Meiotic DNA Double Strand Breaks Requires Cyclin-dependent Kinase and Multiple Nucleases. *J. Biol. Chem.* **285**, 11628–11637 (2010).

99. Huertas, P. & Jackson, S. P. Human CtIP Mediates Cell Cycle Control of DNA End Resection and Double Strand Break Repair. *J. Biol. Chem.* **284**, 9558–9565 (2009).

100. Clerici, M., Mantiero, D., Guerini, I., Lucchini, G. & Longhese, M. P. The Yku70–Yku80 complex contributes to regulate double-strand break processing and checkpoint activation during the cell cycle. *EMBO Rep.* **9**, 810–818 (2008).

101. Mimitou, E. P. & Symington, L. S. Ku prevents Exo1 and Sgs1-dependent resection of DNA ends in the absence of a functional MRX complex or Sae2. *EMBO J.* **29**, 3358–3369 (2010).

102. Zhang, Y. *et al.* Role of Dnl4–Lif1 in nonhomologous end-joining repair complex assembly and suppression of homologous recombination. *Nat. Struct. Mol. Biol.* **14**, 639–646 (2007).

103. Wu, D., Topper, L. M. & Wilson, T. E. Recruitment and Dissociation of Nonhomologous End Joining Proteins at a DNA Double-Strand Break in Saccharomyces cerevisiae. *Genetics* **178**, 1237–1249 (2008).

104. Langerak, P., Mejia-Ramirez, E., Limbo, O. & Russell, P. Release of Ku and MRN from DNA Ends by Mre11 Nuclease Activity and Ctp1 Is Required for Homologous Recombination Repair of Double-Strand Breaks. *PLoS Genet.* **7**, e1002271 (2011).

105. Sun, J., Lee, K.-J., Davis, A. J. & Chen, D. J. Human Ku70/80 Protein Blocks Exonuclease 1-mediated DNA Resection in the Presence of Human Mre11 or Mre11/Rad50 Protein Complex. *J. Biol. Chem.* **287**, 4936–4945 (2012).

106. Lazzaro, F. *et al.* Histone methyltransferase Dot1 and Rad9 inhibit single-stranded DNA accumulation at DSBs and uncapped telomeres. *EMBO J.* **27**, 1502–1512 (2008).

107. Bonetti, D. *et al.* Escape of Sgs1 from Rad9 inhibition reduces the requirement for Sae2 and functional MRX in DNA end resection. *EMBO Rep.* **16**, 351–361 (2015).

108. Ferrari, M. *et al.* Functional Interplay between the 53BP1-Ortholog Rad9 and the Mre11 Complex Regulates Resection, End-Tethering and Repair of a Double-Strand Break. *PLoS Genet.* **11**, e1004928 (2015).

109. Escribano-Díaz, C. *et al.* A Cell Cycle-Dependent Regulatory Circuit Composed of 53BP1-RIF1 and BRCA1-CtIP Controls DNA Repair Pathway Choice. *Mol. Cell* **49**, 872–883 (2013).

110. Giannattasio, M., Lazzaro, F., Plevani, P. & Muzi-Falconi, M. The DNA Damage Checkpoint Response Requires Histone H2B Ubiquitination by Rad6-Bre1 and H3 Methylation by Dot1. *J. Biol. Chem.* **280**, 9879–9886 (2005).

111. Wysocki, R. *et al.* Role of Dot1-Dependent Histone H3 Methylation in G1 and S Phase DNA Damage Checkpoint Functions of Rad9. *Mol. Cell. Biol.* **25**, 8430–8443 (2005).

112. Grenon, M. *et al.* Docking onto chromatin via the Saccharomyces cerevisiae Rad9 Tudor domain. *Yeast* **24**, 105–119 (2007).

113. Granata, M. *et al.* To trim or not to trim: Progression and control of DSB end resection. *Cell Cycle* **12**, 1848 (2013).

114. Downs, J. A., Lowndes, N. F. & Jackson, S. P. A role for *Saccharomyces cerevisiae* histone H2A in DNA repair. *Nature* **408**, 1001–1004 (2000).

115. Shroff, R. *et al.* Distribution and Dynamics of Chromatin Modification Induced by a Defined DNA Double-Strand Break. *Curr. Biol. CB* **14**, 1703–1711 (2004).

116. Toh, G. W.-L. *et al.* Histone H2A phosphorylation and H3 methylation are required for a novel Rad9 DSB repair function following checkpoint activation. *DNA Repair* **5**, 693–703 (2006).

117. Hammet, A., Magill, C., Heierhorst, J. & Jackson, S. P. Rad9 BRCT domain interaction with phosphorylated H2AX regulates the G1 checkpoint in budding yeast. *EMBO Rep.* **8**, 851–857 (2007).

118. Javaheri, A. *et al.* Yeast G1 DNA damage checkpoint regulation by H2A phosphorylation is independent of chromatin remodeling. *Proc. Natl. Acad. Sci. U. S. A.* **103**, 13771–13776 (2006).

119. Granata, M. *et al.* Dynamics of Rad9 Chromatin Binding and Checkpoint Function Are Mediated by Its Dimerization and Are Cell Cycle–Regulated by CDK1 Activity. *PLOS Genet.* **6**, e1001047 (2010).

120. Pfander, B. & Diffley, J. F. X. Dpb11 coordinates Mec1 kinase activation with cell cycle-regulated Rad9 recruitment. *EMBO J.* **30**, 4897–4907 (2011).

121. Chen, X. *et al.* The Fun30 ATP-dependent nucleosome remodeler promotes resection of DNA double-strand break ends. *Nature* **489**, 576–580 (2012).

122. Costelloe, T. *et al.* The yeast Fun30 and human SMARCAD1 chromatin remodelers promote DNA end resection. *Nature* **489**, 581–584 (2012).

123. Eapen, V. V., Sugawara, N., Tsabar, M., Wu, W.-H. & Haber, J. E. The Saccharomyces cerevisiae Chromatin Remodeler Fun30 Regulates DNA End Resection and Checkpoint Deactivation. *Mol. Cell. Biol.* **32**, 4727–4740 (2012).

124. Dibitetto, D. *et al.* Slx4 and Rtt107 control checkpoint signalling and DNA resection at double-strand breaks. *Nucleic Acids Res.* **44**, 669–682 (2016).

125. Ohouo, P. Y., Bastos de Oliveira, F. M., Liu, Y., Ma, C. J. & Smolka, M. B. DNA Repair Scaffolds Dampen Checkpoint Signaling by Counteracting the Rad9 Adaptor. *Nature* **493**, 120–124 (2013).

126. Di Virgilio, M. *et al.* Rif1 Prevents Resection of DNA Breaks and Promotes Immunoglobulin Class Switching. *Science* **339**, 711–715 (2013).

127. Zimmermann, M., Lottersberger, F., Buonomo, S. B., Sfeir, A. & de Lange, T. 53BP1 regulates DSB repair using Rif1 to control 5' end resection. *Science* **339**, 700–704 (2013).

128. Cassani, C. *et al.* Tel1 and Rif2 Regulate MRX Functions in End-Tethering and Repair of DNA Double-Strand Breaks. *PLOS Biol.* **14**, e1002387 (2016).

129. Morin, I. *et al.* Checkpoint-dependent phosphorylation of Exo1 modulates the DNA damage response. *EMBO J.* **27**, 2400–2410 (2008).

130. Jia, X., Weinert, T. & Lydall, D. Mec1 and Rad53 inhibit formation of single-stranded DNA at telomeres of Saccharomyces cerevisiae cdc13-1 mutants. *Genetics* **166**, 753–764 (2004).

131. Clerici, M., Trovesi, C., Galbiati, A., Lucchini, G. & Longhese, M. P. Mec1/ATR regulates the generation of single-stranded DNA that attenuates Tel1/ATM signaling at DNA ends. *EMBO J.* **33**, 198–216 (2014).

132. Gobbini, E. *et al.* Sae2 Function at DNA Double-Strand Breaks Is Bypassed by Dampening Tel1 or Rad53 Activity. *PLoS Genet.* **11**, e1005685 (2015).

133. Cartagena-Lirola, H., Guerini, I., Viscardi, V., Lucchini, G. & Longhese, M. P. Budding Yeast Sae2 is an In Vivo Target of the Mec1 and Tel1 Checkpoint Kinases During Meiosis. *Cell Cycle* **5**, 1549–1559 (2006).

134. Smolka, M. B., Albuquerque, C. P., Chen, S. & Zhou, H. Proteome-wide identification of in vivo targets of DNA damage checkpoint kinases. *Proc. Natl. Acad. Sci. U. S. A.* **104**, 10364–10369 (2007).

135. Liu, Y. *et al.* TOPBP1Dpb11 plays a conserved role in homologous recombination DNA repair through the coordinated recruitment of 53BP1Rad9. *J. Cell Biol.* **216**, 623–639 (2017).

136. Symington, L. S. Mechanism and Regulation of DNA End Resection in Eukaryotes. *Crit. Rev. Biochem. Mol. Biol.* **51**, 195–212 (2016).

137. Ngo, G. H. P. & Lydall, D. The 9-1-1 checkpoint clamp coordinates resection at DNA double strand breaks. *Nucleic Acids Res.* **43**, 5017–5032 (2015).

138. Ngo, G. H. P., Balakrishnan, L., Dubarry, M., Campbell, J. L. & Lydall, D. The 9-1-1 checkpoint clamp stimulates DNA resection by Dna2-Sgs1 and Exo1. *Nucleic Acids Res.* **42**, 10516–10528 (2014).

139. Krejci, L., Altmannova, V., Spirek, M. & Zhao, X. Homologous recombination and its regulation. *Nucleic Acids Res.* **40**, 5795–5818 (2012).

140. Holloman, W. K. Unraveling the mechanism of BRCA2 in homologous recombination. *Nat. Struct. Mol. Biol.* **18**, 748–754 (2011).

141. Sung, P., Krejci, L., Komen, S. V. & Sehorn, M. G. Rad51 Recombinase and Recombination Mediators. *J. Biol. Chem.* **278**, 42729–42732 (2003).

142. Li, J., Holzschu, D. L. & Sugiyama, T. PCNA is efficiently loaded on the DNA recombination intermediate to modulate polymerase δ, η, and ζ activities. *Proc. Natl. Acad. Sci. U. S. A.* **110**, 7672–7677 (2013).

143. Chen, J.-M., Cooper, D. N., Chuzhanova, N., Férec, C. & Patrinos, G. P. Gene conversion: mechanisms, evolution and human disease. *Nat. Rev. Genet.* **8**, 762–775 (2007).

144. Ciccia, A. & Elledge, S. J. The DNA Damage Response: Making it safe to play with knives. *Mol. Cell* **40**, 179–204 (2010).

145. Sarbajna, S. & West, S. C. Holliday junction processing enzymes as guardians of genome stability. *Trends Biochem. Sci.* **39**, 409–419 (2014).

146. Bizard, A. H. & Hickson, I. D. The Dissolution of Double Holliday Junctions. *Cold Spring Harb. Perspect. Biol.* **6**, a016477 (2014).

147. Moynahan, M. E. & Jasin, M. Mitotic homologous recombination maintains genomic stability and suppresses tumorigenesis. *Nat. Rev. Mol. Cell Biol.* **11**, 196–207 (2010).

148. Branzei, D. & Foiani, M. Template Switching: From Replication Fork Repair to Genome Rearrangements. *Cell* **131**, 1228–1230 (2007).

149. Finn, K., Lowndes, N. F. & Grenon, M. Eukaryotic DNA damage checkpoint activation in response to double-strand breaks. *Cell. Mol. Life Sci.* **69**, 1447–1473 (2012).

150. Harrison, J. C. & Haber, J. E. Surviving the Breakup: The DNA Damage Checkpoint. *Annu. Rev. Genet.* **40**, 209–235 (2006).

151. Lazzaro, F. *et al.* Checkpoint mechanisms at the intersection between DNA damage and repair. *DNA Repair* **8**, 1055–1067 (2009).

152. Lempiäinen, H. & Halazonetis, T. D. Emerging common themes in regulation of PIKKs and PI3Ks. *EMBO J.* **28**, 3067–3073 (2009).

153. Bosotti, R., Isacchi, A. & Sonnhammer, E. L. L. FAT: a novel domain in PIK-related kinases. *Trends Biochem. Sci.* **25**, 225–227 (2000).

154. Di Domenico, E. G., Romano, E., Del Porto, P. & Ascenzioni, F. Multifunctional Role of ATM/Tel1 Kinase in Genome Stability: From the DNA Damage Response to Telomere Maintenance. *BioMed Res. Int.* **2014**, 787404 (2014).

155. Smith, J., Mun Tho, L., Xu, N. & A. Gillespie, D. Chapter 3 - The ATM–Chk2 and ATR–Chk1 Pathways in DNA Damage Signaling and Cancer. in *Advances in Cancer Research* (eds. Vande Woude, G. F. & Klein, G.) **108**, 73–112 (Academic Press, 2010).

156. Nakada, D., Matsumoto, K. & Sugimoto, K. ATM-related Tel1 associates with double-strand breaks through an Xrs2-dependent mechanism. *Genes Dev.* **17**, 1957–1962 (2003).

157. You, Z., Chahwan, C., Bailis, J., Hunter, T. & Russell, P. ATM Activation and Its Recruitment to Damaged DNA Require Binding to the C Terminus of Nbs1. *Mol. Cell. Biol.* **25**, 5363–5379 (2005).

158. Dupré, A., Boyer-Chatenet, L. & Gautier, J. Two-step activation of ATM by DNA and the Mre11–Rad50–Nbs1 complex. *Nat. Struct. Mol. Biol.* **13**, 451–457 (2006).

159. Paull, T. T. Mechanisms of ATM Activation. *Annu. Rev. Biochem.* **84**, 711–738 (2015).

160. Fukunaga, K., Kwon, Y., Sung, P. & Sugimoto, K. Activation of Protein Kinase Tel1 through Recognition of Protein-Bound DNA Ends ▿. *Mol. Cell. Biol.* **31**, 1959–1971 (2011).

161. Guleria, A. & Chandna, S. ATM kinase: Much more than a DNA damage responsive protein. *DNA Repair* **39**, 1–20 (2016).

162. Zou, L. & Elledge, S. J. Sensing DNA Damage Through ATRIP Recognition of RPA-ssDNA Complexes. *Science* **300**, 1542–1548 (2003).

163. Paciotti, V., Clerici, M., Lucchini, G. & Longhese, M. P. The checkpoint protein Ddc2, functionally related to S. pombe Rad26, interacts with Mec1 and is regulated by Mec1-dependent phosphorylation in budding yeast. *Genes Dev.* **14**, 2046–2059 (2000).

164. Cortez, D., Guntuku, S., Qin, J. & Elledge, S. J. ATR and ATRIP: Partners in Checkpoint Signaling. *Science* **294**, 1713–1716 (2001).

165. Ball, H. L. *et al.* Function of a Conserved Checkpoint Recruitment Domain in ATRIP Proteins. *Mol. Cell. Biol.* **27**, 3367–3377 (2007).

166. MacDougall, C. A., Byun, T. S., Van, C., Yee, M. & Cimprich, K. A. The structural determinants of checkpoint activation. *Genes Dev.* **21**, 898–903 (2007).

167. Navadgi-Patil, V. M. & Burgers, P. M. A tale of two tails: Activation of DNA damage checkpoint kinase Mec1/ATR by the 9-1-1 clamp and by Dpb11/TopBP1. *DNA Repair* **8**, 996–1003 (2009).

168. Majka, J., Niedziela-Majka, A. & Burgers, P. M. J. The checkpoint clamp activates Mec1 kinase during initiation of the DNA damage checkpoint. *Mol. Cell* **24**, 891–901 (2006).

169. Duursma, A. M., Driscoll, R., Elias, J. E. & Cimprich, K. A. A role for the MRN complex in ATR activation through TOPBP1 recruitment. *Mol. Cell* **50**, 116–122 (2013).

170. Kumagai, A., Lee, J., Yoo, H. Y. & Dunphy, W. G. TopBP1 Activates the ATR-ATRIP Complex. *Cell* **124**, 943–955 (2006).

171. Mordes, D. A., Nam, E. A. & Cortez, D. Dpb11 activates the Mec1–Ddc2 complex. *Proc. Natl. Acad. Sci. U. S. A.* **105**, 18730–18734 (2008).

172. Puddu, F. *et al.* Phosphorylation of the Budding Yeast 9-1-1 Complex Is Required for Dpb11 Function in the Full Activation of the UV-Induced DNA Damage Checkpoint. *Mol. Cell. Biol.* **28**, 4782–4793 (2008).

173. Mantiero, D., Clerici, M., Lucchini, G. & Longhese, M. P. Dual role for Saccharomyces cerevisiae Tel1 in the checkpoint response to double-strand breaks. *EMBO Rep.* **8**, 380–387 (2007).

174. Shiotani, B. & Zou, L. Single-Stranded DNA Orchestrates an ATM-to-ATR Switch at DNA Breaks. *Mol. Cell* **33**, 547–558 (2009).

175. Cicco, G. di, Bantele, S. C. S., Reusswig, K.-U. & Pfander, B. A cell cycle-independent mode of the Rad9-Dpb11 interaction is induced by DNA damage. *Sci. Rep.* **7**, 11650 (2017).

176. Schwartz, M. F. *et al.* Rad9 Phosphorylation Sites Couple Rad53 to the Saccharomyces cerevisiae DNA Damage Checkpoint. *Mol. Cell* **9**, 1055–1065 (2002).

177. Sweeney, F. D. *et al.* Saccharomyces cerevisiae Rad9 Acts as a Mec1 Adaptor to Allow Rad53 Activation. *Curr. Biol.* **15**, 1364–1375 (2005).

178. Gilbert, C. S., Green, C. M. & Lowndes, N. F. Budding Yeast Rad9 Is an ATP-Dependent Rad53 Activating Machine. *Mol. Cell* **8**, 129–136 (2001).

179. Wang, B., Matsuoka, S., Carpenter, P. B. & Elledge, S. J. 53BP1, a Mediator of the DNA Damage Checkpoint. *Science* **298**, 1435–1438 (2002).

180. Stucki, M. *et al.* MDC1 Directly Binds Phosphorylated Histone H2AX to Regulate Cellular Responses to DNA Double-Strand Breaks. *Cell* **123**, 1213–1226 (2005).

181. Goldberg, M. *et al.* MDC1 is required for the intra-S-phase DNA damage checkpoint. *Nature* **421**, 952–956 (2003).

182. Lou, Z. *et al.* MDC1 Maintains Genomic Stability by Participating in the Amplification of ATM-Dependent DNA Damage Signals. *Mol. Cell* **21**, 187–200 (2006).

183. Luo, K., Yuan, J. & Lou, Z. Oligomerization of MDC1 Protein Is Important for Proper DNA Damage Response. *J. Biol. Chem.* **286**, 28192–28199 (2011).

184. Wu, L., Luo, K., Lou, Z. & Chen, J. MDC1 regulates intra-S-phase checkpoint by targeting NBS1 to DNA double-strand breaks. *Proc. Natl. Acad. Sci. U. S. A.* **105**, 11200–11205 (2008).

185. Stucki, M. & Jackson, S. P. γH2AX and MDC1: Anchoring the DNA-damage-response machinery to broken chromosomes. *DNA Repair* **5**, 534–543 (2006).

186. Jungmichel, S. & Stucki, M. MDC1: The art of keeping things in focus. *Chromosoma* **119**, 337–349 (2010).

187. Chen, S. & Zhou, H. Reconstitution of Rad53 Activation by Mec1 through Adaptor Protein Mrc1. *J. Biol. Chem.* **284**, 18593–18604 (2009).

188. Giannattasio, M. & Branzei, D. S-phase checkpoint regulations that preserve replication and chromosome integrity upon dNTP depletion. *Cell. Mol. Life Sci.* **74**, 2361–2380 (2017).

189. Alcasabas, A. A. *et al.* Mrc1 transduces signals of DNA replication stress to activate Rad53. *Nat. Cell Biol.* **3**, 958–965 (2001).

190. Durocher, D., Henckel, J., Fersht, A. R. & Jackson, S. P. The FHA Domain Is a Modular Phosphopeptide Recognition Motif. *Mol. Cell* **4**, 387–394 (1999).

191. Patil, M., Pabla, N. & Dong, Z. Checkpoint kinase 1 in DNA damage response and cell cycle regulation. *Cell. Mol. Life Sci. CMLS* **70**, 4009–4021 (2013).

192. Zhang, Y. & Hunter, T. Roles of Chk1 in Cell Biology and Cancer Therapy. *Int. J. Cancer J. Int. Cancer* **134**, 1013–1023 (2014).

193. Bartek, J., Falck, J. & Lukas, J. Chk2 kinase — a busy messenger. *Nat. Rev. Mol. Cell Biol.* **2**, 877–886 (2001).

194. Zannini, L., Delia, D. & Buscemi, G. CHK2 kinase in the DNA damage response and beyond. *J. Mol. Cell Biol.* **6**, 442–457 (2014).

195. Medema, R. H. & Macůrek, L. Checkpoint control and cancer. *Oncogene* **31**, 2601–2613 (2012).

196. Shibata, A. *et al.* Role of ATM and the Damage Response Mediator Proteins 53BP1 and MDC1 in the Maintenance of G2/M Checkpoint Arrest. *Mol. Cell. Biol.* **30**, 3371–3383 (2010).

197. Syljuåsen, R. G., Jensen, S., Bartek, J. & Lukas, J. Adaptation to the Ionizing Radiation–Induced G2 Checkpoint Occurs in Human Cells and Depends on Checkpoint Kinase 1 and Polo-like Kinase 1 Kinases. *Cancer Res.* **66**, 10253–10257 (2006).

198. Clémenson, C. & Marsolier-Kergoat, M.-C. DNA damage checkpoint inactivation: Adaptation and recovery. *DNA Repair* **8**, 1101–1109 (2009).

199. Chan, Y. A., Hieter, P. & Stirling, P. C. Mechanisms of genome instability induced by RNA processing defects. *Trends Genet. TIG* **30**, 245–253 (2014).

200. Dutertre, M., Lambert, S., Carreira, A., Amor-Guéret, M. & Vagner, S. DNA damage: RNA-binding proteins protect from near and far. *Trends Biochem. Sci.* **39**, 141–149 (2014).

201. Aguilera, A. & García-Muse, T. R Loops: From Transcription Byproducts to Threats to Genome Stability. *Mol. Cell* **46**, 115–124 (2012).

202. Huertas, P. & Aguilera, A. Cotranscriptionally Formed DNA:RNA Hybrids Mediate Transcription Elongation Impairment and Transcription-Associated Recombination. *Mol. Cell* **12**, 711–721 (2003).

203. Santos-Pereira, J. M., Herrero, A. B., Moreno, S. & Aguilera, A. Npl3, a new link between RNA-binding proteins and the maintenance of genome integrity. *Cell Cycle* **13**, 1524–1529 (2014).

204. Lenzken, S. C., Loffreda, A. & Barabino, S. M. L. RNA Splicing: A New Player in the DNA Damage Response. *Int. J. Cell Biol.* **2013**, 153634 (2013).

205. Tan, A. Y. & Manley, J. L. The TET Family of Proteins: Functions and Roles in Disease. *J. Mol. Cell Biol.* **1**, 82–92 (2009).

206. Deka, P., Bucheli, M. E., Moore, C., Buratowski, S. & Varani, G. Structure of the yeast SR protein Npl3 and Interaction with mRNA 3'-end processing signals. *J. Mol. Biol.* **375**, 136–150 (2008).

207. Dermody, J. L. *et al.* Unphosphorylated SR-like protein Npl3 stimulates RNA polymerase II elongation. *PloS One* **3**, e3273 (2008).

208. Rajyaguru, P., She, M. & Parker, R. Scd6 Targets eIF4G to Repress Translation: RGG Motif Proteins as a Class of eIF4G-Binding Proteins. *Mol. Cell* **45**, 244–254 (2012).

209. Kress, T. L., Krogan, N. J. & Guthrie, C. A single SR-like protein, Npl3, promotes pre-mRNA splicing in budding yeast. *Mol. Cell* **32**, 727–734 (2008).

210. Gilbert, W. & Guthrie, C. The Glc7p nuclear phosphatase promotes mRNA export by facilitating association of Mex67p with mRNA. *Mol. Cell* **13**, 201–212 (2004).

211. McBride, A. E. *et al.* Arginine methylation of yeast mRNA-binding protein Npl3 directly affects its function, nuclear export, and intranuclear protein interactions. *J. Biol. Chem.* **280**, 30888–30898 (2005).

212. Tutucci, E. & Stutz, F. Keeping mRNPs in check during assembly and nuclear export. *Nat. Rev. Mol. Cell Biol.* **12**, 377–384 (2011).

213. Moehle, E. A., Ryan, C. J., Krogan, N. J., Kress, T. L. & Guthrie, C. The Yeast SR-Like Protein Npl3 Links Chromatin Modification to mRNA Processing. *PLOS Genet.* **8**, e1003101 (2012).

214. Lee-Soety, J. Y. *et al.* Yeast hnRNP-related proteins contribute to the maintenance of telomeres. *Biochem. Biophys. Res. Commun.* **426**, 12–17 (2012).

215. Santos-Pereira, J. M. *et al.* The Npl3 hnRNP prevents R-loop-mediated transcription-replication conflicts and genome instability. *Genes Dev.* **27**, 2445–2458 (2013).

216. Bucheli, M. E. & Buratowski, S. Npl3 is an antagonist of mRNA 3' end formation by RNA polymerase II. *EMBO J.* **24**, 2150–2160 (2005).

217. Bucheli, M. E., He, X., Kaplan, C. D., Moore, C. L. & Buratowski, S. Polyadenylation site choice in yeast is affected by competition between Npl3 and polyadenylation factor CFI. *RNA* **13**, 1756–1764 (2007).

218. Wong, C.-M. *et al.* Yeast arginine methyltransferase Hmt1p regulates transcription elongation and termination by methylating Npl3p. *Nucleic Acids Res.* **38**, 2217–2228 (2010).

219. Russell, I. D. & Tollervey, D. NOP3 is an essential yeast protein which is required for pre-rRNA processing. *J. Cell Biol.* **119**, 737–747 (1992).

220. Vitaliano-Prunier, A. *et al.* H2B ubiquitylation controls the formation of export-competent mRNP. *Mol. Cell* **45**, 132–139 (2012).

221. Lee, M. S., Henry, M. & Silver, P. A. A protein that shuttles between the nucleus and the cytoplasm is an important mediator of RNA export. *Genes Dev.* **10**, 1233–1246 (1996).

222. Baierlein, C. *et al.* Monosome Formation during Translation Initiation Requires the Serine/Arginine-Rich Protein Npl3. *Mol. Cell. Biol.* **33**, 4811–4823 (2013).

223. Symington, L. S., Rothstein, R. & Lisby, M. Mechanisms and regulation of mitotic recombination in Saccharomyces cerevisiae. *Genetics* **198**, 795–835 (2014).

224. Villa, M., Cassani, C., Gobbini, E., Bonetti, D. & Longhese, M. P. Coupling end resection with the checkpoint response at DNA double-strand breaks. *Cell. Mol. Life Sci. CMLS* **73**, 3655–3663 (2016).

225. Wickramasinghe, V. O. & Venkitaraman, A. R. RNA Processing and Genome Stability: Cause and Consequence. *Mol. Cell* **61**, 496–505 (2016).

226. Eberle, A. B. & Visa, N. Quality control of mRNP biogenesis: networking at the transcription site. *Semin. Cell Dev. Biol.* **32**, 37–46 (2014).

227. Fox, M. J. & Mosley, A. L. Rrp6: Integrated roles in nuclear RNA metabolism and transcription termination. *Wiley Interdiscip. Rev. RNA* **7**, 91–104 (2016).

228. García-Muse, T. & Aguilera, A. Transcription-replication conflicts: how they occur and how they are resolved. *Nat. Rev. Mol. Cell Biol.* **17**, 553–563 (2016).

229. Janke, R. *et al.* Nonsense-mediated decay regulates key components of homologous recombination. *Nucleic Acids Res.* **44**, 5218–5230 (2016).

230. Lei, E. P., Krebber, H. & Silver, P. A. Messenger RNAs are recruited for nuclear export during transcription. *Genes Dev.* **15**, 1771–1782 (2001).

231. Holmes, R. K. *et al.* Loss of the Yeast SR Protein Npl3 Alters Gene Expression Due to Transcription Readthrough. *PLoS Genet.* **11**, e1005735 (2015).

232. McKinney, J. S. *et al.* A multistep genomic screen identifies new genes required for repair of DNA double-strand breaks in Saccharomyces cerevisiae. *BMC Genomics* **14**, 251 (2013).

233. Pan, X. *et al.* A DNA integrity network in the yeast Saccharomyces cerevisiae. *Cell* **124**, 1069–1081 (2006).

234. Lee, S. E. *et al.* Saccharomyces Ku70, mre11/rad50 and RPA proteins regulate adaptation to G2/M arrest after DNA damage. *Cell* **94**, 399–409 (1998).

235. Pellicioli, A., Lee, S. E., Lucca, C., Foiani, M. & Haber, J. E. Regulation of Saccharomyces Rad53 checkpoint kinase during adaptation from DNA damage-induced G2/M arrest. *Mol. Cell* **7**, 293–300 (2001).

236. Zhao, X., Muller, E. G. & Rothstein, R. A suppressor of two essential checkpoint genes identifies a novel protein that negatively affects dNTP pools. *Mol. Cell* **2**, 329–340 (1998).

237. Redon, C. *et al.* Yeast histone 2A serine 129 is essential for the efficient repair of checkpoint-blind DNA damage. *EMBO Rep.* **4**, 678–684 (2003).

238. Nakada, D., Shimomura, T., Matsumoto, K. & Sugimoto, K. The ATM-related Tel1 protein of Saccharomyces cerevisiae controls a checkpoint response following phleomycin treatment. *Nucleic Acids Res.* **31**, 1715–1724 (2003).

239. Ohle, C. *et al.* Transient RNA-DNA Hybrids Are Required for Efficient Double-Strand Break Repair. *Cell* **167**, 1001-1013.e7 (2016).

240. Li, L. *et al.* DEAD Box 1 Facilitates Removal of RNA and Homologous Recombination at DNA Double-Strand Breaks. *Mol. Cell. Biol.* **36**, 2794–2810 (2016).

241. Castellano-Pozo, M., García-Muse, T. & Aguilera, A. R-loops cause replication impairment and genome instability during meiosis. *EMBO Rep.* **13**, 923–929 (2012).

242. Hegnauer, A. M. *et al.* An N-terminal acidic region of Sgs1 interacts with Rpa70 and recruits Rad53 kinase to stalled forks. *EMBO J.* **31**, 3768–3783 (2012).

243. Manfrini, N. *et al.* RNA-processing proteins regulate Mec1/ATR activation by promoting generation of RPA-coated ssDNA. *EMBO Rep.* **16**, 221–231 (2015).

244. Sokolsky, T. & Alani, E. EXO1 and MSH6 are high-copy suppressors of conditional mutations in the MSH2 mismatch repair gene of Saccharomyces cerevisiae. *Genetics* **155**, 589–599 (2000).

245. Longhese, M. P., Plevani, P. & Lucchini, G. Replication factor A is required in vivo for DNA replication, repair, and recombination. *Mol. Cell. Biol.* **14**, 7884–7890 (1994).

246. Giannattasio, M. *et al.* Exo1 competes with repair synthesis, converts NER intermediates to long ssDNA gaps, and promotes checkpoint activation. *Mol. Cell* **40**, 50–62 (2010).

247. Baejen, C. *et al.* Transcriptome maps of mRNP biogenesis factors define pre-mRNA recognition. *Mol. Cell* **55**, 745–757 (2014).

248. Hurowitz, E. H. & Brown, P. O. Genome-wide analysis of mRNA lengths in Saccharomyces cerevisiae. *Genome Biol.* **5**, R2 (2003).

249. Burkard, K. T. & Butler, J. S. A nuclear 3'-5' exonuclease involved in mRNA degradation interacts with Poly(A) polymerase and the hnRNA protein Npl3p. *Mol. Cell. Biol.* **20**, 604–616 (2000).

250. Garcia, V., Phelps, S. E. L., Gray, S. & Neale, M. J. Bidirectional resection of DNA double-strand breaks by Mre11 and Exo1. *Nature* **479**, 241–244 (2011).

251. Shibata, A. *et al.* DNA double-strand break repair pathway choice is directed by distinct MRE11 nuclease activities. *Mol. Cell* **53**, 7–18 (2014).

252. Jazayeri, A. *et al.* ATM- and cell cycle-dependent regulation of ATR in response to DNA double-strand breaks. *Nat. Cell Biol.* **8**, 37–45 (2006).

253. Myers, J. S. & Cortez, D. Rapid activation of ATR by ionizing radiation requires ATM and Mre11. *J. Biol. Chem.* **281**, 9346–9350 (2006).

254. Emili, A. MEC1-dependent phosphorylation of Rad9p in response to DNA damage. *Mol. Cell* **2**, 183–189 (1998).

255. Vialard, J. E., Gilbert, C. S., Green, C. M. & Lowndes, N. F. The budding yeast Rad9 checkpoint protein is subjected to Mec1/Tel1-dependent hyperphosphorylation and interacts with Rad53 after DNA damage. *EMBO J.* **17**, 5679–5688 (1998).

256. Sun, Z., Hsiao, J., Fay, D. S. & Stern, D. F. Rad53 FHA domain associated with phosphorylated Rad9 in the DNA damage checkpoint. *Science* **281**, 272–274 (1998).

257. Pellicioli, A. *et al.* Activation of Rad53 kinase in response to DNA damage and its effect in modulating phosphorylation of the lagging strand DNA polymerase. *EMBO J.* **18**, 6561–6572 (1999).

258. Falck, J., Coates, J. & Jackson, S. P. Conserved modes of recruitment of ATM, ATR and DNA-PKcs to sites of DNA damage. *Nature* **434**, 605–611 (2005).

259. Lee, J.-H. & Paull, T. T. ATM activation by DNA double-strand breaks through the Mre11-Rad50-Nbs1 complex. *Science* **308**, 551–554 (2005).

260. Berkovich, E., Monnat, R. J. & Kastan, M. B. Roles of ATM and NBS1 in chromatin structure modulation and DNA double-strand break repair. *Nat. Cell Biol.* **9**, 683–690 (2007).

261. Usui, T., Ogawa, H. & Petrini, J. H. A DNA damage response pathway controlled by Tel1 and the Mre11 complex. *Mol. Cell* **7**, 1255–1266 (2001).

262. Cassani, C. *et al.* Structurally distinct Mre11 domains mediate MRX functions in resection, end-tethering and DNA damage resistance. *Nucleic Acids Res.* **46**, 2990–3008 (2018).

263. Tishkoff, D. X., Filosi, N., Gaida, G. M. & Kolodner, R. D. A novel mutation avoidance mechanism dependent on S. cerevisiae RAD27 is distinct from DNA mismatch repair. *Cell* **88**, 253–263 (1997).

264. Moreau, S., Ferguson, J. R. & Symington, L. S. The nuclease activity of Mre11 is required for meiosis but not for mating type switching, end joining, or telomere maintenance. *Mol. Cell. Biol.* **19**, 556–566 (1999).

265. Debrauwère, H., Loeillet, S., Lin, W., Lopes, J. & Nicolas, A. Links between replication and recombination in Saccharomyces cerevisiae: a hypersensitive requirement for homologous recombination in the absence of Rad27 activity. *Proc. Natl. Acad. Sci. U. S. A.* **98**, 8263–8269 (2001).

266. Hardy, J., Churikov, D., Géli, V. & Simon, M.-N. Sgs1 and Sae2 promote telomere replication by limiting accumulation of ssDNA. *Nat. Commun.* **5**, 5004 (2014).

267. Fishman-Lobell, J., Rudin, N. & Haber, J. E. Two alternative pathways of double-strand break repair that are kinetically separable and independently modulated. *Mol. Cell. Biol.* **12**, 1292–1303 (1992).

268. Ivanov, E. L., Sugawara, N., Fishman-Lobell, J. & Haber, J. E. Genetic requirements for the single-strand annealing pathway of double-strand break repair in Saccharomyces cerevisiae. *Genetics* **142**, 693–704 (1996).

269. Vaze, M. B. *et al.* Recovery from checkpoint-mediated arrest after repair of a double-strand break requires Srs2 helicase. *Mol. Cell* **10**, 373–385 (2002).

270. Lobachev, K. S., Gordenin, D. A. & Resnick, M. A. The Mre11 Complex Is Required for Repair of Hairpin-Capped Double-Strand Breaks and Prevention of Chromosome Rearrangements. *Cell* **108**, 183–193 (2002).

271. Kim, H.-S. *et al.* Functional interactions between Sae2 and the Mre11 complex. *Genetics* **178**, 711–723 (2008).

272. Trujillo, K. M. & Sung, P. DNA structure-specific nuclease activities in the Saccharomyces cerevisiae Rad50*Mre11 complex. *J. Biol. Chem.* **276**, 35458–35464 (2001).

273. Toczyski, D. P., Galgoczy, D. J. & Hartwell, L. H. CDC5 and CKII control adaptation to the yeast DNA damage checkpoint. *Cell* **90**, 1097–1106 (1997).

274. Nakada, D., Hirano, Y. & Sugimoto, K. Requirement of the Mre11 complex and exonuclease 1 for activation of the Mec1 signaling pathway. *Mol. Cell. Biol.* **24**, 10016–10025 (2004).

275. Zierhut, C. & Diffley, J. F. X. Break dosage, cell cycle stage and DNA replication influence DNA double strand break response. *EMBO J.* **27**, 1875–1885 (2008).

276. Libri, D. *et al.* Interactions between mRNA export commitment, 3'-end quality control, and nuclear degradation. *Mol. Cell. Biol.* **22**, 8254–8266 (2002).

277. Hilleren, P., McCarthy, T., Rosbash, M., Parker, R. & Jensen, T. H. Quality control of mRNA 3'-end processing is linked to the nuclear exosome. *Nature* **413**, 538–542 (2001).

278. Kallehauge, T. B., Robert, M.-C., Bertrand, E. & Jensen, T. H. Nuclear retention prevents premature cytoplasmic appearance of mRNA. *Mol. Cell* **48**, 145–152 (2012).

279. Babour, A. *et al.* The Chromatin Remodeler ISW1 Is a Quality Control Factor that Surveys Nuclear mRNP Biogenesis. *Cell* **167**, 1201-1214.e15 (2016).

280. Cotta-Ramusino, C. *et al.* Exo1 processes stalled replication forks and counteracts fork reversal in checkpoint-defective cells. *Mol. Cell* **17**, 153–159 (2005).

281. Maringele, L. & Lydall, D. EXO1-dependent single-stranded DNA at telomeres activates subsets of DNA damage and spindle checkpoint pathways in budding yeast yku70Delta mutants. *Genes Dev.* **16**, 1919–1933 (2002).

282. Myler, L. R. *et al.* Single-molecule imaging reveals the mechanism of Exo1 regulation by single-stranded DNA binding proteins. *Proc. Natl. Acad. Sci. U. S. A.* **113**, E1170-1179 (2016).

283. Tsubouchi, H. & Ogawa, H. Exo1 roles for repair of DNA double-strand breaks and meiotic crossing over in Saccharomyces cerevisiae. *Mol. Biol. Cell* **11**, 2221–2233 (2000).

284. Savage, K. I. *et al.* Identification of a BRCA1-mRNA splicing complex required for efficient DNA repair and maintenance of genomic stability. *Mol. Cell* **54**, 445–459 (2014).

285. Bonetti, D., Martina, M., Clerici, M., Lucchini, G. & Longhese, M. P. Multiple pathways regulate 3' overhang generation at S. cerevisiae telomeres. *Mol. Cell* **35**, 70–81 (2009).

286. Longhese, M. P., Paciotti, V., Neecke, H. & Lucchini, G. Checkpoint proteins influence telomeric silencing and length maintenance in budding yeast. *Genetics* **155**, 1577–1591 (2000).

287. Baldo, V., Testoni, V., Lucchini, G. & Longhese, M. P. Dominant TEL1-hy mutations compensate for Mec1 lack of functions in the DNA damage response. *Mol. Cell. Biol.* **28**, 358–375 (2008).

288. Kaye, J. A. *et al.* DNA breaks promote genomic instability by impeding proper chromosome segregation. *Curr. Biol. CB* **14**, 2096–2106 (2004).